CREEP CAVITATION IN 304 STAINLESS STEEL

by

I-WEI CHEN

B.S., National Tsinghua University
(1972)

M.S., University of Pennsylvania
(1975)

SUBMITTED IN PARTIAL FULFILLMENT

OF THE REQUIREMENTS FOR THE

DEGREE OF

DOCTOR OF PHILOSOPHY

at the

MASSACHUSETTS INSTITUTE OF TECHNOLOGY

February 1980

Signature of Author _____
Department of Materials Science and Engineering
January 11, 1980

Certified by _____
Ali S. Argon
Thesis Supervisor

Accepted by _____
Regis M. N. Pelloux
Chairman, Departmental Graduate Committee

CREEP CAVITATION IN 304 STAINLESS STEEL

by

I-WEI CHEN

Submitted to the Department of Materials Science and Engineering on January 11, 1980 in partial fulfillment of the requirements for the Degree of Doctor of Philosophy in Metallurgy.

ABSTRACT

A micromechanical analysis of deformation and fracture in creeping alloys is presented based on a mechanistic approach using continuum mechanics. The analysis was first carried out on a coarse microscopic level in which the self-consistent theory of Hill was employed to treat the steady state creep of heterogeneous alloys with coarse microstructures allowing for grain boundary sliding. Processes operating on a finer scale than the grain size such as grain boundary diffusion and surface diffusion were subsequently included in the analysis. It was found that the high stresses required for cavity nucleation occur at intergranular particles only in transients of grain boundary sliding, and that two modes of cavity growth result corresponding to rate control by each of the abovementioned diffusional processes.

Creep cavitation in 304 stainless steel in the neighborhood of 0.5 T_m was studied experimentally to test these theoretical models. Our results suggest that a broad spectrum of interfacial energy may exist and that microstructural changes such as those caused by twins can alter cavitation behavior drastically. Cavities grow in most cases by grain boundary diffusion coupled with matrix creep, somewhat restricted by surface diffusion. However, the grain boundary sliding can be a dominant mode of cavity growth at high stresses and for large cavities.

Thesis Supervisor: Dr. Ali S. Argon
Title: Professor of Mechanical Engineering

TABLE OF CONTENTS

TABLE OF CONTENTS (Cont'd.)

TABLE OF CONTENTS (Cont'd.)

TABLE OF CONTENTS (Cont'd.)

LIST OF ILLUSTRATIONS AND FIGURES

LIST OF ILLUSTRATIONS AND FIGURES (Cont'd.)

LIST OF ILLUSTRATIONS AND FIGURES (Cont'd.)

ACKNOWLEDGEMENTS

I owe a great debt to my thesis advisor, Professor Ali S. Argon; his guidance and, more importantly, his example have nurtured in me an aspiration to excellence that will serve me well in years to come. My interaction with him has been a personally and professionally rewarding experience.

Professors F. A. McClintock and J. Bassani, and Mr. A. W. Lau, coworkers under the DOE Contract "Micromechanical Modeling of Damage Production at Elevated Temperature in Heterogeneous Alloys," have shaped my thinking in many important ways. Their approach to significant engineering problems has had a profound effect on the direction of this study.

I am also grateful to Professors R. M. Cannon, M. P. Cleary, N. J. Grant, J. W. Hutchinson, R.M.N. Pelloux and F. Prinz for helpful discussions and criticism.

Finally, I am thankful to my parents, sisters and wife, without whose unwavering support and love this work would never have been accomplished.

Financial support from the Department of Mechanical Engineering at MIT (the du Pont Fund) and the U.S. Department of Energy (Contract No. EG-77-S-02-4461) is gratefully acknowledged.

LIST OF SYMBOLS*

σ_∞	distant stress
σ_n	normal stress
σ_o	stress unit in non-dimensional representation
τ_a	applied shear stress
E	Young's modulus
L^{-1}	compliance
ν	Poisson's ratio
Δ	δ-function tensor that relates strain rate to diffusional displacement
$\dot{\varepsilon}$	distant strain rate
$\dot{u}_{GB}$	rate of grain boundary sliding
ε_r	rupture strain
t_r	rupture time
t_o	time unit in non-dimensional representation
τ_b	relaxation time due to grain boundary diffusion
τ_s	relaxation time due to surface diffusion
ℓ	dimension of elastic stress concentration
ℓ_o	length unit in non-dimensional representation
ℓ_D	diffusion distance in creep
m, A	creep coefficient in $\dot{\varepsilon} = A\sigma^m$
ϕ	stress function
η	viscosity in $\sigma = \eta\dot{\varepsilon}$
η'	plain strain viscosity ($\eta' = 4/3\eta$ if $\nu = 1/2$)
G	influence function in linear viscous deformation

*These symbols are used in Chapters 5-8.

LIST OF SYMBOLS (Cont'd.)

K_n	wave vector in Fourier series
K_D	diffusion wave vector
λ	wave length of grain boundary steps
h_n	Fourier coefficient of grain boundary steps
h	height of grain boundary steps
ξ	coupling coefficient in visco-diffusive deformation
J_s	atomic flux along surface
J_b	atomic flux along grain boundary
D_s	Surface diffusion coefficient
D_b	grain boundary diffusion coefficient
δ_s	effective thickness of surface diffusion path
δ_b	effective thickness of grain boundary diffusive path
γ_s	surface energy
γ_b	grain boundary energy
k	Boltzman Constant
R	gas constant
Ω	atomic volume
χ	increase of interfacial energy in nucleating a cavity
ΔG^*	energy of critical nuclei
ΔG_b	activation energy of grain boundary diffusion
ΔG_s	activation energy of surface diffusion
r^*	radius of critical nuclei
$\dot{\zeta}$	nucleation rate per nucleation site
ψ	tip angle of cavity ($2\gamma_s \cos \psi = \gamma_b$)

LIST OF SYMBOLS (Cont'd.)

b_o	cavity spacing
d	cavity diameter
v	cavity volume
a	major radius of an axisymmetric cavity
$h(\psi)$	geometric constant, $v = 4\pi/3\ a^3\ h(\psi)$
F_v	geometric constant, $v = F_v a^3$
f_L	ratio of coverage of carbides on grain boundaries on planar section
f_A	area coverage of grain boundary particles
n_L	number density of carbides of grain boundaries on a planar section
$p_{\|\|}$	carbide size along grain boundaries on a planar section
$p_{\|}$	carbide size normal to grain boundaries on a planar section
v_f	volume fraction of carbides
N_L^*	number density of cavities of grain boundaries on a planar section
N_A^*	number density of cavities of grain boundaries
F_A	area fraction of cavitated grain boundaries
ϕ	inclination between normal of the grain boundaries and the applied stress
α	coefficient that prescribes the ratio of J_s to J_b
α'	coefficient that prescribes the ratio of J_s to J_b
$F(a/\ell_D)$	normalized growth rate of cavity
d_G	grain size

*We follow notation as found in standard texts of quantitative metallography. In particular, N_L is defined as the number of cavity interceptions per unit length of the lines which represent the intersections of the grain boundaries with the picture plane, and N_A is defined as the number of cavities per unit area of grain boundaries projected onto the picture plane. No attempt is made to infer the actual area from those projections.

CHAPTER 1

OVERVIEW

Creep deformation and intergranular failure are of great concern in the design of structures which operate at elevated temperatures. The performance of engineering materials intended for high temperature applications is often determined by their creep resistance and their ductility. Since most structural materials contain, often by design, a small to intermediate volume fraction of hard phases to improve the performance, their behavior is extremely sensitive to microstructures and composition. It is necessary however, for the purpose of fundamental understanding, to seek to identify mechanisms which are common to most materials, recognizing that the regime of temperature and stress in which a particular mechanism dominates will differ from one material to another.

The scope of creep deformation and intergranular failure can be best envisioned by examination of mechanisms which operate at elevated temperature. In a polycrystal, deformation of constituents is mutually accommodated by a combination of elastic deformation, localized plastic deformation, non-uniform creep, grain boundary sliding and diffusional flow through the grains, along grain boundaries and free surfaces. In heterogeneous alloys, further accommodation occurs at interfaces of distinct phases which in general raises the deformation resistance both intragranularly and intergranularly. It is also known that second phase particles are often responsible for cavity production which leads to intergranular failures. The initiation, ripening and development of such cavities and macro-cracks are likely related to one or several of

the deformation mechanisms mentioned earlier.

In this study, we proceed with a micromechanical analysis of these problems by the continuum analysis of specific mechanisms. Guided by the choice of plausible mechanistic models pertaining to various stages in the deformation and fracture process, we shall conduct comprehensive analyses using continuum mechanics. Results of such analyses are compared with phenomenology and, whenever possible, with specific measurements of relevant experiments.

A structural material of sufficient complexity and with broad applications, 304 stainless steel, was chosen for experimental studies.

The main body of this thesis can be further divided into three parts. In the first part, composed of Chapter 3 and Chapter 4, the continuum analysis is carried out on a coarse microscopic level in which the individual grain and the grain boundary are taken to be constituent phase domains of a heterogeneous material. This allows us to draw an analogy between the multiphase polycrystals with or without grain boundary sliding and the conventional composite materials. The self-consistent theory of Hill is then employed to treat the overall deformation of heterogeneous materials. In Chapter 3 we study the steady state power law creep of two-phase materials of coarse microstructure and later, in Chapter 4, the same technique is extended to cover grain boundary sliding and interface sliding in a power law creeping matrix.

For problems such as the determination of interfacial stresses at elevated temperature or the nucleation and growth of intergranular cavities, microscopic processes which operate at a scale finer than grain size need to be taken into account. These processes include grain

boundary diffusion and surface diffusion; their formulations and applications to the problems mentioned above form the major themes of the second part of the thesis. In Chapter 5 the relaxation of internal stresses in viscous solids which also undergo diffusional flow is treated in great detail. In addition, the overall deformation of a polycrystal with sliding grain boundaries is again examined with inclusion of diffusional flow. The result of these studies with regard to internal stresses is then related to the nucleation of intergranular cavities. Subsequently, in Chapter 6, we develop a simple theoretical approach to the general problem of cavity growth in which the intricate interplay between surface diffusion, grain boundary diffusion and matrix creep is taken into account. Two modes of cavity growth are predicted by this theory which embraces most of the features of previous successful models in the field and is possible to furnish a satisfactory account of the process of cavity growth (see Eqns (6.7) and (6.8)).

The third part of the thesis, an experimental study of creep cavitation in 304 stainless steel, is presented in Chapter 7. Emphasis of the effort was directed toward creep cavitation near 0.5 T_m. Quantitative measurement pertaining to nucleation and growth of cavities is used for comparison with the analysis. The most rewarding outcome of this study is however the microscopic observation which sheds some light on the nature of intergranular fracture in engineering alloys. In particular, a shearing mode caused by grain boundary sliding was unambiguously identified, this was found to be responsible for the growth of cavities at high strain rates. The occurrence of this additional mode of cavity growth is shown to be explained by the competition between

surface diffusion and grain boundary sliding.

Although this thesis is felt to be a coherently organized unit, the reader should feel free to read any part of the thesis separately. Each chapter is sufficiently coherent and complete to allow its review in isolation by readers of different interests. Indeed alternative arrangements may offer the advantage of providing a focus on the mechanistic aspects, by first reading Chapters 5 and 6, or on the experimental aspects, by first reading Chapter 7. Hopefully these suggestions will encourage every interested reader to review this study.

CHAPTER 2

REVIEW OF CREEP AND FRACTURE IN HETEROGENEOUS ALLOYS

2.1. Introduction

The current state of understanding of creep and fracture in heterogeneous alloys is reviewed in this chapter. The survey is not intended to be comprehensive, as such expositions exist in the literature. Rather the survey offers a general background of the field which includes a broader perspective than what is required for our specific developments. Specific references of particular relevance to the analysis will be brought up later in appropriate chapters.

2.2. Response of Heterogeneous Materials

Two complementary and equally powerful approaches exist for computation of the response of heterogeneous materials having coarse microstructures. The first one is based on the bounding theorems which state in simple terms that for a given deformation: lower bounds are obtained from stress distributions that satisfy equilibrium and the constitutive laws; while upper bounds are obtained from displacement distributions that satisfy compatibility and the constitutive laws (1). Numerous straigtforward applications of these theorems can be found using the uniform strain upper bound and the uniform stress lower bound, for example, widely used the laws of mixture (2) and Taylor's polycrystal analysis (3). Efforts of extending these techniques to creep were due to Hill (4), Ashby et al. (5).

It should be noted that the power of bounding theorems is limited

by our ability to construct approximate yet adequate deformation fields that provide realistic bounds for the exact solution. Unfortunately, there is no systematic way for constructing these approximate fields in general and assumptions of uniform deformation usually lead to incorrect asymptotic limits. Several useful techniques have been widely employed. One is Hashin-Shtrikman's method (6) which amounts to, for most applications, constructing concentric spherical shells* made of the two constituent materials (their order is permuted between the upper bound configuration and its lower bound counterpart) for which solutions can be obtained and bounds thereby established (7). The recent model of yield loci for porous materials of Gurson was also of this kind (8). Another useful technique is the finite element analysis or the finite difference analysis for which typically a periodic array somewhat representative of the heterogeneous material permits numerical computations. Depending on the chosen configuration, the solution can be regarded as either a upper bound or a lower bound. Examples of such applications for linear constitutive properties are numerous in the field of composite materials, but non-linear computations are far fewer.

The second approach to the determination of the response of heterogeneous materials invokes the concept of an effective medium and is generally called the self-consistent method (9). The heterogeneous material in question is viewed as a whole as an effective medium in which an individual phase is embedded, that locally is further divided into a

---

* For that matter, they can be ellipsoidal shells as well.

number of "inclusions"* having the deformation resistance of an individual phase. For self-consistency, the overall deformation response of the effective medium is taken to depend on the average stress and strains of all inclusions so constructed.

As it applies to linearly elastic polycrystals and composites, the self consistent method has been developed by Hershey (10), Kröner (11), Budiansky (12) and Hill (13, 14). Hill's formulation is particularly useful for it incorporates incremental linearity to handle non-linear problems. This subject was further studied by Hutchinson for elastic-plastic behavior (15) and creep of polycrystalline (16) but single phase materials.

It is interesting to note that, as in the case of the previous approach based on bounding theorems, the power of the self consistent method is also limited by our ability to construct simple but adequate solutions, in this case for inclusion problems (17,18), on which estimation of overall response can be made. This situation is particularly acute in non-linear materials in which the inclusion problem depends on the local stresses in the surroundings of the inclusion.

An attempt to include this modification was made by Huang (17) for the plane deformation of a non-linear material with rigid circular fibers. This work, as well as that of Hutchinson's (16), had the advantage of dealing with essentially only one kind of constitutive relation in the form of a power-law for all constituent phases. For the more general

---

* The term "inclusion" is used here in a general sense to indicate included material of different deformation resistance, see also Chapter 3.

case, we present an approximate analysis in Chapter 3.

Finally, to make contact with the microscopic theory of work hardening in an alloy with dispersed particles which is most comprehensively developed by Brown and Stobbs (19, 30, 21), we remark that most self consistent models with regard to hardening, including the one we shall present, contributes to an alternative view of the so called "image stress" in the microscopic theory. In our development to be presented in Chapter 3, both the non-local interactions and the local relaxations of stress due to dislocations are omitted. Indeed, it is our aim to examine the validity of this omission there.

2.3. Grain Boundary Sliding and Internal Stresses

For most practical purposes, Zener's simple picture of grain boundaries at elevated temperature remains useful and convenient (22). Grain boundaries at elevated temperature were envisioned by many authors as a layer of viscous fluid a few atoms thick (23, 24). Since the shearing resistance of grain boundaries is much less than that of individual grains themselves, at elevated temperature, shear tractions across grain boundaries are usually fully relaxed at the steady state and their viscous deformation gives rise to internal friction during transients.

Modern theoretical views of grain boundary structures has substantially modified this simple picture. [For a review, See Gleiter (25).] Most importantly, it points out that significant variation in grain boundary properties exists near certain coincident misorientations of high angle grain boundaries. Although these properties and other microscopic considerations must be very important in understanding processes such as

creep cavitation, they do not yet lend themselves to computations in most applications involving polycrystals.

Zener (22) made the first computation of the loss of modulus that would result from grain boundaries which carry no shear stress, by applying the theory of elasticity to find the reduction in strain energy associated with deforming a sphere in the absence of any surface shear stresses, but otherwise not bothering to satisfy compatibility with the surrounding material. Its extension to nonlinear creep was first attempted by Hart using a phenomenological spring-dashpot approach (26). Although he correctly explained the response of polycrystals in terms of compatible deformation of grains and the grain boundaries, his prediction was not deterministic and relied on experimental fitting.

Crossman and Ashby (27), and more recently, Ghahremani (28), employed finite element analysis to obtain the solution for idealized polycrystals containing hexagons with sliding interfaces in material with a power-law type constitutive behavior. Their results showed qualitative agreement with Hart's model, namely that, at both high and low strain rates, the polycrystal flows according to the power-law creep of the grains, while the flow at low strain rates is somewhat accelerated by a grain boundary sliding. A transition occurs at a rate where the sliding boundaries and the deforming matrix contribute to the overall strain rate equally. Lau and Argon (29), in a different approach based on Hutchinson's method (30), obtained detailed expressions for stress concentrations at triple junctions of sliding boundaries in a power-law matrix.

It should be noted that although steady state was often assumed in

analyses and indeed achieved in these kinds of calculations this is only an operational steady state on a macroscopic scale. Transients of grain boundary sliding are known to occur even at steady state, presumably due to grain boundary migration at pinning points and other semi-abrupt microstructural alternations (31). Direct observations of this phenomenon have been reported by Chang and Grant in a set of classical experiments (31).

In considerations of tractions across a grain boundary, it is essential to take into account the effect of diffusional smoothing. Indeed in steady diffusional Nabarro-Herring flow, sliding of grain boundaries is an inevitable by-product of the mass transport across non-deforming grains or along grain boundary channels (32), and no additional strain is attributable to grain boundary sliding in this context. In the past, when continuum deformation of the matrix was taken into account, this was only for elastic response and was coupled with diffusional flow (32). In this instance grain boundary sliding provides additional compliance in the material. This amounts to the transient analysis that has been adequately described by Raj (33). When power-law creep occurs in the grain matrix additional deformations can occur at steady state and accompanying grain boundary sliding will accelerate the steady state creep rate. Such an analysis is given in Chapter 5.

2.4. Intergranular Cavitation in Creep

Perry (34) gave a most comprehensive review of cavitation in creep. Phenomenologically, this process refers to the observation that most metals which are normally ductile at their operating temperature fail by intergranular cavitation after a limited extension when held under a

relatively low constant stress for a prolonged period in the temperature range of 0.3 to 0.9 of their melting temperatures. Two specific types of intergranular damage have been reported based on light microscopy: namely wedge cracking at grain boundary triple junctions or w-type cavities, and rounded cavities along grain boundaries or r-type cavities (35).

The transition between these two kinds of damages, referred to as the Stroh-McLean transition (36), occurs over a very diffuse range of temperature and stress. In general, the round hole type cavitation seems to be favored at lower stresses and higher temperatures whereas wedge cracking at triple-points seems to be favored by higher stresses and lower temperatures.

Although the problem of wedge cracking has been treated by the theory of Zener (37) and Stroh (38) based on stress concentration produced in an elastic matrix in the presence of grain boundary sliding, the full process of intergranular creep cavitation has never been fully understood. The original proposal of Greenwood (39) that lattice vacancies agglomerated together under the action of the applied stress onto grain boundaries was later modified to allow heterogeneous nucleation (40, 41) and stress concentration due to grain boundary sliding (42, 43, 44).

The sites of heterogeneous nucleation and stress concentration were thought to be either grain boundary discontinuities such as jogs (42, 43, 44) or second-phase particles (40, 45). Despite very widespread and continued reference to this possibility, it has been shown, repeatedly (45, 46) that such jogs or ledges cannot exist nor can they act as

stress concentrators either due to diffusional smoothing or grain boundary migration. Indeed, second phase particles were often found to be necessary in most cases to reduce grain boundary migration and to cause cavitation (47, 48).

It is important to point out that in considering creep cavitation, caution has to be exercised to justify the mechanisms in light of very effective recovery processes at elevated temperature. In general steady state deformation is only adequately described by power law creep, while in the vicinity of grain boundaries, short range stress concentrations are subject to diffusional smoothing. Obviously many proposed models, unfortunately, did not satisfy these requirements. Indeed, in Chapter 5 we come to the conclusion that only transient grain boundary sliding offers significant stress concentrations at second phase particles that might serve as nucleation sites for cavities.

The argument for particles as nucleation sites was put forth first by Balluffi, Seigle and Resnick (40, 41), even though the experimentally observed connection goes back to Grant (47). The former concluded that homogeneous nucleation by vacancies required too high a vacancy supersaturation for the applied stress and would be possible only at sites such as grain boundary particles where energy balance is more favorable.

Direct association between cavities and particles which was first reported by Hyam (49) is not completely unambiguous however. In most cases, the particles in question were small ones since massive inclusions on grain boundaries often completely inhibited grain boundary sliding and reduced cavitation, especially in nickel based alloys (50). In general,

no one-to-one correspondence between cavities and inclusions were found and the association may be due to the cavities enveloping particles during growth.

One conjecture related to second phase particles as nucleation sites suggested that certain particles had either pre-existing (gas) pockets (51) formed in processing or non-wetting interfaces (52, 53). Although this is certainly possible occasionally, it is difficult to reconcile the fact that, in most fractures under conditions other than creep, holes do not nucleate intergranularly or even easily.

The nucleation of cavities has been found to continue with increasing strain in all studies. In most studies, cavities were found at a fairly early stage in creep (54, 55, 56, 57, 58). The rate of increase in their number usually slowed down at steady state creep but never vanished. Nevertheless there is no general agreement as to the exact functional form of these variations.

The distribution of cavitated grain boundaries with respect to the applied tensile stress has been found invariably to favor those boundaries that are nearly perpendicular to the stress axis, at least in monotonic loading (39). Some observations (59), which were more relevant to the growth mechanisms, however, showed the distribution tend to shift to the 45° boundaries at higher strain rate, indicative of a change of growth mechanisms.

2.5. Creep Cavitation and Cavity Growth

It is not surprising, considering the complexity and uncertainty of the problem, that much controversy still exists with regard to cavity

growth mechanisms. Two schools of thought are prominent, one in favor of diffusional growth and the other deformation controlled growth. For the former, an equilibrium shape of cavity consisting of spherical caps was usually assumed. However, cavities with crystallographic facets were reported in several studies, for example in magnesium by Presland and Hutchinson (60), in copper and iron by Taplin (61, 62). In contrast, cavities were sometimes found to be elongated or finger-like, with one specific orientation for all such cavities on one grain boundary (62). This latter observation, mostly due to Taplin also, was generally made at higher strain rates and grain boundary sliding was thought to be responsible for its occurrence.

Aside from this occasional, microscopic evidence, arguments for both mechanisms were centered around the stress dependence of growth processes, Hull and Rimmer (63), noting that cavitation depends on the difference between tensile and hydrostatic stress, proposed a diffusive growth theory which predicted that growth of the volume of the cavities is a linear function of the applied stress and of time. Several modification were made to this theory, with essentially the same prediction (64, 65). The preferential distribution of cavities with respect to the applied stress axis that was discussed previously with reference to nucleation was often cited as supportive evidence. Nevertheless, it is well known that the predicted stress dependence is not valid in almost all experiments.

Despite the deficiencies in its usual description as a precise model, grain boundary sliding has been frequently regarded as being responsible for cavity growth, either by providing a direct displacement or by causing enhanced diffusion (66, 67). Since grain boundary sliding is generally

proportional to overall creep, the general correlation between steady state strain rates and rupture time (68) is cited as evidence in support of this mechanism. In addition, it has been found by Gittins (69) that the largest cavities occurred on grain boundaries which slid the most, and by Kramer and Machlin (70, 67) and several others that the cavity area (or cavity length on a planar section) was linearly related to creep time or creep strain. Another observation first noted by Intrater and Machlin (71) was that the area of visible cavities was independent of temperature.

Recently, several new models for diffusive growth have been proposed. First, Ashby suggested that diffusive growth of crack-like cavities would be unstable under certain circumstances and would grow into a finger-like morphology (72). Some of the observations by Taplin and Wingrone (66, 66) certainly were due to this effect. The crack like morphology were further studied by Chuang and Rice focusing on the effect of surface diffusion in relation to grain boundary diffusion and the tip advancement velocity (73, 65). It is found, nevertheless, that the modification has only a minor effect on the stress dependence of the growth rate. In general, the solution predicted a growth rate proportional to $\sigma^{1-1.5}$ for cavities ranging from equilibrium shape to crack-like shape.

Another dimension was added when Beere and Speight (74) proposed that creep within the matrix could significantly alter the diffusional flow near a cavity and in general can reduce the diffusion distance. Edward and Ashby (75) elaborated on this model. Their result showed that, despite certain improvement, this model still could not resolve all the

differences between a diffusive growth model and the empirical deformation controlled growth. These points will be taken up again in Chapter 6.

CHAPTER 3

STEADY STATE POWER-LAW CREEP IN HETEROGENEOUS ALLOYS WITH COARSE MICROSTRUCTURES

3.1. Introduction

Creep resistant engineering alloys are almost always multi-phase substances, where individual phases have different creep behavior. In such alloys, a question that often arises is: if individual phases have different creep constitutive relations, what is the creep constitutive relation of the composite alloy?

It is observed that in power-law creep, pure metals and solid solution alloys usually have stress exponents of the creep rate in the range of 3 to 6, in comparison to about 7 or higher in engineering alloys which are often multiphase. In plastic deformation at low temperature, the stress exponent of the strain rate is commonly in the vicinity of 50. In view of this observation, it is interesting to explore whether the higher values of stress exponents in creep for multiphase alloys are merely a consequence of the mechanical restraint exerted on the matrix deformation by the reinforcing particles, derivable from the theory of particle-reinforced composites.

The deformation of such composites is necessarily non-linear and inhomogeneous. The non-linearity stems from the local stress strain-rate relation, while the inhomogeneity of deformation is a direct result of the heterogeneous nature of the material. When the heterogeneities are on a large enough scale in comparison with the scale of the inherently non-uniform deformation of crystal plasticity or creep involving dislocations, the mutual mechanical interactions between phases will be weak

and the deformations may be treated by continuum mechanics. Although the phase scale where this division occurs is never clearly definable (76), the deformations around particles in excess of several microns in size can usually be treated by continuum mechanics. This will be the approach taken in this chapter, recognizing that the results will not apply to composites with very fine particles or to alloys with fine precipitates where such particles cause qualitatively different, very strong interactions with the surrounding matrix.

The exact solution of the general problem of composite moduli is quite complicated even in linear elasticity where, however, when only the overall constitutive relations of the composite are of interest, it is often possible to make predictions on the basis of bounding theorems (6, 16, 77, 78, 79). Although this approach is fruitful in application to estimation of elastic properties of composites where moduli of the constituent phases are not very different, such bounds are very far apart whenever the moduli of any constituent phase go to extremes. Examples are composites containing rigid inclusions or voids, and composites with two power-law hardening materials. In these instances, the self-consistent method offers a much more accurate approach. This method of Hershey (10) and Kröner (11) was originally proposed for aggregates of crystal grains. In that connection it has been elaborated and reformulated by Hill (13) to extend the theory to deal with incrementally linear behavior in non-linear problems. For composites, a very similar formulation has also been developed by Hill (14).

The self-consistent method for heterogeneous elastic media draws on the familiar solution of Eshelby (18) of the problem of a uniformly

stressed infinite continuum containing an ellipsoidal inhomogeneity (or inclusion)*. In applying this solution to the problem of the composite in which particulate phases are surrounded by a continuous one-phase matrix, each particulate phase is considered to be an isolated ellipsoidal inclusion. The properties and orientation of the particulate phase are assigned to the inclusion, while the surrounding of the inclusions is given the same macroscopic properties of the composite. Thus the stresses and the strains in all particulate phases can be calculated. This in turn leads to knowledge of the average stresses and the average strains in the matrix phase, between them the constitutive equations of the matrix phase need to be satisfied. Therefore a self-consistent scheme can be set up to solve the overall moduli of the composite.

Here we extend the self-consistent theory to deal with steady state creep in nonlinear composites. At each increment of stress, the above method is employed to determine the stress strain-rate relationship assuming incrementally linear behavior for all phases. Since operationally the problem involves monotonic loading we make use of the well-known analogy (80) between a creeping material having a stress strain-rate law $\sigma = \sigma(\dot{\varepsilon})$ and a strain hardening material having a similar stress strain law $\sigma = \sigma(\varepsilon)$, and consider our problem as if it were a boundary value problem in nonlinear elasticity of the deformation of a heterogeneous incompressibe medium. In the next section we restate the system of

---

*

Eshelby calls an inclusion a region that has undergone a shear transformation with or without a volume change, and an inhomogeneity a region that has merely different elastic properties. Here we will use the word inclusion in its engineering sense as an included region of different properties. Hence in the context of this paper the two terms will be synonymous and will be used interchangeably although the term inclusion will be generally preferred.

equations of the self-consistent theory and apply them in Section 3.3 to the solution of the problem posed in the outset of this chapter. Finally, the accuracy of the results together with their significance are discussed in Section IV and contrasted with results of other authors.

3.2. Self-Consistent Theory

3.2.1. Formulation

Consider a composite in which N ellipsoidal inclusions, which need not be of the same phase or crystallographic orientation, are embedded in a matrix. The subscript i will be used to denote the ith inclusion and the subscript o the matrix. Since the overall composite is on a very large scale homogeneous with apparent overall moduli, an increment of the overall strain rate $d\underset{\sim}{\varepsilon}^*$ can be imposed which is taken to be equal to the increment of average strain rate over the composite and is related to the increment of the stress $d\underset{\sim}{\sigma}$ by

$$d\underset{\sim}{\sigma} = \underset{\sim}{L}\, d\underset{\sim}{\varepsilon} \quad \text{or} \quad d\underset{\sim}{\varepsilon} = \underset{\sim}{M}\, d\underset{\sim}{\sigma} \tag{3.1}$$

where $\underset{\sim}{L}$ is the composite creep modulus, and $\underset{\sim}{M}$, its inverse, is the composite creep compliance. We wish to calculate the current overall creep moduli $\underset{\sim}{L}$ incrementally in terms of current individual moduli. To do this, we treat the typical inclusion as an ellipsoid with uniform current moduli $\underset{\sim}{L}_i$ embedded in an infinite matrix with current moduli $\underset{\sim}{L}$ and solve the problem as if it were an incrementally linear problem.

---

*Here all lower case bold face symbols stand for second order tensors while capital bold face symbols stand for fourth order tensors that relate second order tensors to each other. The choice of symbols is the same as that of other authors in this field, e.g. Hutchinson (16).

Under this approximation, Eshlby's solution provides

$$d\underset{\sim}{\varepsilon}_i = \underset{\sim}{A}_i \, d\underset{\sim}{\varepsilon} \quad \text{and} \quad d\underset{\sim}{\sigma}_i = \underset{\sim}{B}_i \, d\underset{\sim}{\sigma} \tag{3.2}$$

where $d\underset{\sim}{\varepsilon}_i$ is the increment of strain rate in the ith inclusion which is uniform by virtue of ellipsoidal geometry and $\underset{\sim}{A}_i$ and $\underset{\sim}{B}_i$ are fourth order strain rate and stress concentration tensors respectively. These concentration tensors are functions of the aspect ratio of the elipsoid, of $\underset{\sim}{L}$ or $\underset{\sim}{M}$, and of $\underset{\sim}{L}_i$ or $\underset{\sim}{M}_i$, which are the moduli and compliances of the inclusions given by

$$d\underset{\sim}{\sigma}_i = \underset{\sim}{L}_i \, d\underset{\sim}{\varepsilon}_i \quad \text{and} \quad d\underset{\sim}{\varepsilon}_i = \underset{\sim}{M}_i \, d\underset{\sim}{\sigma}_i \tag{3.3}$$

We can formally <u>define</u> "average concentration factors" $\underset{\sim}{A}_o$ and $\underset{\sim}{B}_o$ in the matrix similarly as

$$d\underset{\sim}{\varepsilon}_o = \underset{\sim}{A}_o \, d\underset{\sim}{\varepsilon} \, , \quad \text{and} \quad d\underset{\sim}{\sigma}_o = \underset{\sim}{B}_o \, d\underset{\sim}{\sigma} \tag{3.4}$$

where $d\underset{\sim}{\varepsilon}_o$ and $d\underset{\sim}{\sigma}_o$ are respectively the average strain rate and stress tensors in the matrix. The self-consistency condition now provides the necessary equation to solve for $\underset{\sim}{A}_o$ and $\underset{\sim}{B}_o$, namely

$$\sum_{i=1}^{N} c_i \underset{\sim}{A}_i + c_o \underset{\sim}{A}_o = \underset{\sim}{I}, \qquad \sum_{i=1}^{N} c_i \underset{\sim}{B}_i + c_o \underset{\sim}{B}_o = \underset{\sim}{I} \tag{3.5}$$

where $\underset{\sim}{I}$ is the unit tensor and c's are volume fractions of the inclusions and the matrix. Finally, the constitutive equations of the matrix are assumed to be satisfied, i.e.

$$d\underset{\sim}{\sigma}_o = \underset{\sim}{L}_o \, d\underset{\sim}{\varepsilon}_o \quad \text{or} \quad d\underset{\sim}{\varepsilon}_o = \underset{\sim}{M}_o \, d\underset{\sim}{\sigma}_o \tag{3.6}$$

Elimination of $\underset{\sim}{A}_o$ and $\underset{\sim}{B}_o$ in Equations (3.4), (3.5) and (3.6) yields the following two identical equations which allow only one set of connection tensors $\underset{\sim}{L}$, $\underset{\sim}{M}$ to assure self-consistency

$$(\underset{\sim}{I} - \sum_{i=1}^{N} c_i \underset{\sim}{B}_i) \underset{\sim}{L} = \underset{\sim}{L}_o (\underset{\sim}{I} - \sum_{i=1}^{N} c_i \underset{\sim}{A}_i) \qquad (3.6a)$$

and

$$(\underset{\sim}{I} - \sum_{i=1}^{N} c_i \underset{\sim}{A}_i) \underset{\sim}{M} = \underset{\sim}{M}_o (\underset{\sim}{I} - \sum_{i=1}^{N} c_i \underset{\sim}{B}_i) \qquad (3.6b)$$

Either Equation (3.6a) or (3.6b) can be used to solve $\underset{\sim}{L}$ or $\underset{\sim}{M}$ in terms of c_i, c_o, $\underset{\sim}{L}_i$ and $\underset{\sim}{L}_o$. In doing so, it is assumed that $\underset{\sim}{\varepsilon}_i$ and $\underset{\sim}{\varepsilon}_o$, and consequently $\underset{\sim}{L}_i$, $\underset{\sim}{L}_o$ are known at the overall strain rate $\underset{\sim}{\varepsilon}$. It remains to complete the system of equations by integrating the incremental Equations (3.1 - 4) and (3.6a, b) from the state of zero stress to the overall stress along a path of proportional loading. The system of equations can thus be integrated to a total form.

3.2.2. Features of the Formulation

The application of the self-consistent theory to problems in linear elasticity, and attendant limitations of the approach have been extensively discussed recently (81. 82). We note particularly that interactions between inclusions do not enter the calculation explicitly in this theory, beyond the consideration that assigns to the surroundings of the typical inclusion the average properties of the composite. Furthermore, the use of Eshelby's solution in each linear increment in the non-linear problem necessitates that the moduli of the surroundings of the inclusion be "smoothed out" and taken to depend on the average strain rate of the matrix and not on the local strain rates in the matrix (16). In the non-linear problems considered here where the modulus decreases with

increasing strain, such smoothing artifically inhibits strain concentrations in problems involving large local strain variations. As a consequence (see also Section 3.4) our self-consistent theory for non-linear material overestimates the deformation resistance and the creep modulu. A further approximation of considerably lesser consequence will be introduced in Section 3.3.1. in connection with the incremental constitutive behavior of the material. These features will be discussed further in the following sections in relation to the specific examples which we will consider.

3.3. Application to Creep of two Phase Composites with Non-sliding Interfaces

3.3.1. Spherically Shaped Phase Domains

In this section we develop specific results for the creep moduli of composites by the self-consistent approach. To simplify the calculation at no important sacrifice in results, we choose a spherical particle model for each phase.

We shall consider a two-phase composite comprised of two isotropic incompressible phases creeping according to a power law, with constitutive equations

$$\varepsilon_1 = F_1 \sigma_1^{m_1} , \quad \varepsilon_2 = F_2 \sigma_2^{m_2} \tag{3.7}$$

where $m_1 > m_2 > 1$ and the ε, σ are equivalent strain rates and equivalent stresses, respectively. In simple tension, we shall approximate the incremental relationship of deformation by a simple isotropic relation

$$d\varepsilon_{ij} = ds_{ij}/2\mu \tag{3.8}$$

where s_{ij} is the stress deviator given as

$$s_{ij} = \sigma_{ij} - \frac{1}{3}\sigma_{kk}\delta_{ij} \tag{3.9}$$

and the creep shear moduli can be shown to be

$$\mu_1 = \frac{1}{3}\frac{d\sigma_1}{d\varepsilon_1}, \quad \mu_2 = \frac{1}{3}\frac{d\sigma_2}{d\varepsilon_2}, \quad \mu = \frac{1}{3}\frac{d\sigma}{d\varepsilon} \tag{3.10}$$

We should emphasize here that the correct incremental relationship of deformation in conventional flow theory based on the attainment of a critical deviatoric stress (or equivalent stress) is only transversely isotropic in simple tension. Namely, for a given form of associated flow rule

$$\varepsilon_{ij} = \frac{3}{2} f(\sigma)\, s_{ij} \tag{3.11}$$

the incremental relationship is

$$d\varepsilon_{ij} = \frac{3}{2} f(\sigma)\, ds_{ij} + \left(\frac{3}{2}\right)^2 \frac{f'(\sigma)}{\sigma}\, s_{ij}\, s_{kl}\, ds_{kl} \tag{3.12}$$

In simple tension, it can be easily seen from symmetry that

$$s_{11} = s_{22} = -\frac{1}{2} s_{33}, \quad s_{12} = s_{23} = s_{31} = 0 \tag{3.13}$$

are satisfied in all phases, and the equivalent stress for these average stresses is $\frac{3}{2} s_{33}$. Therefore, the incremental strain rate-stress relation is transversely isotropic as follows:

$$d\varepsilon_{11} = (\alpha+\beta)\left(d\sigma_{11} - \frac{d\sigma_{22}+d\sigma_{33}}{2}\right) - \frac{3}{4}\beta\,(d\sigma_{11}-d\sigma_{22}) \tag{3.14a}$$

$$d\varepsilon_{22} = (\alpha+\beta)\left(d\sigma_{22} - \frac{d\sigma_{33}+d\sigma_{11}}{2}\right) - \frac{3}{4}\beta\,(d\sigma_{22}-d\sigma_{11}) \tag{3.14b}$$

$$d\varepsilon_{33} = (\alpha+\beta)\left(d\sigma_{33} - \frac{d\sigma_{11}+d\sigma_{22}}{2}\right) \tag{3.14c}$$

$$d\varepsilon_{ij} = \frac{3}{2}\alpha d\sigma_{ij} = \frac{3}{2}(\alpha+\beta)\, d\sigma_{ij} - \frac{3}{2}\beta d\sigma_{ij}, \quad (i \neq j) \tag{3.14d}$$

where $\alpha = f(\sigma)$, $\beta = \sigma f'(\sigma)$. (3.14e, f)

In the above relations, the first term in each equation is exactly the isotropic compliance of Equation (3.10). Generally speaking, in shear, the isotropic compliance is larger than the transverse isotropic compliance while these compliances are roughly equal in tension if we observe that $d\sigma_{11} = d\sigma_{22}$ in simple tension. The consequence of this additional approximation which overestimates the shear compliance of the matrix is the overestimation of the composite compliance. Its significance will be discussed further in Section 3.4.1.

Equations (3.2), (3.4) and (3.5) reduced to the following form with the aid of Eshelby's solution

$$\frac{d\sigma_1}{d\sigma} = \frac{5\mu_1}{3\mu+2\mu_1}, \qquad \frac{d\sigma_2}{d\sigma} = \frac{5\mu_2}{3\mu+2\mu_2} \tag{3.15a, b}$$

$$c_1 \frac{5\mu_1}{3\mu+2\mu_1} + c_2 \frac{5\mu_2}{3\mu+2\mu_2} = 1 \tag{3.16}$$

We note that it is sufficient to consider equivalent stresses here due to symmetry and incompressibility. The hydrostatic stress, $-\frac{\sigma}{3}$, is uniform in the composite, therefore it needs no separate consideration. From Equation (3.16), μ can be solved in terms of μ_1 and μ_2, which are in turn only functions of σ_1 and σ_2. Hence, Equations (3.15a, b) are the system of simultaneous differential equations for σ_1 and σ_2. Equations (3.15a and 15b) can be integrated with the initial condition of

$$\sigma_1 = \sigma_2 = 0 \quad \text{at } \sigma = 0 \tag{3.17}$$

From this, Equation (3.8) can be integrated to give the strains.

In general, numerical calculation is needed to obtain solutions. However, asymptotic solutions at $\sigma \gtrsim 0$ and at $\sigma \gtrsim \infty$ are readily obtainable. At these limits, the right hand sides of Equations (3.15a) and (3.15b) reduce to constants which can be determined from Equations (3.7) and (3.16). After integration, we obtain σ_1, σ_2 and ε. These asymptotic solutions are:

At $\sigma \gtrsim 0$

$$\varepsilon = F_2 \, (1 - 2.5 \, c_1)^{m_2} \, c_2 \left(\frac{\sigma}{c_2}\right)^{m_2}, \quad (c_1 < 0.4)$$

$$\varepsilon = F_1 \left(\frac{1}{1 - \frac{5}{3} c_2}\right) \, c_1 \left(\frac{\sigma}{c_1}\right)^{m_1}, \quad (c_1 > 0.4) \qquad (3.18a)$$

and at $\sigma \gtrsim \infty$

$$\varepsilon = F_1 \, (1 - 2.5 \, c_2)^{m_1} \, c_1 \left(\frac{\sigma}{c_1}\right)^{m_1}, \quad (c_2 < 0.4)$$

$$\varepsilon = F_2 \left(\frac{1}{1 - \frac{5}{3} c_1}\right) \, c_2 \left(\frac{\sigma}{c_2}\right)^{m_2}, \quad (c_2 > 0.4) \qquad (3.18b)$$

The main conclusion derived from these calculations and asymptotic forms is that the creep in the majority phase governs the overall creep behavior at both the small and the large stress limits only to be amplified or attenuated by the presence of the minority phase to a much less important extent. Between these two extreme limits, the overall creep goes through a transition which can be best quantified by defining an effective creep exponent for the overall creep of the composite,

$$m_{eff} \equiv \frac{d\ell n \varepsilon}{d\ell n \sigma} \qquad (3.19)$$

A specific example of the variation of m_{eff} with stress for $m_1 = 10$ and $m_2 = 5$ is shown in Fig. 3.1, where without loss of generality, we have normalized stresses and strain rates with σ_c and ε_c where the two stress strain-rate curves cross over. The figure shows that the presence of very small amounts of a second phase has little effect. The variation of m_{eff} with stress becomes larger when the amount of second phase becomes 0.1 or larger. The figure shows also that for small volume fractions of an entrapped reinforcing phase ($c_1 < 0.3$) the maximum change in effective exponent, Δm_{eff}, is almost linear in the concentration. Only in a composite comprised of roughly equal amounts by volume of phase does the behavior with larger m dominate at small stresses. In comparison with these results, the upper bound computation based on constant strain in all phases predicts that phase 1 dominates composite behavior at low stress and phase 2 at high stress regardless of volume fraction (see Appendix).

Clearly, the behavior in Fig. 3.1, showing a transition of response in the two limits from that of phase 2 to that of phase 1 (i.e., from smaller m to larger m) with increasing volume fraction of phase 1 takes place roughly when a phase inversion occurs. For a quasi-spherical phase shape this occurs when the two volume fractions are about equal.

The maximum in m_{eff} occurs when $\mu_1 \approx \mu_2$. A crude estimate can be made by simply letting $\sigma_1 = \sigma_2 = \sigma$. The actual maximum will shift more towards the lower stress side (for the case when $c_1 < 0.4$), due to the stress concentration in phase 1. In general, the peak in m_{eff} remains narrow as long as c_1 is small and $m_1 - m_2$ is large. This narrowness is due to the decrease in disparity in the stress distribution between the two phases as a result of the decreased total load-bearing capacity

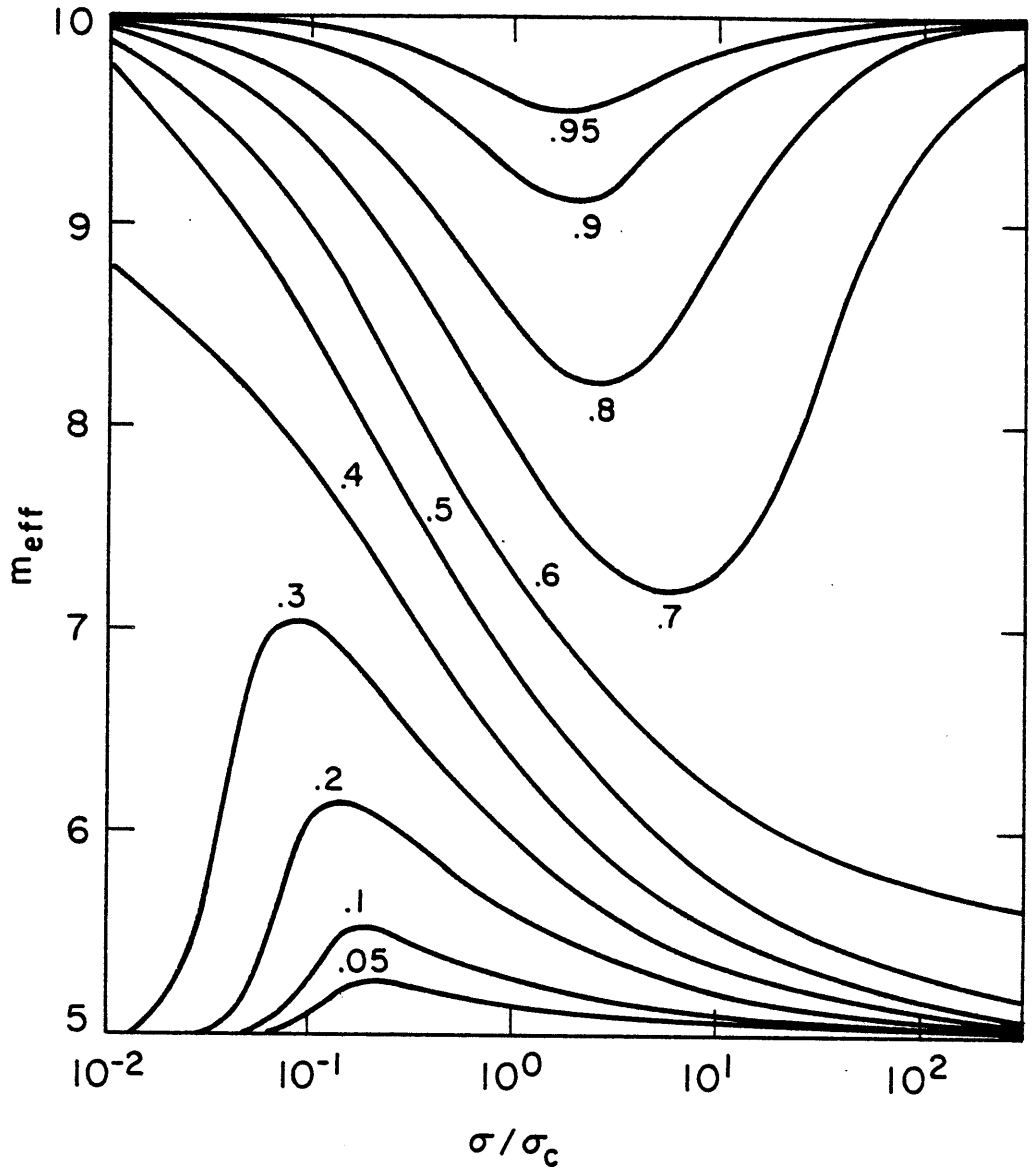

Fig. 3.1 - The effective stress exponent m_{eff} v.s. normalized stress σ/σ_c for $m_1 = 10$ and $m_2 = 5$. The volume fractions c_1 are shown by the number on each curve.

of phase 1 when c_1 is small, and to the greater variation of creep resistance of phase 1 with stress when m_1 is large. Both indicate that for conditions in ordinary engineering alloys where only a moderate amount of strengthening phase of very high creep resistance is present, the peak in m_{eff} should be rather narrow and the overall behavior very much like that of the matrix phase. For instance, a two-fold variation of stress will cause a 10^{10} variation of μ_1/μ_2, for $m_1 - m_2 = 35$. From the above discussion it is clear that the major strengthening effect of hard particles in creep of real alloys is of a very different origin than the reinforcement of the matrix by the deformation constraint of the less deformable phase, where both act as continua, and where all non-local effects requiring consideration of specific interactions of dislocations with obstacles are ignored.

To illustrate the effects of F_1, F_2, m_1, m_2, c_1 and c_2 on the behavior of the composite, we introduce a somewhat modified notation and write Equation (3.7) in the following form:

$$\frac{\varepsilon_1}{\varepsilon_{standard}} = \left(\frac{\sigma_1}{\sigma_{y1}}\right)^{m_1}, \quad \frac{\varepsilon_2}{\varepsilon_{standard}} = \left(\frac{\sigma_2}{\sigma_{y2}}\right)^{m_2} \tag{3.7a}$$

where σ_{y1}, and σ_{y2} are creep flow stresses of material 1 and 2 respectively, when tested at the standard strain rate $\dot{\varepsilon}_{standard}$. We further choose to use reduced strain rates ε_{ri} and reduced stresses σ_{ri} in units of $\dot{\varepsilon}_{standard}$ and σ_{y2} (customarily $\sigma_{y1} > \sigma_{y2}$ if $m_1 > m_2$) for which Equation (3.7a) now becomes

$$\varepsilon_{r1} = F_{r1}\,\sigma_{r1}^{m_1}, \quad \varepsilon_{r2} = \sigma_{r2}^{m_2} \tag{3.7b}$$

where F_{r1} is given by (for $F_{r2} = 1$, by definition)

$$F_{r1} = \left(\frac{\sigma_{y2}}{\sigma_{y1}}\right)^{m_1} \tag{3.7c}$$

Using the reduced creep constitutive Equations (3.7b) and (3.7c), we have computed the behavior of the composite for six possible limiting combinations of behavior of constituent phases having creep exponents $m_1 = 20$ and $m_2 = 5$ and consisting of:

a) $(\sigma_{y2}/\sigma_{y1}) = 1$, $c_1 = 0.1$

b) $(\sigma_{y2}/\sigma_{y1}) = 0.3$, $c_1 = 0.1$

c) $(\sigma_{y2}/\sigma_{y1}) = 0.1$, $c_1 = 0.1$

d) $(\sigma_{y2}/\sigma_{y1}) = 1$, $c_1 = 0.3$

e) $(\sigma_{y2}/\sigma_{y1}) = 0.3$, $c_1 = 0.3$

f) $(\sigma_{y2}/\sigma_{y1}) = 0.1$, $c_1 = 0.3$

The computed behavior is shown in Fig. 3.2 and furnishes a direct demonstration of the transitional behavior summarized in Fig. 3.1 and the rather modest effect that appreciable volume fractions of a reinforcing phase (with a higher creep resistance) produces on the overall behavior of the composite by continuum considerations alone. In Fig. 3.2, the diagonal line with unit slope represents $\sigma_r^5 = \varepsilon_r$, which is the behavior of phase 2 in pure form. We note from Fig. 2 that at a constant volume fraction of the hard phase, the transition--where this hard phase begins to deform appreciably--shifts to larger stresses as the ratio of σ_{y2}/σ_{y1} decreases.

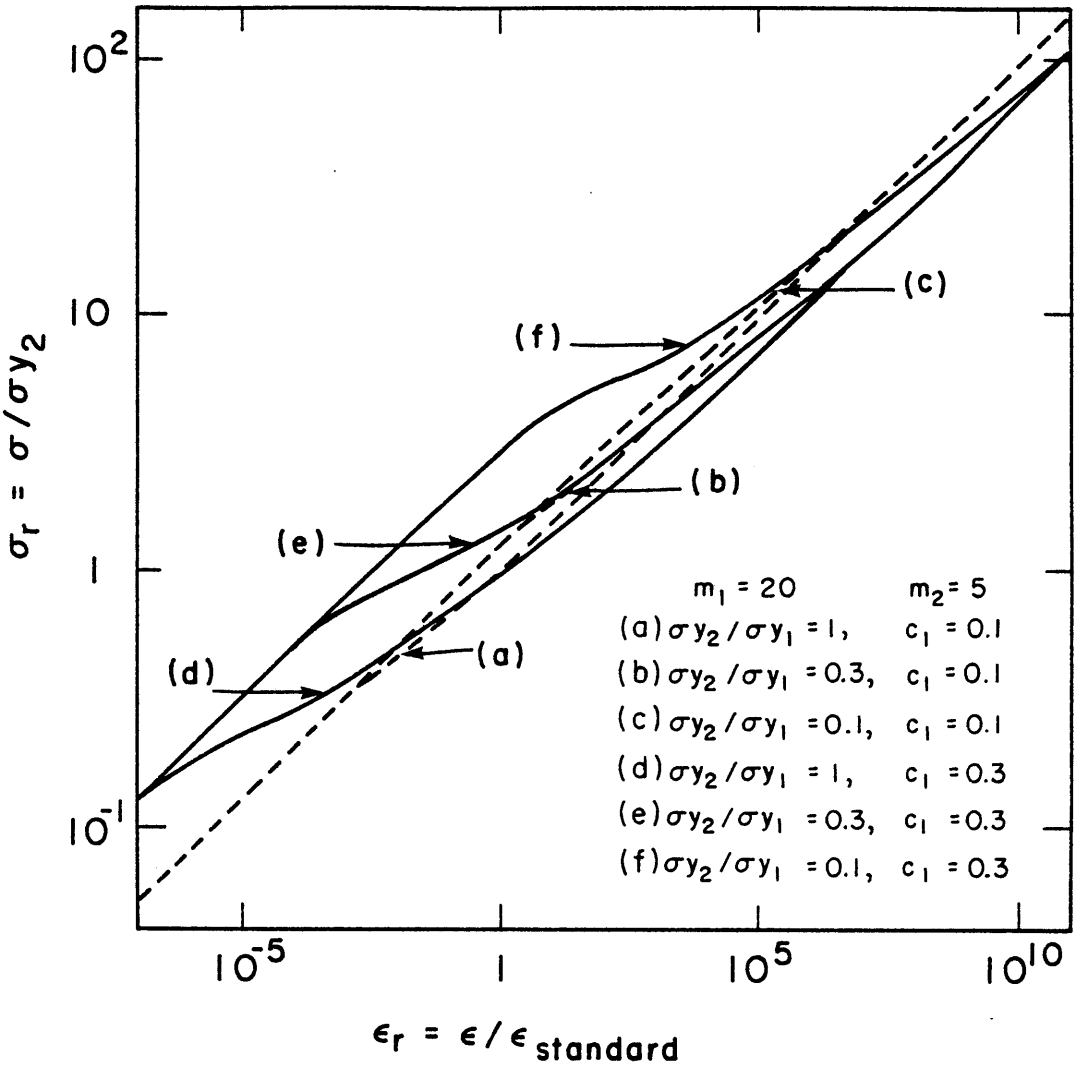

Figure 3.2 - Six different types of creep constitutive behavior of a two phase heterogeneous alloy with three different ratios of flow stress of individual phases at a reference strain rate and at two levels of volume fraction of the less deformable phase.

3.3.2. Circular Cylindrical Phase Domains in Plane Strain

A corresponding analysis for circular cylindrical phase domains in plane strain can also be developed readily and is often useful in discussing idealized models. Following a procedure similar to that for spherically shaped domains we obtain the following asymptotic equations for plane strain:

at $\underset{\sim}{\sigma} \approx 0$

$$\varepsilon = F_2(1 - 2\,c_1)^{m_2}\, c_2 \left(\frac{\sigma}{c_2}\right)^{m_2}, \quad (c_1 < 0.5) \tag{3.20a}$$

$$\varepsilon = F_1 \left(\frac{1}{1 - 2\,c_2}\right) c_1 \left(\frac{\sigma}{c_1}\right)^{m_1}, \quad (c_1 > 0.5)$$

at $\underset{\sim}{\sigma} \approx \infty$

$$\varepsilon = F_1(1 - 2\,c_2)^{m_1}\, c_1 \left(\frac{\sigma}{c_1}\right)^{m_1}, \quad (c_2 < 0.5) \tag{3.20b}$$

$$\varepsilon = F_2 \left(\frac{1}{1 - 2\,c_1}\right) c_2 \left(\frac{\sigma}{c_2}\right)^{m_2}, \quad (c_2 > 0.5)$$

3.4. Discussion

3.4.1. Approximations in the Method

The effects of the approximations in the use of the self-consistent method for non-linear materials by incremental steps within which the constituents are considered linear throughout in the computation of the steady state creep resistance need to be assessed. During each increment of stress the "smoothing out" of the changes in the local moduli in the surroundings of inclusions in non-linear materials of the type we have considered overestimates the creep moduli of the composite for two reasons.

First, any redistribution of stresses in an initially uniformly stressed homogeneous matrix will always produce an increase in the local average strains. Second, in a heterogeneous alloy, a stiffer inclusion in a non-linear matrix is stressed less than in a linear matrix, while a more compliant inclusion in a non-linear matrix is strained more than a linear matrix. This always results in a larger compliance in the composite for each incremental step which is not accounted for by the incrementally linear idealization of the constituents. As a consequence, the application of the self-consistent theory to non-linear problems by the technique discussed in this paper gives overestimates of the deformation resistance.

The neglect of the anisotropic portion of the incremental constitutive relation (3.12) results in the underestimation of the creep shear moduli of the matrix around the inclusion. This, in turn, gives an underestimation of the overall moduli, i.e., the creep resistances. Although this underestimation partially compensates the overestimation resulting from the "modulus smoothing" in each linear step of the self-consistent theory, detailed calculation has indicated that the effect of this additional approximation due to neglect of anisotropy is usually less than the effect of modulus smoothing. Consequently, our application of the self-consistent theory generally overestimates the creep deformation resistance.

3.4.2. Comparison with Other Investigators

It is interesting to compare our results with those of others for nonlinear material behavior. Huang (17) has carried out a calculation for the plane deformation of a power-law material with rigid transverse

circular fibers using a self-consistent model in which Eshelby's solutions for concentration factors are replaced by their nonlinear equivalents obtained by a finite difference method (16). His result is, in our notation

$$\varepsilon = F_2 (1 - c_1 R)^{m_2} c_2 \left(\frac{\sigma}{c_2}\right)^{m_2} \tag{3.21}$$

where R, the stress concentration factor in rigid circular fibers, varies between 2 and 1.4 as m varies between 1 to 7. This is to be compared with the first Equation of (3.20a). From this comparison it is clear that due to the long range response in the non-linearly hardening matrix, a lower stress concentration is built up in the less strain rate sensitive phase. It is to be noted that although Huang obtained improved estimates of stress concentrations in the inclusion, he still used the self-consistent model in which the matrix was taken to be homogeneous, as in our case, without further consideration being given to the effect of stress variations in the matrix. (See Section 3.4.1.) We therefore expect that even Huang's result is an overestimation of deformation resistance of the nonlinear material. Fortunately, this was shown to be not serious; Huang's result agrees well with that of the finite element calculation of Needleman (84).

In summary, the spherical-grain self-consistent model does provide a qualitatively different and more realistic description of the overall deformation of nonlinear composites than that of bound analysis. The major uncertainty of this method is more likely in the use of Eshelby's solution to estimate concentration factors in inclusions for a nonlinear system than in the picture of replacing the surrounding of the inclusion

by a homogeneous matrix for which only the averages of stresses and strain rates are specified. Hence, self-consistent approaches give qualitatively correct results which, however, lead to overestimates of the deformation resistance.

3.4.3. Non-local Interactions

When the dramatic increases in creep resistance, frequently achievable in practice by the addition of relatively small volume fractions of very small (~ 100 Å) hard particles into ductile matrices, are compared with the computed creep resistance of Fig. 2, the latter are found to be very modest in comparison. This is an illustration of the non-local nature of interaction of the very small particles with dislocations and subgrain boundaries in a scale range where continuum concepts are inapplicable (76). Our computations in this paper are meant to apply only over volume elements and inclusion sizes very large in comparison with mean dislocation spacings, and subgrain sizes.

Furthermore, inspection of Fig. 1 shows that the effect of small volume fractions of non-creeping but only plastically deformable (large m) reinforcing phases in a creeping matrix (small m) is only a very modest rise in m_{eff} of the alloy. Thus the relatively large creep exponents in composite alloys, in relation to the exponents of the pure matrix, is also not attributable to the deformation restraint of the less readily deformable reinforcing phase. Although the exact cause of this so-called power-law breakdown behavior is still not clear, according to the best current understanding, the reinforcing particles appear to effectively inhibit normal recovery processes and retain a non-characteristically fine subgrain structure in the creeping alloy.

APPENDIX TO CHAPTER 3

UPPER AND LOWER BOUNDS FOR CREEPING NON-LINEAR COMPOSITES

Unlike in the case of linear composites, the various accurate bounding approaches such as that of Hashin and Strickman (6) are no longer applicable for non-linear materials (16). The only available bounding technique which continues to apply is the uniform strain-rate upper bound and the uniform stress lower bound. The application of these bounds for a two-phase composite described by Equations (3.7 - 3.10) gives the upper bound

$$\sigma = c_1 \left(\frac{\dot{\varepsilon}}{F_1}\right)^{\frac{1}{m_1}} + c_2 \left(\frac{\dot{\varepsilon}}{F_2}\right)^{\frac{1}{m_2}} \qquad (A.1)$$

and the lower bound

$$\dot{\varepsilon} = c_1 F_1 \sigma^{m_1} + c_2 F_2 \sigma^{m_2} \qquad (A.2)$$

The derivations are straightforward and are omitted. In the two limits of small stress and large stress these bounds reduce to the following forms: the upper bound

$$\dot{\varepsilon} = F_1 \left(\frac{\sigma}{c_1}\right)^{m_1}, \quad (\sigma \to 0) \qquad (A.3)$$

$$\dot{\varepsilon} = F_2 \left(\frac{\sigma}{c_2}\right)^{m_2}, \quad (\sigma \to \infty)$$

and the lower bound

$$\dot{\varepsilon} = c_2 F_2 \sigma^{m_2}, \quad (\sigma \to 0) \qquad (A.5)$$

$$\varepsilon = c_1 F_1 \sigma^{m_1}, \quad (\sigma \to \infty) \tag{A.6}$$

Clearly the results of the self-consistent theory given by Equations (3.18) and (3.20) lie within these bounds. Furthermore, we note that the upper and lower bounds do not lead to the same stress exponents at the high and low stress limits as is physically required and as the self-consistent theory gives.

CHAPTER 4

GRAIN BOUNDARY AND INTERFACE BOUNDARY SLIDING IN POWER LAW CREEP

4.1. Introduction

In the preceding chapter we studied the overall steady state creep behavior of heterogeneous alloys with coarse microstructure. The approach was to treat each individual phase as a continuum inclusion, and to follow the formulation of the self-consistent theory of Hill (9). Specific results were derived for heterogeneous alloys with coarse, equiaxed phases which were modeled as spherical inclusions.

The problem studied in this paper is the other extreme in composites in which inclusions are of very large aspect ratio and small volume fraction. This model is applied to obtain an analytic estimate of the effective creep equation of a polycrystal creeping according to a power law with viscous grain boundaries or incoherent phase boundaries which are modelled as randomly distributed thin circular disks of a critical volume concentration N that gives a high probability of contiguous grain boundary surfaces through the material. A similar problem in elasticity has been studied by Wu (85) and more recently by Budiansky and O'Connell (86).

4.2. Theory*

4.2.1. Grain Boundary Sliding Among Equiaxed Quasi-spherical Grains

For simplicity, the grain boundary taken as an ellipsoidal disk of some large aspect ratio a/b where a and b are lengths of the semi-major

---

* The notation used in this chapter is the same as that in Chapter 3. In particular $\dot{\varepsilon}$ stands for strain rate.

axes respectively, is modelled in the corresponding elastic analog as an anisotropic medium with a low shear modulus in the plane of the disk, but with a modulus equal to that of the matrix along the principal directions of the disk as shown in Fig. 4.1. More precisely, for the creeping material, we assume the following:

1. that both the matrix and the disks are incompressible,

2. that the matrix (grain interior) follows a power-law in creep, i.e., $\varepsilon_g = F_g \sigma_g^m$,

3. that the disk (grain boundary) is isotropic in its plane with a Newtonian viscous shear response, i.e., $d\varepsilon_{13} = d\varepsilon_{31} = 1/2\mu_{gb}\, d\sigma_{13} = 1/2\mu_{gb}\, d\sigma_{31}$,

4. that the disk is indistinguishable from the matrix in its normal stress response along the principal axes of the disk.

As in Chapter 3, we shall approximate the incremental deformation of the matrix to be isotropic. As discussed there, we expect that this approximation will result in an overestimate of the overall creep moduli for $m > 1$. In addition, as discussed in Chapter 3 and as will become clearer later on in this paper, we recognize that this necessary simplification leads to useful results for only small m (say $m \lesssim 5$). For larger m, the interaction between neighboring boundaries becomes overwhelming, making the self-consistent method in the sense that it is used here an increasingly poor model.

Consider a typical disk at an inclination θ with the tensile direction $\hat{3}$ (Fig. 4.1). The coplanar sets of axes 1, 3, $\hat{1}$, $\hat{3}$ are chosen to lie in the vertical plane. The incremental loading at distant boun-

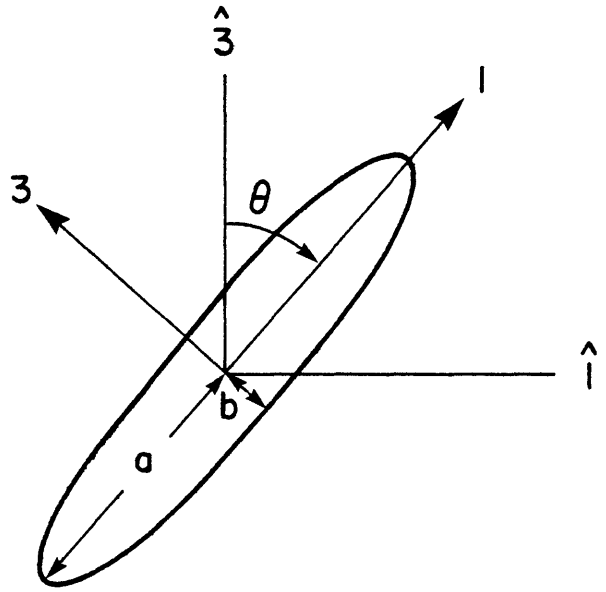

Fig. 4.1 - Circular disk shaped grain boundary with its principal axis 1, inclined at an angle θ with respect to the tensile axis $\hat{3}$. The coplanar sets of axes 1,3 and $\hat{1},\hat{3}$ lie in the vertical plane as shown while the other major axis 2 coincides with $\hat{2}$ and is perpendicular to the plane of the paper.

daries is

$$d\varepsilon_{33}^{\wedge\wedge} = -2d\varepsilon_{11}^{\wedge\wedge} = -2d\varepsilon_{22}^{\wedge\wedge} = d\,\varepsilon \tag{4.1a}$$

$$d\sigma_{33}^{\wedge\wedge} = d\,\sigma \tag{4.1b}$$

with all other components not present. It is possible to decompose this deformation into planar shear components in the disc coordinates, e.g.

$$d\varepsilon_{13} = d\varepsilon_{31} = \frac{3}{2}\cos\theta\,\sin\theta\,d\,\varepsilon \tag{4.2a}$$

and

$$d\sigma_{13} = d\sigma_{31} = \cos\theta\,\sin\theta\,d\,\sigma \tag{4.2b}$$

Since the disk is indistinguishable from the matrix for all other deformation modes, the composite simply creeps uniformly except for planar shear modes.*

Treating the matrix as a homogeneous continuum with effective shear viscosity μ and still obeying Eshelby's solution, we have in his own notation (18)

$$S_{1313} = \frac{1}{2}\left(1 - \frac{3}{4}\frac{b}{a} + 0\left(\frac{b}{a}\right)^2\right) \tag{4.3a}$$

$$d\varepsilon_{13_{gb}} = \frac{\mu}{\mu_{gb} + \frac{3\pi}{4}\left(\frac{b}{a}\right)(\mu-\mu_{gb})}\, d\varepsilon_{13} = d\varepsilon_{31_{gb}} \tag{4.3b}$$

$$d\sigma_{13_{gb}} = \frac{\mu_{gb}}{\mu_{gb} + \frac{3\pi}{4}\left(\frac{b}{a}\right)(\mu-\mu_{gb})}\, d\sigma_{13} = d\sigma_{31_{gb}} \tag{4.3c}$$

where S_{1313} is the only component in Eshelby's transformation matrix which is needed to obtain the final forms given in Equations (4.3b) and (4.3c). The total contribution of sliding which comes from the planar

---

*The use of superposition is permissible during each linear increment within the spirit of the approximation used in deriving Equations (4.2) and of Chapter 3.

shear mode is obtained by averaging Equation (4.3b) over all solid angles of inclination of the disk shaped inclusions. Thus the self-consistent equations are, for tensile components $d\varepsilon_{33}^{\wedge\wedge}$ and $d\sigma_{33}^{\wedge\wedge}$,

$$d\varepsilon_{33}^{\wedge\wedge} = \nu_{gb}\,\frac{2}{5}\,\frac{\mu}{\mu_{gb} + \frac{3\pi}{4}\left(\frac{b}{a}\right)(\mu-\mu_{gb})}\,d\varepsilon + (1-\nu_{gb})\,d\varepsilon_g = d\varepsilon \qquad (4.4a)$$

$$d\sigma_{33}^{\wedge\wedge} = \nu_{gb}\,\frac{4}{15}\,\frac{\mu_{gb}}{\mu_{gb} + \frac{3\pi}{4}\left(\frac{b}{a}\right)(\mu-\mu_{gb})}\,d\sigma + (1-\nu_{gb})\,d\sigma_g = d\sigma \qquad (4.4b)$$

where the first term in each equation is the contribution of boundary sliding in which $\nu_{gb} = N\,\frac{4\pi}{3}\,a^2 b$ (N is the volume concentration of the number of grain boundary disks), and the second term is that of the grains.

The value of the volume concentration N of the number of grain boundaries can be determined in reference to an analogous system in which a volume concentration N of number of shear cracks in an elastic matrix has reduced the overall tensile modulus to zero. Such critically cracked solids were investigated by Budiansky and O'Connell (86) and have very similar properties to polycrystals with continuously connected sliding grain boundaries. Very much like the elastic solid with contiguous planar cracked regions the polycrystal with sliding boundaries would have come apart were it not for the fact that grain boundaries are not allowed to deform freely normal to their plane. A similar calculation using our self-consistent method leads to $N\,a^3 = 9/16$ (i.e., $\nu_{gb} \approx \frac{3\pi}{4}\left(\frac{b}{a}\right)$ for $b/a \ll 1$), which is the same result obtained by Budiansky and O'Connell (86) using a much more complicated method in the energy description of the self-consistent theory.

Thus, from Equations (4.4a, b) in the limit of $a/b \gg 1$ and $\mu_{gb}/\mu \ll 1$,

$$\mu = \frac{1}{3}\frac{d\sigma}{d\varepsilon} = \frac{1}{3}\frac{1 - \frac{2}{5}\left(\frac{\mu}{\mu^*_{gb} + \mu}\right)}{F_g\, m\sigma^{m-1}}$$

where μ^*_{gb}, the "grain equivalent" boundary viscosity is defined by $\mu^*_{gb} = \frac{4}{3\pi}\left(\frac{a}{b}\right)\mu_{gb}$, and the previously assumed form $\varepsilon_g = F_g\sigma_g^m$ is utilized. In Equation (4.5), μ can be solved explicitly as a function of σ. Therefore, the constitutive equation for the polycrystal is directly integrable. As before, we can obtain asymptotic solutions

$$\varepsilon = \frac{5}{3}F_g\sigma^m \quad \text{at} \quad \sigma \lesssim 0 \tag{4.6a}$$

$$\varepsilon = F_g\sigma^m \quad \text{at} \quad \sigma \gtrsim \infty \tag{4.6b}$$

which lead to the following limiting behavior

$$d\varepsilon_g = \frac{3}{5}d\varepsilon \quad \text{at } \sigma \lesssim 0 \text{ and } d\varepsilon_g = d\varepsilon \text{ at } \sigma \gtrsim \infty \tag{4.7}$$

while $d\sigma_g = d\sigma$ always holds.

This confirms results obtained by several others workers (26, 27), that both in the low strain rate limit when boundaries are fully relaxed and the stress distribution is inhomogeneous, and in the high strain rate limit when boundaries are unrelaxed and the stress is homogeneous, the strain rate of the polycrystal has the same stress dependence as the grain matrix. At an intermediate but narrow range of the stress when the grain boundaries slide effectively with equal ease as the grains deform (i.e., $\mu_g \gtrsim \mu^*_{gb}$), the strain rate sensitivity of the flow stress goes

through a minimum (Crossman and Ashby (27) (*), Hart (26)).

4.2.2. Grain Boundary Sliding Among Rod Shaped Grains in Plane Strain

It is very instructive to perform a similar calculation for grain boundary sliding in creep in a plain strain geometry which has been assumed most often in the past. Equations (4.3a-c) are now:

$$S_{1313} = \frac{1}{2}\left(1 - \frac{2b}{a} + 0\left(\frac{b}{a}\right)^2\right) \tag{4.8a}$$

$$d\varepsilon_{13_{gb}} = \frac{\mu}{\mu_{gb} + \frac{2b}{a}(\mu - \mu_{gb})}\, d\varepsilon_{13} = d\varepsilon_{31_{gb}} \tag{4.8b}$$

$$d\sigma_{13_{gb}} = \frac{\mu_{gb}}{\mu_{gb} + \frac{2b}{a}(\mu - \mu_{gb})}\, d\sigma_{13} = d\sigma_{31_{gb}} \tag{4.8c}$$

where

$$d\varepsilon = d\varepsilon_{\hat{3}\hat{3}} = -\, d\varepsilon_{\hat{1}\hat{1}}, \quad d\sigma = d\sigma_{\hat{3}\hat{3}} = 2d\sigma_{\hat{2}\hat{2}}$$

$$d\varepsilon_{31} = d\varepsilon_{13} = 2\cos\theta \sin\theta\, d\varepsilon, \quad d\sigma_{13} = \cos\theta \sin\theta\, d\sigma$$

Similarly it is found that $N a^2 = \frac{1}{\pi}$ (or $\nu_{gb} = \frac{b}{a}$). Therefore,

$$\mu = \frac{1}{4}\frac{d\sigma}{d\varepsilon} = \frac{1}{4}\,\frac{1 - \frac{1}{4}\left(\frac{\mu}{\mu_{gb}^{*} + \mu}\right)}{F_g m \sigma^{m-1}} \tag{4.9}$$

where $\mu_{gb}^{*} = \frac{a}{2b}\mu_{gb}$ and $\varepsilon_g = F_g \sigma_g^{m}$ is taken. This leads to corresponding asymptotic solutions

$$\varepsilon = \frac{4}{3} F_g\, \sigma^m, \quad (\sigma \lesssim 0) \tag{4.10a}$$

$$\varepsilon = F_g \sigma^m, \quad (\sigma \gtrsim \infty),$$

(*) In comparing our result with that of Crossman and Ashby, we note some errors in their paper. In their Fig. 8, the apparent A at $\sigma \gtrsim \infty$ does not agree with the value of A given in the figure caption; the same error occurs in their Fig. 9, in their strain rate scale.

and

$$d\varepsilon_g = \frac{3}{4}\, d\varepsilon \quad \text{at } \sigma = 0 \text{ and } d\varepsilon_g = d\varepsilon \text{ at } \sigma \gtrsim \infty \tag{4.11}$$

As a check on our results, we find that Equation (4.6a) or (4.5) agrees with the result of Budiansky and O'Connell for the effective moduli for an elastic body permeated at the same volume concentration by flat cracks that are filled with an ideal fluid, as might be expected. Furthermore, the coefficient in (4.6a) is larger than that in (4.10a), as expected from the observation that there is more grain boundary area among equiaxed quasi-spherical grains than among rod shaped grains.

4.2.3. An Instructive Computation

Figure 4.2 demonstrates graphically the effect of grain boundary sliding in a specific case of plane strain configuration subjected to a shear stress τ. Using a familiar creep constitutive equation

$$\gamma = A\,(\frac{\tau}{G})^m \quad ; \quad (A = \sqrt{3}\, F_g\, (\sqrt{3}G)^m) \tag{4.12}$$

between shear strain rate γ and shear stress τ (G is shear modulus), Equation (4.9) was integrated for the typical values of $A = 10^{18}\ \text{sec}^{-1}$, $(G/\mu_{gb}^*) = 10\ \text{sec}^{-1}$, and $m = 5$ to give the resulting behavior shown in Fig. 2. The transition between relaxed and unrelaxed behavior occurs at $\log \tau/G = -4.20$ where the effective exponent m_{eff} reaches its minimum value of 4.77. At the transition, the contribution of the sliding grain boundaries to the overall strain rate equals that of the deforming grains, i.e., where $\mu_{gb}^* = \mu$. This occurs at the intersection of the power law creep curve of the grain $\gamma = A(\tau/G)^5$ and the "grain equivalent" flow law of the grain boundary $\gamma_{gb}^* = \gamma_{gb}\, \nu_{gb} = \tau/2\, \mu_{gb}^*$. The position of the

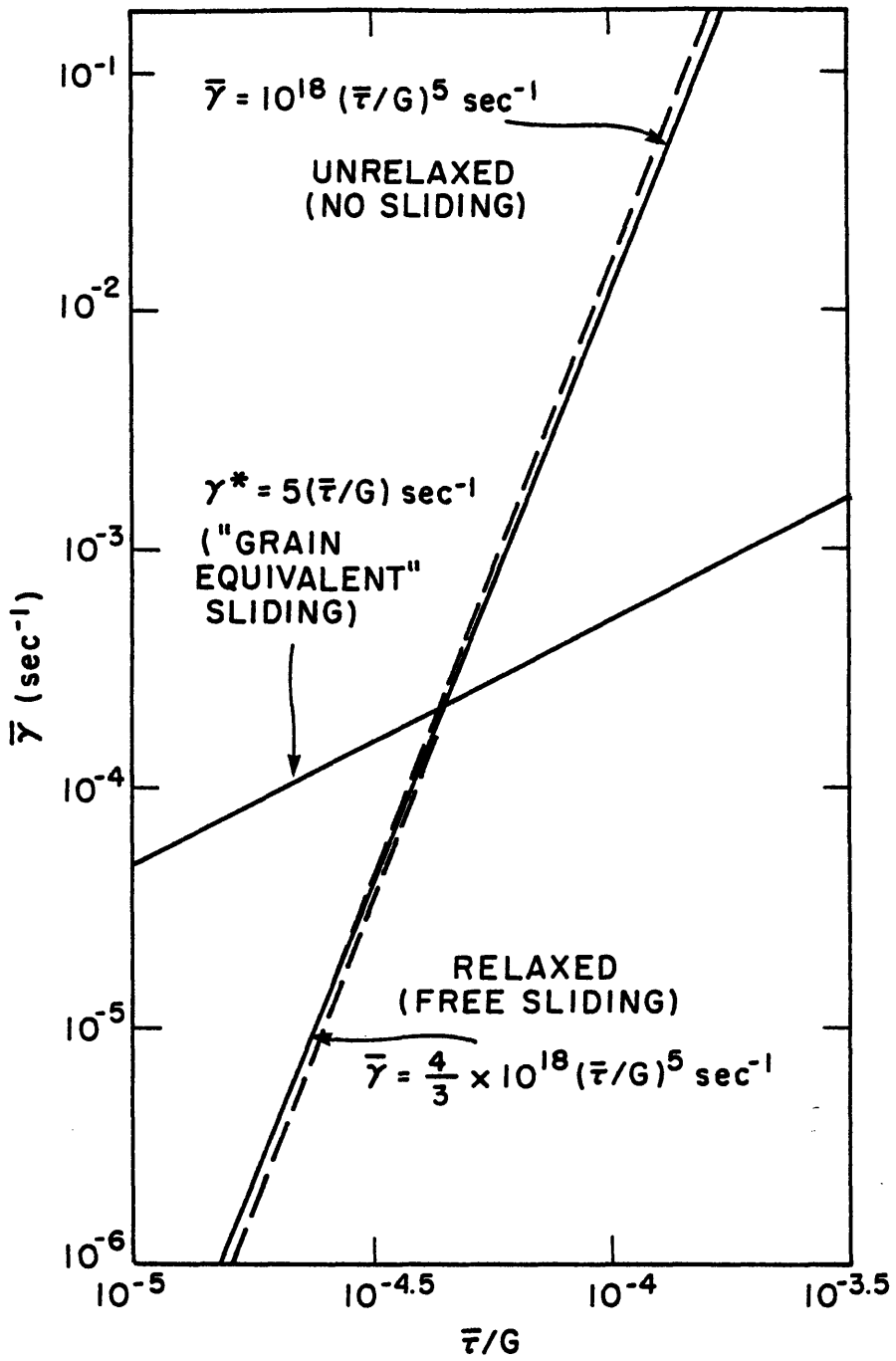

Fig. 4.2 - Transition between relaxed to unrelaxed behavior of grain boundaries with increasing stress in plane strain geometry, in a polycrystal in which the grain matrix creeps according to a law $\gamma = A(\tau/G)^5$, obtained from Equation (4.9), and where $G/\mu^*_{gb} = 10$ sec^{-1}, $A = 10^{18}$ sec^{-1} were chosen. The transition of behavior, where a minimum in $m_{eff} = 4.77$ is achieved, occurs at log $\tau/G = -4.20$.

transition, of course, depends on grain size through the chosen volume fraction $\nu_{gb} = b/a$ where b can be taken as the boundary half thickness and a as the grain radius. Apart from the small change in slope of the asymptotic lines for relaxed and unrelaxed behavior, that results from our choice of m = 5, and the specific strain rate amplification factor 4/3 for the fully relaxed case, (Eqn. 4.11), our results are almost indistinguishable from the results of Crossman and Ashby (27).

4.3. Interface Boundary Sliding in Heterogeneous Alloys

In many alloys, interface boundaries are largely incoherent and permit sliding of the phases relative to each other. Similarly, grain boundary sliding can occur in heterogeneous alloys with or without sliding interfaces. Thus, there would be many applications where the results of Chapter 3 on heterogeneities without sliding interfaces and the results of this paper on sliding boundaries and interfaces need to be combined. Clearly, dealing with the combined problem all at once would be beyond the capacity of the self-consistent theory as used here. Instead, we propose to deal with such problems in two stages: first the effect of nonsliding but non-linearly deformable heterogeneities are considered by the method of Chapter 3 to compute the constitutive behavior of the composite for full traction transmitting boundaries followed by the additional effect of sliding of contiguous viscous boundaries and interfaces plus the sliding of the interfaces of the entirely entrapped heterogeneities by the method presented here. In taking account of the effect of sliding of the entrapped non-contiguous interfaces of heterogeneities it is, of course, necessary to use the actual volume fraction of these

sliding entrapped interfaces.

4.4. Discussion

4.4.1. Grain Boundaries as Ellipsoidal Disks

Consider an idealized hexagonal two-dimensional geometry of grains as shown in Fig. 4.3. The volume concentration of number of grain boundaries in this equiaxed hexagonal array is $N = \frac{1}{2\sqrt{3}} \frac{1}{a^2}$, or $\nu_{gb} = \frac{\pi}{2\sqrt{3}} \frac{b}{a}$ if grain boundaries are taken to be ellipses of aspect ratio a/b. This volume concentration is 91% of that used in the self-consistent theory of randomly distributed ellipsoidal disks. It is to be recognized that any slightly distorted non-equiaxed hexagonal array has a higher N and ν_{gb}, as has any other periodic array in two dimensions. This observation indicates that the volume fraction of grain boundaries considered in our self-consistent theory is quite realistic.

The choice of ellipsoidal geometry and the feature of uniform strain rate inside the ellipsoid (Equations 4.8a-c) results in the rate of shear displacement across the boundary that satisfies the following equation at low strain rates

$$\left(\frac{\Delta u}{2a\varepsilon \sin 2\theta}\right)^2 + \frac{u^2}{a^2} = 1 \qquad (4.13)$$

where Δu is the rate of shear displacement and u is the coordinate along the major axis. This result is identical to the estimate of Brunner and Grant (87) and is supported by their experiments.

In spite of the successful features of the ellipsoidal disks as grain boundaries in the context of the incrementally linear self-consistent

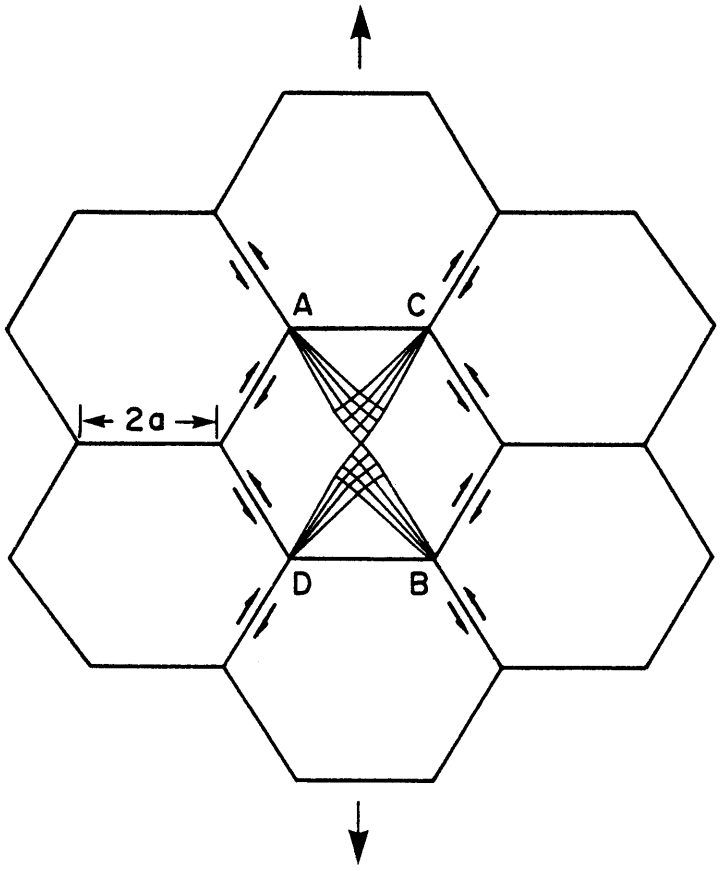

Fig. 4.3 - Idealized two-dimensional hexagonal array of grains. Grain boundary sliding and the slip lines obtained by plasticity theory are shown in one grain.

method, there are a number of severe shortcomings. First, grain boundaries form triple point junctions where the local stress concentrations differ in character from that obtainable at the tip of an ellipsoidal disk as has been shown by Lau and Argon (29). More importantly, however, grain boundaries on opposite sides of a grain interact, and the shear strain concentration between them accentuates steadily with increasing stress exponent m as has been shown by the finite element model computations of Crossman and Ashby (27). In the limit as $m \to \infty$, the shear strain across grains concentrate into a set of slip lines connecting up the sliding boundaries on opposite sides of the grains. Such strong interactions of grain boundaries which is a direct result of the nonlinearity in the creep law fall entirely outside the scope of the self-consistent method as utilized here. Thus, the developments of Section 4.4 which ignore such interactions lead to quantitatively useful results only for small m. As m becomes large, the results deteriorate both qualitatively and quantitatively.

4.4.2. Strain Rate Enhancement and Stress Enhancement

Our result for strain rate enhancement due to sliding grain boundaries can be taken to be correct for $m = 1$.

Instead of considering a strain rate enhancement, we may find it more satisfactory to refer to a stress enhancement factor f that produces the same increase in strain rate in a reference material without any boundaries (27). This factor f is defined as

$$\varepsilon = F_g (f\sigma)^m \quad (\text{for } \sigma \to 0) \tag{4.14}$$

Thus, at m = 1, our result shows f to be 4/3 in plane strain.

For the other limiting case of $m \to \infty$, as we have discussed above, the grain interiors become an ideally plastic, non-hardening medium, where now f can be inferred from slip line theory, where the sliding boundaries will be linked by a series of slip line fields inside the grains (88). Considering the hexagonal grains of Fig. 4.3 as an ordered limiting arrangement of grain boundaries and approximating the curved slip lines of Fig. 4.3 by straight ones, one can obtain readily a stress enhancement factor of 1.3 in tension along the vertical or horizontal axes of the figure. If the tension axes depart from these symmetry axes, higher stress enhancement factors result with a maximum of 1.5 corresponding to simple shear along the symmetry axes. An orientation average can be readily obtained and gives 1.43. This slip line model is an upper bound with the actual deformation resistance of the material being lower, and the actual stress enhancement factor being somewhat higher. It is now interesting to note that the stress enhancement factor ranges only from 1.33 to 1.43 as m goes from 1 to ∞. The stress enhancement factor for behavior in between these limits is expected to lie on a monotonically rising function. The behavior for a three-dimensional arrangement of quasi-spherical grains is expected to give somewhat higher results on the basis that f = 5/3 for m = 1 (Eqn. 4.7). These conclusions are qualitatively in agreement with those of Crossman and Ashby (27).

In view of this discussion we expect that the effect of sliding boundaries is an almost constant shift, independent of m, along the

stress axis of the log σ, log ε behavior between totally relaxed and totally unrelaxed boundaries, as given in Fig. 2 for the specific case of $m = 5$.

4.4.3. Comparison with Results of Earlier Investigators

Zener (22) calculated the effect of grain boundary sliding in elasticity by modeling the grains as isolated spheres free of surface shear traction. By superposing three appropriate sets of displacement functions, Zener was able to satisfy this boundary condition. However, by considering the grains in isolation, Zener failed to take the important compatibility restraints of the rest of the matrix into account. Also the spherical grains of Zener have a lower surface to volume ratio than any realistic three-dimensional grain configuration which is space filling and equiaxed. A much better result in our opinion is that of Budiansky and O'Connell (86) for elastic solids containing contiguously connected shear cracks filled with an ideal fluid. As we have mentioned before, their result and ours are essentially the same.

Recently, Speight (89) considered a model of cubic grains free of surface shear traction, and having a uniform strain rate throughout the polycrystal to satisfy compatibility. Hence, the assumed uniform shear strain rate along the cubic surfaces must be supplied by different normal tractions across grain boundaries for different grain orientations. As a consequence, the stresses in the cubes, though uniform within each cube, are different from cube to cube and an overall strain rate enhancement (or stress enhancement) is expected. However, Speight (in calculating the overall stresses as a function of overall strain rates)

incorrectly assumed that $\langle\sigma^2\rangle$ averaged over all grains is equal to σ^2. If instead, $\langle\sigma_{33}^{\wedge\wedge}\rangle$ averaged over all cubical grains in a cross section is equated to σ, as would be required by equilibrium. Speight's problem would become a special case of an upper bound model, since $\varepsilon_{33}^{\wedge\wedge}$ is assumed to be uniform and equal to ε. In that case, the stress enhancement factor f would vary from 2.11 to 1.55 as m varies from 1 to ∞ for cubical grains in three dimensions; and from 2 to 1.57 for square rod-shaped grains in plane strain. These values are significantly higher than Speight's original evaluation and also those of both Crossman and Ashby and ours. The reason for this probably lies in the overestimate of density of grain boundaries in a cubical grain model. For example, in two dimension, N is 1/2 a^2 for a square array of grains, which is significantly higher than the N used in the self-consistent theory.

4.4.4. Diffusional Creep

In diffusional creep, mass transport is always perpendicular to the grain boundaries and grain boundary sliding is an essential and integral part that becomes necessary to preserve continuity of the polycrystalline aggregate (90). Hence the diffusional creep rate is proportional to the reciprocal square of the grain size for volume diffusion (Nabarro-Herring) and to the reciprocal cube of the grain size for surface diffusion (Coble). The boundary sliding that is required for compatibility and continuity does not produce any enhancement of the overall strain rate in comparison with the strain rate in a collection of isolated grains of the same size, which now must be taken as the reference material. Without boundary sliding (or decohesion)

material transport cannot occur between different faces of a grain and diffusional flow would have to occur only between the external surfaces of a body and such internal surfaces that are perpendicular to principal stress directions across which no sliding is necessary. This would, of course, result in very substantial increases (by several orders of magnitude) of the length of the diffusion path and would therefore reduce the rate of diffusional creep drastically (by the reciprocal square or cube of the increase of the path length).

CHAPTER 5

INTERFACIAL STRESS IN VISCOUS MATERIALS WITH DIFFUSIONAL FLOW AND ITS APPLICATION TO NUCLEATION OF CAVITIES

5.1. Introduction

At elevated temperature where grains deform primarily by power law creep, grain boundaries also undergo significant material transport by diffusional flow leading to overall deformation. Generally deformation under this condition can be labeled as "visco-diffusive". This combination is of particular relevance in consideration of processes occurring along grain boundaries such as grain boundary sliding and intergranular cavitation. In this chapter we examine the nature of visco-diffusive deformation and apply the result to obtain interfacial stresses which could lead to cavitation.

When a load or a displacement rate is applied to a visco-diffusive body the initial response is elastic deformation. Subsequently dislocation creep and grain boundary diffusion will over the time smooth the stress field which, at steady state eventually, becomes independent of the initial elasticity. Examination of the steady state field frequently finds, near each geometric asperity or similar perturbation along the grain boundary, a diffusion zone within which diffusion dominates. It is thus convenient, as a first step, to determine the time and the length over which the elastic stress relaxes and diffusion dominates. On this basis, furthermore, the problem of a visco-diffusive deformation can be divided into separate regimes within each of which there is only one dominant process. Meanwhile the global analysis is completed after coupling these regimes together.

The rigorous implementation of this procedure is made difficult by the nonlinear nature of power law creep. Often the problem is only tractable by numerical analysis which deals with the coupling interactively. Much insight can be gained, however, if we first obtain the nondimensional form of the governing equations in which the scaling is built in. Further insight is also possible when strategically chosen simple samples are solved. The most useful application of this method, confirmed fully by exact numerical analysis, is presented in the next chapter on cavity growth.

The method is applied here to obtain interfacial stresses at an inclusion on a grain boundary. With a review of classical nucleation theory of cavitation, it is concluded that such stresses, enhanced in their magnitude by stress concentration due to grain boundary sliding, are responsible for cavitation at elevated temperature in engineering alloys.

The symbols used in this chapter have been listed at the beginning of this thesis.

5.2. Nondimensional form of Governing Equations in Visco-Diffusive Materials

We consider the following field equations, in the symbolic notation of Luré (91) in which $\nabla \times A \times \overleftarrow{\nabla}$ stands for $e_{npj}\, e_{\ell mi}\, \partial^2 A_{jm}/\partial x_p\, \partial x_i$,

$$\nabla \cdot \sigma = 0 \quad \text{(Equilibrium equation)} \tag{5.1}$$

and

$$\nabla \times \dot{\varepsilon} \times \overleftarrow{\nabla} = 0 \quad \text{(Compatibility equation)} \tag{5.2}$$

In a visco-diffusive material the constitutive law can be written, again in a symbolic notation, as

$$\dot{\varepsilon} = L^{-1}\dot{\sigma} + A\sigma^m - \frac{D_b \delta_b \Omega}{kT} \frac{\partial^2 \sigma_n}{\partial s^2} \Delta (r - s_o - s) \tag{5.3}$$

The first and the second term of RHS are the familiar elastic and power-law creep components. The strain rates due to the grain boundary diffusion, which adds additional normal displacements at grain boundaries, is introduced in the last term using the abbreviated form of tensor Δ which in the full form contains delta-functions, $\delta(r - s_o - s)$, in its components. The origin of boundary coordinate, s, is displaced by s_o from the origin of the space coordinate. Equation (5.2) now appears as

$$\nabla \times (L^{-1}\dot{\sigma} + A\sigma^m - \frac{D_b \delta_b \Omega}{kT} \frac{\partial^2 \sigma_n}{\partial s^2} \Delta(r - s_o - s)) \times \overleftarrow{\nabla} = 0 \tag{5.4}$$

The nondimensional form of governing Equations (5.1), (5.2) are, after substitution of σ by $\sigma_o \tilde{\sigma}$, t by $t_o \tilde{t}$, and r, s by $\ell_o \tilde{r}$, $\ell_o \tilde{s}$, with corresponding substitution of $(\cdot)$ by $1/t_o (^*)$ and ∇ by $1/\ell_o \tilde{\nabla}$,

$$\tilde{\nabla} \cdot \tilde{\sigma} = 0 \tag{5.5}$$

and

$$\tilde{\nabla} \times \{(L^{-1} \frac{\sigma_o}{t_o}) \overset{*}{\tilde{\sigma}} + (A\sigma_o^m) \tilde{\sigma}^m - (\frac{D_b \delta_b \Omega \sigma_o}{kT\ell_o^3}) \frac{\partial^2 \tilde{\sigma}}{\partial \tilde{s}^2} \Delta (\tilde{r} - \tilde{s}_o - \tilde{s})\} \times \overleftarrow{\tilde{\nabla}} = 0 \tag{5.6}$$

Under a stress boundary condition with some representative measure of the nominal stress σ_N, we can let $\sigma_o = \sigma_N$ and choose t_o and ℓ_o according to (recognizing that L, the stiffness matrix, is of the same order as E, the Young's modulus)

$$\frac{\sigma_o}{Et_o} = A\,\sigma_o^{\,m} = \frac{D_b \delta_b \Omega}{kT}\,\frac{\sigma_o}{\ell_o^{\,3}} \tag{5.7}$$

This operation, or any other similar ones which obey Equation (5.7) in the choice of scaling dimensions, renders all the coefficients in Equation (5.6) the same value which can be factored out. Thus, we are left with a compatibility equation in the simple form

$$\tilde{\nabla} \times \{\overset{*}{\tilde{\sigma}} + \tilde{\sigma}^m - \frac{\partial^2 \tilde{\sigma}}{\partial \tilde{s}^2}\,\Delta\,(\tilde{r}-\tilde{s}_o-\tilde{s})\} \times \overset{\leftarrow}{\tilde{\nabla}} = 0 \tag{5.8}$$

in which all the material constants are left out. The normalization procedure is now completed.

It is now obvious that the solution of the stress field in a visco-diffusive material obtained for a given stress boundary condition with the representative measure of the nominal stress σ_N, can be used to deduce the solution of the stress field in the same material for the same boundary condition but with a different representative measure of the nominal stress $\alpha\sigma_N$, simply by following the above normalization procedure and let $\sigma_o = \alpha\sigma_N$ while choosing t_o and ℓ_o accordingly.

We conclude this section by rewriting Equation (5.7), by assigning $\sigma_o = \sigma_N$ and $\dot{\varepsilon}_{N,\,creep} = A\sigma_N^{\,m}$, in the following form

$$\ell_o = \left(\frac{D_b \delta_b \Omega}{kT}\,\frac{\sigma_N}{\dot{\varepsilon}_{N,creep}}\right)^{1/3} \tag{5.9}$$

and

$$t_o = \frac{\sigma_N}{E\dot{\varepsilon}_{N,\,creep}} \tag{5.10}$$

5.3. Stress Relaxation

5.3.1. Elastic stress

Stress relaxation in visco-diffusive materials can be best envisioned by inspection of Eqn. (5.8). For a given regime of space and time the magnitude of each term in the equation can often be estimated easily for useful inference. For example, during a fast transient the elastic response ($\overset{*}{\sigma}$) will dominate, it being smoothed out locally by diffusion ($\partial^2\tilde{\sigma}/\partial\tilde{s}^2\ \Delta(\tilde{r}-\tilde{r}_o-\tilde{s})$) and elsewhere by power-law creep ($\tilde{\sigma}^m$). The latter might take considerable time, depending on the rate of transient loading.

Quantitative evaluation becomes feasible if one of the three terms in Equation (5.8) is negligible. For relaxation of the elastic stress, the short range smoothing can be calculated considering only diffusion. The characteristic relaxation time of the simplified equation obtained by Raj (33) and Chuang et al. (65) using Fourier analysis, is

$$\tau_b = \frac{kT}{D_b\delta_b\Omega E}\left(\frac{\ell}{2\pi}\right)^3 \qquad (5.11)$$

where ℓ is the range of the elastic stress concentration. The effect of creep smoothing has also been studied recently analytically by Riedel (92) and numerically by Bassani (93) and Lau (88). Generally speaking, a creep zone associated with an elastic stress singularity will gradually expand, and a self similar solution can sometimes be found in the limit of "small scale yielding". The characteristic time for this kind of relaxation can be defined as the time taken for the creep zone to cover the entire space (or an entire grain in the triple point

problem).

We note, in passing, that the transient analysis for relaxation of elastic stresses by diffusive flow invariably yields a very short transient for submicron asperities above roughly 0.45 T_m (33). For this reason a grain boundary without significant asperities or any portion between major asperities can be regarded as relaxed and free of shear tractions. This view is in agreement with a large body of measurement of relaxation time using the internal friction technique at elevated temperature (25).

5.3.2. Creep field

Following a transient of loading or a perturbation (e.g., nucleation of a cavity), the steady state field of visco-diffusive deformation prevails. Hence the term $\overset{*}{\sigma}$ can be dropped in Equation (5.8) for a steady state solution. Consideration of this problem has received little attention and only recently. For cavity growth and crack growth problems, both approximate (74, 75) and more exact solutions (94) were developed. Also of relevance to the nucleation of cavities is the development of interfacial stress at an inclusion on a grain boundary. It might be possible that, given a grain boundary free of shear traction, the load transfer to the inclusions could result in considerable stress concentration even with diffusional smoothing at the steady state.

Choosing σ_o and ℓ_o as before, $\tilde{\sigma}$'s in Equation (5.8) are of the order of unity. Let $\tilde{s} = 0$ be the origin of a stress concentration, diffusion is important only within a distance $\tilde{s} < 1$, namely $s < \ell_o$.

Indeed if $\tilde{s} << 1$, the normal stress should exhibit a variation characteristic of that of a diffusion field, e.g., parabolic if the displacement rate is a constant. As for $\tilde{s} >> 1$, diffusion should hardly affect the distant field that is governed by power-law creep. In either case, Equation (5.8) reduces to one in which only the dominant process is responsible for the asymptotic solution, although the amplitude of the asymptotic solution could be affected by the coupling between the two modes of deformation as well as by the boundary conditions.

At this time, it is worthwhile to re-examine Equation (5.9) to explore its physical meaning. After rearrangement it becomes

$$\dot{\varepsilon}_N = \frac{D_b \delta_b \Omega}{kT} \frac{\sigma_N}{\ell_o^3} \tag{5.12}$$

(We dropped the subscript "creep" since elastic strain rate does not exist at steady state.) We recall that ℓ_o is the length of the diffusion zone. Equation (5.12) suggests further that the width of the zone should be of the same order as its length, and that the effective strain rate resulting from diffusion under the nominal stress σ_N be $\dot{\varepsilon}_N$ within the zone.*

The specific calculation in the next section and that for hole growth (Chapter 6) verify that Equation (5.12) furnishes an excellent correlation. This is further established by numerical calculation that demonstrates that a simple substitution of the diffusion zone radius into

---

* To emphasize the association of ℓ_o with diffusion in visco-diffusive deformation, ℓ_o as defined by Eqn. (5.9) shall be denoted as ℓ_D hereafter.

a rigid-grain model (i.e., only diffusion operating) yields ℓ_o in Equation (5.12). This is astonishing considering the complexity of the creep field surrounding the cavity in Needleman's numerical solution (94).

5.4. Linear Visco-Diffusive Deformation

5.4.1. General Solution

Equation (5.8) at steady state ($\overset{*}{\tilde{\sigma}} = 0$) for linear visco-diffusive material can be readily solved by the integral equation technique for which the influence functions are well known from the theory of elasticity. Let σ_v be the stress distribution in the absence of diffusion, then Eqn. (5.4) of diffusional smoothing becomes

$$\sigma = \sigma_v + \frac{D_b \delta_b \Omega \eta}{4\pi(1-\nu^2)\ kT} \int G(s,s') \frac{\partial^2 \sigma}{\partial s'^2} ds' \tag{5.13}$$

Here η is a viscosity defined by $\dot{\varepsilon} = \sigma/\eta$ and G is the influence function for the normal "misfit" stress at s exerted by a unit increment of "edge dislocation" rate at s'. Choosing $\sigma_v = \sigma_{vK} e^{iKs}$ as a Fourier component for obtaining any arbitrary stress distribution by superposition, and considering a straight grain boundary in plane strain, we find from Timoshenko's theory of elasticity (95)

$$\sigma = \frac{\sigma_{vK}}{1 + |K|K^2/K_D^3} e^{iKs} \tag{5.14}$$

where

$$K_D = \left(\frac{D_b \delta_b \Omega \eta}{4(1-\nu^2)\ kT}\right)^{-1/3} \tag{5.15}$$

This Fourier transformation operation demonstrates that the characteristic length of diffusion is $\pi/2\ K_D^{-1}$ which is ($\nu = 1/2$) of the same order

of ℓ_o. For smaller K, corresponding to the distant stress, σ reduces to σ_v.

We shall apply this method to grain boundary sliding. Following Raj and Ashby (32), the grain boundary is modeled by a non-planar surface described by a cosine series (Fig. 5.1) $y = \sum_1^\infty h_n \cos K_n x$ for which $\theta = 2h/\lambda << 1$ and $K_n = 2\pi n/\lambda$. Sliding of magnitude $\dot{u}_{GB}$ creates a normal displacement rate

$$\dot{u} = -\frac{\dot{u}_{GB}}{2} \sum_1^\infty K_n h_n \sin K_n x$$

which can be incorporated in Eqn. (5.4), again using the method of Timoshenko's (95) to result in a normal stress

$$\sigma = \frac{\eta \dot{u}_{GB}}{3} \sum_1^\infty \frac{h_n K_n^2}{1 + (K_n/K_D)^3} \sin K_n x \qquad (5.16)$$

Numerical evaluation of this series was performed and the results are shown in Fig. (5.1) for $h_n/h = 4/n^2\pi^2 \sin^2 n\pi/2$ corresponding to a saw-tooth profile of a grain boundary shown in the same figure. We find the maxima of σ at locations $0.9\ \lambda/4\ (K_1/K_D)^3$, which are in agreement with ℓ_o within 1%. The average shear stress which equals the applied stress is

$$\tau_a = \frac{\eta \dot{u}_{GB}}{\lambda} \left(\frac{h}{\lambda}\right)^2 \sum_{n=1}^\infty \frac{\frac{4}{3} n^3 \pi^3 \left(\frac{h_n}{h}\right)^2}{1 + \left(\frac{K_n}{K_D}\right)^3} \qquad (5.17)$$

or for $K_1/K_D < 1$,

$$\tau_a = \frac{\eta \dot{u}_{GB}}{\lambda} \left(\frac{2}{9\pi}\right) \left(\frac{h}{\lambda}\right)^2 \left(\frac{n^2\pi^2 h_n}{h}\right) \ell n \left(\frac{K_1^3}{K_D^3}\right) \qquad (5.18)$$

where $n^2\pi^2 h_n/h$ is a constant independent of n or h.

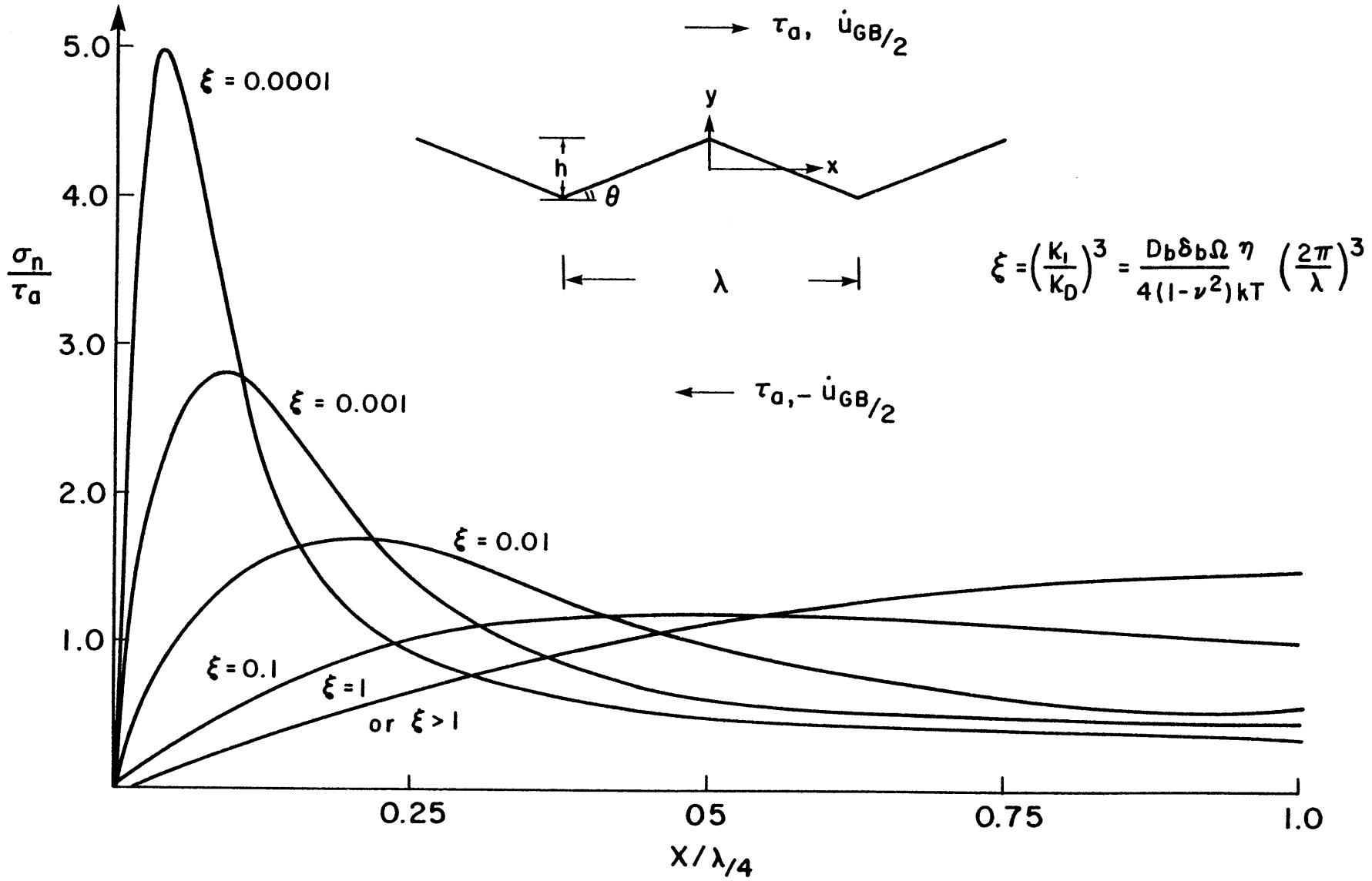

Fig. 5.1 - Coordinate System and Interfacial Stresses Evaluated for Several $\xi(\xi = (K_1/K_D)^3)$ of a serrated grain boundary. The stresses are plotted for $\lambda/h=2$

The stress at $x > \ell_D$ varies as 1/r, as expected from visualizing the configuration as one involving a co-linear array of edge dislocations of alternating signs. This feature is merely artificial and is a result of modeling the sliding grain boundary by normal displacement of alternating sign along a planar boundary. This artifact also makes the short wavelength contributions as a whole felt even at large distances from the origin, a feature not likely to occur in a more realistic treatment. Despite this, the far field has the variation of 1/r in all cases as expected from the Fourier analysis in the beginning of this section.

5.4.2. Interfacial Stresses at Grain Boundary Particles

The result of Section 5.4.1 can be applied to other problems. We now consider the general case of a sliding boundary containing steps of the kind described in Section 5.4.1 but only at a small area fraction f_A ($f_A = p/\lambda_p$ in Figure 5.2). It can be shown that the results of Section 5.4.1 are applicable, namely the interfacial stress has spikes with maxima at a distance ℓ_D away from the apex of each asperity. The magnitude of the stress remains the same for a given $\dot{u}_{GB}$ but the average shear stress at steady state is smaller by a factor f_A.

If these steps are interpreted as grain boundary particles, typically of submicron or micron size, ℓ_D can often exceed the particle size. For example, for $\delta_b D_b = 10^{-21} m^3/sec$, $T = 973°K$, $\Omega = 10^{-29} m^3$, $\sigma/\dot{\varepsilon} = 10^8$ MPA-sec, as typical conditions for fast creep in stainless steel, we find $\ell_D = 4$ μm. This means that any particle up to 4 μm size will be in the diffusion zone and the stress on interface is low and varies smoothly

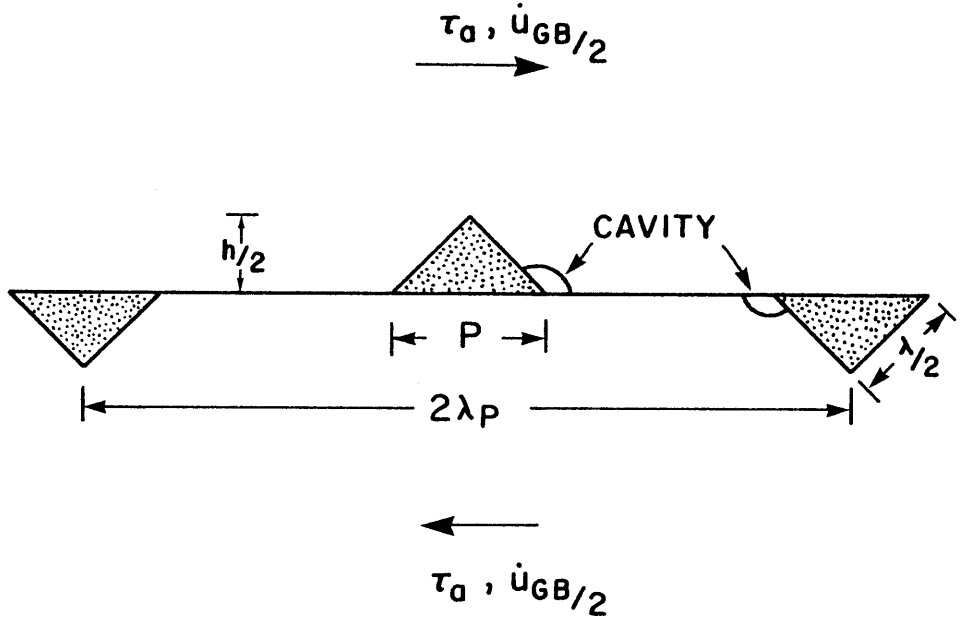

Fig. 5.2 - Particles and cavities on the grain boundary

around the particle. The magnitude of the stress can be estimated approximately from Equation (5.17) by choosing $\lambda \sim \sqrt{2}\, h$, $\ell_D > h$ for the purpose of estimation. The major term in Eqn. (5.17) gives a stress of the order of

$$\sigma_{\text{GB Particle}} = 0.1 \left(\eta \frac{\dot{u}_{GB}}{\ell_D}\right) \left(\frac{h}{\ell_D}\right)^2 \tag{5.19}$$

which invariably is much smaller than the applied stress.

It is evident that relatively fast rates of sliding are required for substantial stress at inclusions. In steady state creep, the average rate of sliding simply is too small for that. Furthermore, the average shear traction along grain boundary at steady state is smaller than the inclusion stress by a factor p/λ_p, the area fraction of particles on grain boundary.

There is another possibility which could result in substantial interfacial stresses at inclusions. During a transient, the stress along a grain boundary relaxes much faster than the stresses at inclusions. In the limit, shear traction on a grain boundary which is still of the order of the applied traction, is only supported by inclusions. Very high stresses can exist in such case, and they seem to be the only source of high interfacial stresses in a creeping solid at elevated temperature.

5.5. Linear Visco-Diffusive Creep in a Polycrystal Containing Hexagonal Grains

Linear visco-diffusive creep in an "ideal" polycrystal containing a periodic array of hexagonal grains with sliding interfaces is considered here (Fig. 5.3). The technique employs series expansion using nonorthogonal functions (95, 100). In this technique, the stress function ϕ is written as (100)

$$\phi = \sum_n \cos \beta_n x \, [B_n \cosh \beta_n y + C_n \beta_n y \sinh \beta_n y]$$

$$+ \sum_k \cos \alpha_k y \, [F_k \cosh \alpha_k x + G_k \alpha_k x \sinh \alpha_k x] \qquad (5.20)$$

and in-plane stresses are, as usual

$$\sigma_{xx} = \frac{\partial^2 \phi}{\partial y^2} \, , \quad \sigma_{yy} = \frac{\partial^2 \phi}{\partial x^2} \, , \quad \sigma_{xy} = -\frac{\partial^2 \phi}{\partial x \partial y}$$

The displacement rates are integrated from strain rates

$$\dot{\varepsilon}_{xx} = \frac{\sigma_{xx} - \sigma_{yy}}{\eta'} = - \dot{\varepsilon}_{yy}$$

where $\eta' = 4/3 \, \eta$ corresponds to the in-plane viscosity of a linear viscous material ($\sigma = \eta \dot{\varepsilon}$) under plain strain condition. The origin is chosen as fixed in the integration.

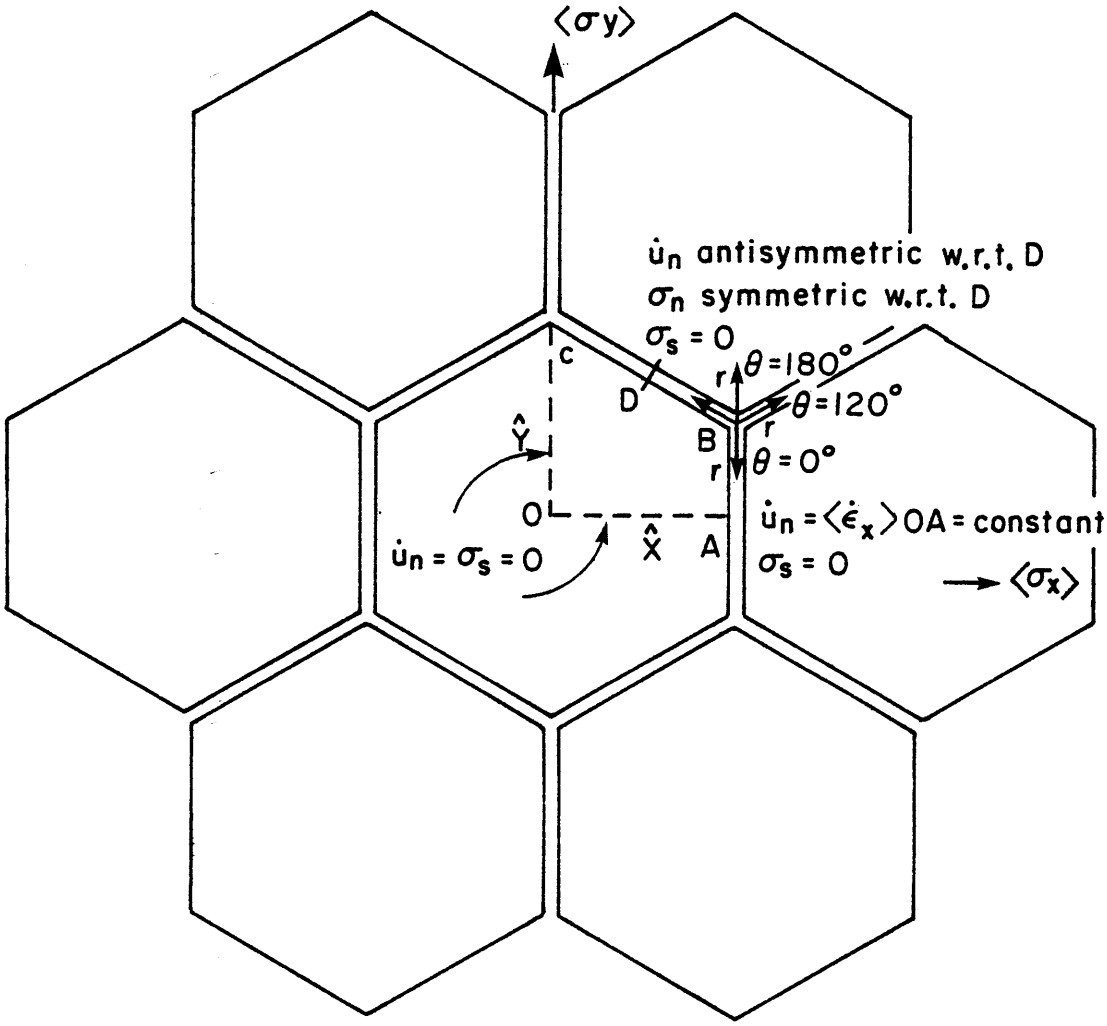

Fig. 5.3 - "Ideal" polycrystal containing hexagonal grains with sliding boundaries under symmetric loading where $\langle\sigma_{xy}\rangle=0$

Boundary conditions of symmetric loading are obtained by inspection. First, $\sigma_{xy} = \dot{u}_y = 0$ on OA and $\sigma_{xy} = \dot{u}_x = 0$ on OC are explicitly satisfied in the choice of the form of ϕ. Second, $\dot{u}_x - D_b\delta_b\Omega/kT\ \partial^2\sigma_x/\partial y^2 = \langle\dot{\varepsilon}_x\rangle_{AB}$ = constant and $\sigma_{xy} = 0$ are demanded on AB. Lastly, $\dot{u}_n - D_b\delta_b\Omega/kT\ \partial^2\sigma_n/\partial t^2$ is anti-symmetric with respect to D on BC, where at D the normal displacement rate is one half of that along AB with its direction reversed. Also, shear stress vanishes along BC but normal stress is symmetric with respect to D.

These conditions are sufficient to determine ϕ within an arbitrarily constant hydrostatic stress. For this, we have chosen $\sigma_{xx} = 0$ at B. Due to grain boundary sliding, this also implies $\sigma_{yy} = \sigma_{xy} = 0$. This choice is also explicitly satisfied through the choice of the form of ϕ.

Boundary collocation technique with least square criterion was used to find coefficients in the series expansion of ϕ (100). From which stress and displacement were obtained according to the relations previously listed.

The results are plotted in Fig. 5.4, where

$$\xi \equiv \frac{D_b\delta_b\Omega}{kT}\frac{\eta'}{(AB)^3} = \frac{4}{3}\left(\frac{\ell_D}{AB}\right)^3$$

covers a wide range of conditions of practial interest (ξ = 0.1 - 0.001). Note that the stress concentrations at triple points B and C are substantially reduced by diffusion. Boundary tractions rapidly relax as ξ becomes larger and have possessed much of the parabolic feature of diffusion governed stresses before ξ = 0.1. It is also noted that in

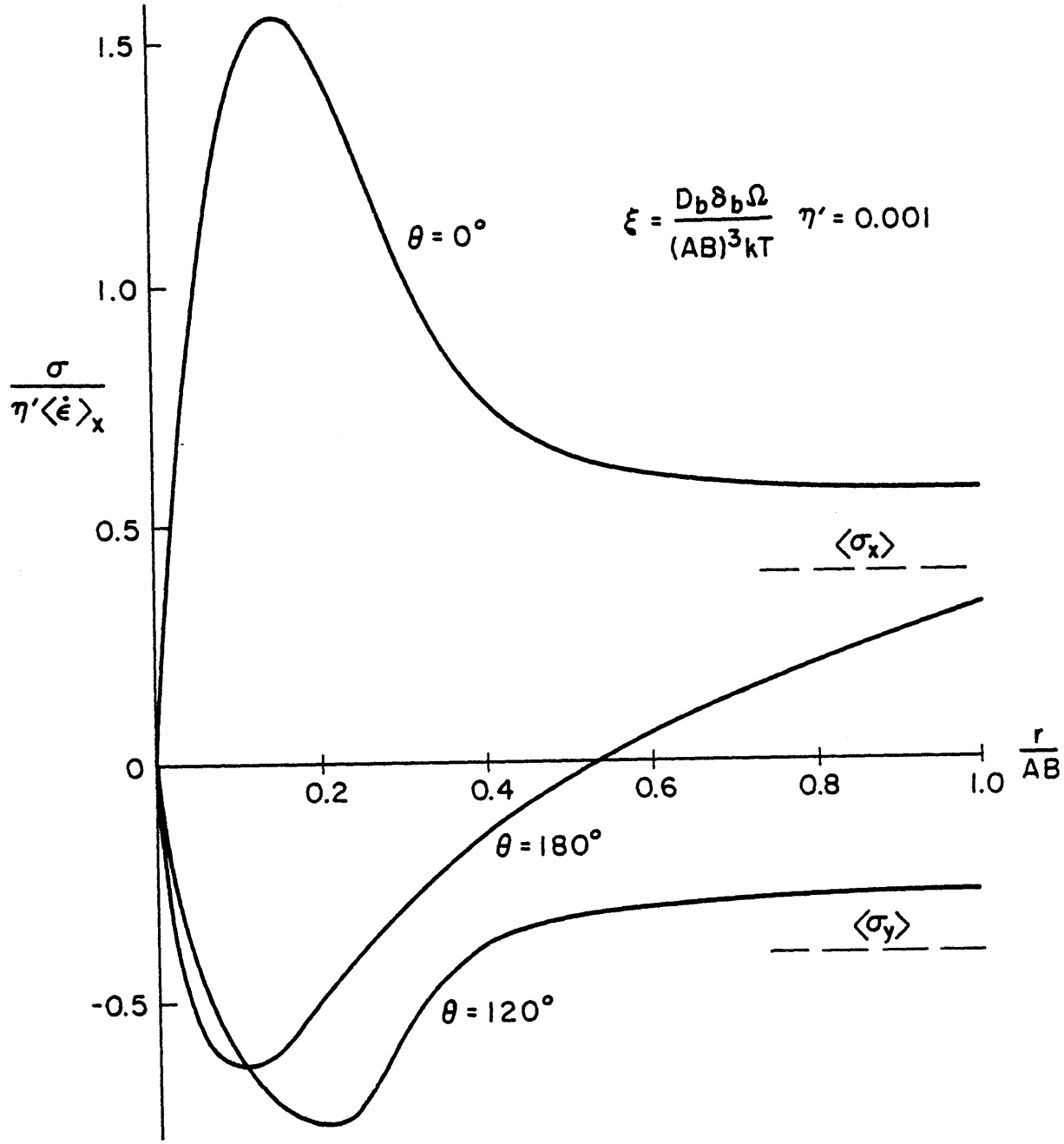

Fig. 5.4a - Stress distribution along grain boundaries near a triple point

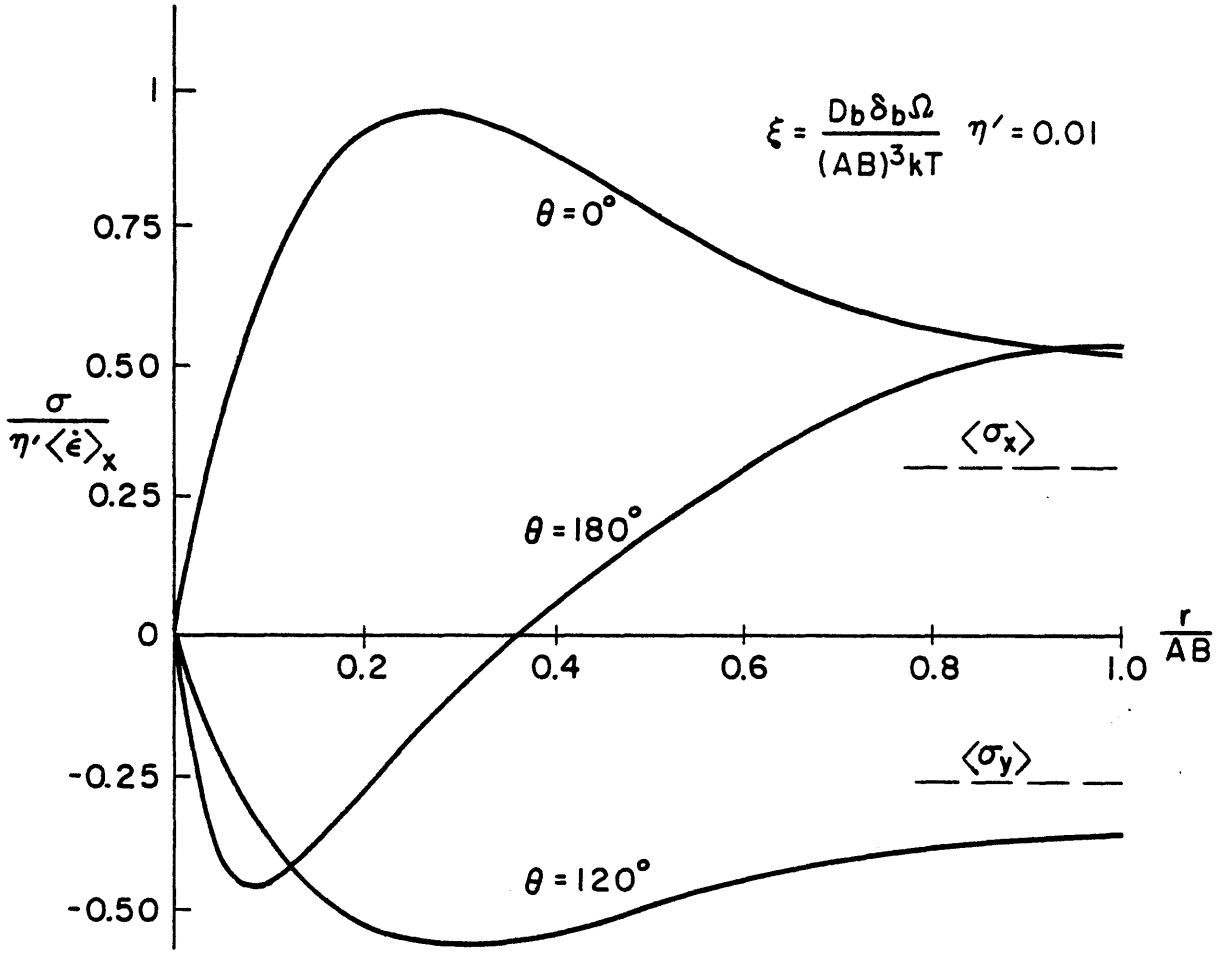

Fig. 5.4b - Stress distribution along grain boundaries near a triple point

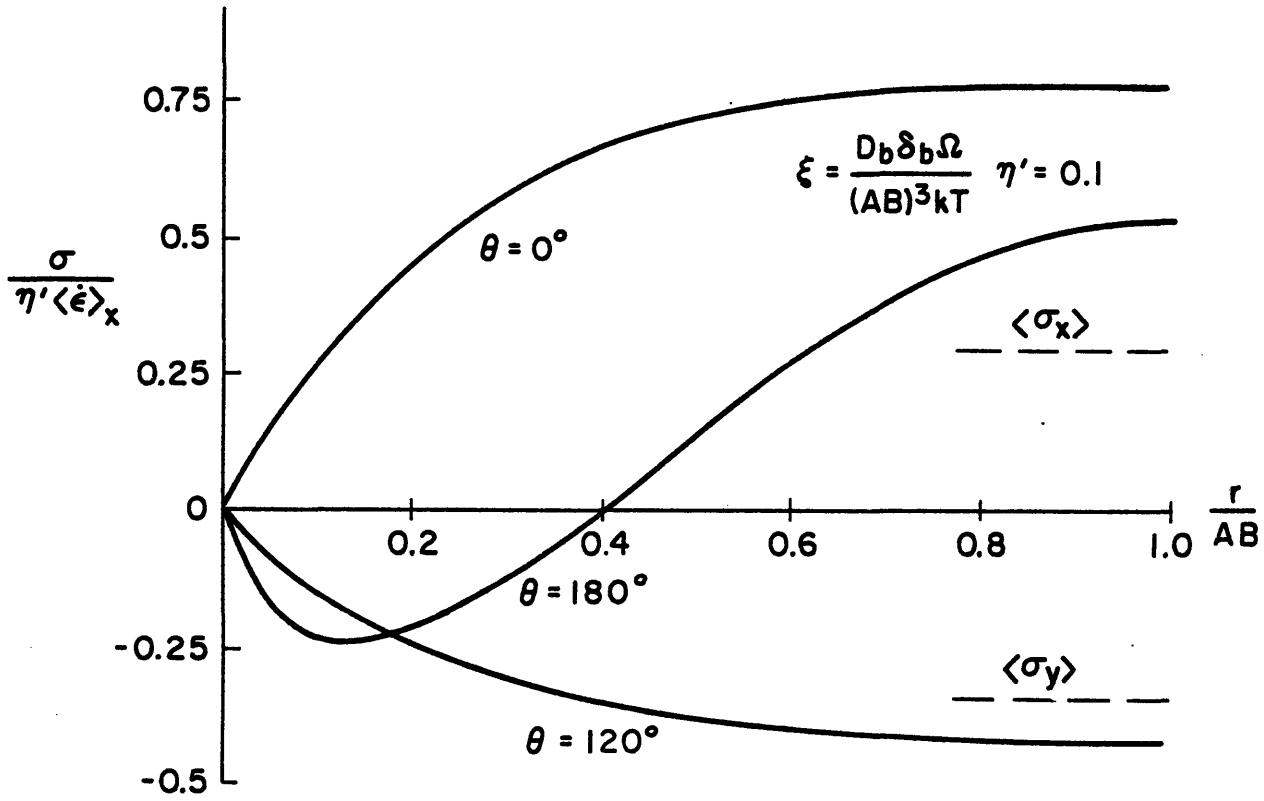

Fig. 5.4c - Stress distribution along grain boundaries near a triple point

the matrix along the extension of the grain boundary AB, a region of compression exists and the overall profile of stress along OC remains the same for all ξ's.

The average stress $\langle\sigma_{xx}\rangle - \langle\sigma_{yy}\rangle = \langle\sigma\rangle$ necessary for the deformation was also evaluated. For ξ = 0.1, 0.01 and 0.001, it is respectively $\langle\sigma\rangle/(\eta' \dot{u}_x/OA) = 0.62$, 0.74 and 0.80. These results can be compared with that computed by Ghahremani (28) using the same configuration but neglecting diffusion ($\langle\sigma\rangle/(\eta' \dot{u}_x/OA) = 0.86$) and our estimation, also neglecting diffusion, for a random but contiguous array of grain boundaries ($\sigma/(\eta' \dot{u}_x/OA) = 0.75$) of Chapter 4.

Although this calculation is applicable only to linear viscous deformation, it is generally regarded that the stress concentrations in the nonlinear material are somewhat less pronounced than those in the linear material. For this reason, we might conclude that in slow creep at elevated temperature, interfacial stresses at most favorably oriented triple junctions are typically twice the applied stress or less. It is not likely that such modest stress concentrations can cause triple-point cracking as was previously thought by McLean (36) and Zener (37) who made their observation based on elastic stress concentration ignoring creep relaxation. Nevertheless, the possibility of more substantial stress concentrations at triple points may still exist as in the cases of very fast creep (small ℓ_D), elastic stress transient (Section 4.3.1) or in coarse grain materials (large AB).

5.6. Nucleation of Cavities on Grain Boundaries

Recently Argon (97) proposed a modified classical nucleation theory of cavitation which was originally due to Raj and Ashby (98, 53). In calculating the nucleation barrier, the driving force for the condensation of vacancies is taken as $\sigma_n \Omega$, where σ_n is the normal component of the local stress on the grain boundary. Obviously the local stress must be evaluated with the effect of grain boundary sliding and diffusional flow taken into consideration. This point has been adequately covered in the preceding section.

The reciprocal time for nucleation of a cavity at a site is, according to this theory

$$\dot{\zeta} = \frac{2\pi r^* D_b \delta_b}{\Omega^{4/3}} \exp\left(-\frac{\Delta G^*}{kT}\right) \tag{5.21}$$

where $r^* = 2\gamma_s/\sigma_n$ is the critical radius and $\Delta G^* = 4\chi^3 F_v/\sigma_n 2$ is the activation energy. In these relations, F_v is a geometric factor related to the cavity and χ is related to the surface energy in which a correlation is made due to the recovery of interface energy during a nucleation process. The reader is referred to Argon and Raj and Ashby for details. For most materials and testing conditions, the pre-exponential factor is roughly 10^{10} sec^{-1}. Thus at temperature between 600°C and 700°C, $\dot{\zeta}$ is practically zero if ΔG^* is greater than 2 e.v. $(3.2 \times 10^{-12}$ erg$)^*$

---

* $D_b \delta_b = 10^{-21}$ m^3/sec, $r^* = 3 \times 10^{-9}$ m, $\Omega = 10^{-29}$ m^3

The magnitude of local stress necessary for appreciable nucleation can now be estimated. Taking χ = 300 erg/cm^2 and F_v = 0.5, σ_n is found to be 410 MPA. This is within reach in our experiments using the estimate for local stress at grain boundary particles given previously.

The choice of values for χ and F_v needs some discussion. Raj (53), arguing that a varying degree of "non-wettingness" may be responsible for cavity nucleation, treated F_v as an adjustable parameter that was made to vary 5 orders of magnitude in his theory. Since $\dot{\zeta}$ is extremely sensitive to ΔG^*, this choice apparently is too liberal. We cannot find any direct evidence to support this argument in our experiments where grain boundary carbides were always well adhered to the matrix. Instead we fix the value of F_v as 0.5 that should be typically met in most good quality structural alloys at particle-grain boundary interfaces. Secondly, the magnitude of χ is chosen to be 0.5 γ_s, where γ_s, the surface energy, is drawn from the recent data of Mortimer and Nicholas for 316 stainless steel (99). These authors also noted in their study that grain boundary energies can be of the same magnitude, or even slightly higher, as the surface energy. Although γ_s at 600 ergs/cm^2 reported by Mortimer and Nicholas is somewhat lower than the surface energy for pure austenitic iron and nickel, it is nevertheless possible that solute segregation (such as B reported by Mortimer et al.) may be responsible for a reduced surface energy at nucleation sites.

At any rate, it is reasonable to expect that nucleation of cavities by vacancy condensation can occur under an enhanced local stress. Thus there is no need to postulate the existence of nearly nonwetting

particles, although such problems can indeed occur in low quality alloys. Grain boundary sliding can result in local stresses substantially higher than the applied stress even at the macroscopic steady state in the presence of diffusional smoothing, since even then transients of grain boundary sliding are known to exist. Yet nucleation no doubt will still be heterogeneous and take place preferentially at sites where surface energy is lowered or energy balance involving other interfaces is most favorable.

CHAPTER 6

DIFFUSIVE GROWTH OF GRAIN-BOUNDARY CAVITIES

6.1. Introduction

Diffusive growth of grain-boundary cavities has been studied extensively (for a review see Perry) (34). Existing models (63, 64) for the diffusive growth of cavities are for the most part based on the quasi-equilibrium assumption that surface diffusion is so rapid that the cavity has a rounded, equilibrium shape. Hence in such models cavity growth is rate-limited only by grain boundary diffusion.

However, the assumption that the cavity has an equilibrium shape may not always be satisfied. Very often flat, disk shaped cavities are observed. In a recent study of cavitation Cane and Greenwood (101) reported that the height of cavities that grew in the early stage stayed unchanged later in their evolution. This is clearly an indication of the transition of the growth mode from a quasi-equilibrium shape to a non-equilibrium one.

Several treatments have now been developed that avoid the above assumption. These models of Chuang et al. (65, 73) and more recently of Pharr and Nix (102) in turn are based on other restrictive assumptions. Commonly, the rigid grain approximation is used so that no attention is paid to creep deformation in the surrounding. In addition, in one model that claimed best agreement with experiments (102, 103), the authors postulated D_b/D_s to be much greater than one, even though there is practically no metallic system that falls into this category as noted by Gjostein (104).

More often, diffusion along a grain boundary tends to restrict the flow of matter from the cavity and affects the geometry accordingly. Moreover diffusional flow along grain boundaries is coupled to matrix creep which is usually appreciable. The coupling process, which has been examined recently by Beere and Speight (74) and most recently by Edward and Ashby (75), serves to shorten the grain boundary diffusion distance. Thereby it gives rise to faster growth of cavities.

Thus the problem in its entirety involves three processes: surface diffusion, grain boundary diffusion, and matrix creep. They are to be coupled together sequentially in order to satisfy conservation of mass and continuity or compatibility of displacement. In this paper we treat these coupling relations first separately, taking advantage of the known relation between cavity shape and total flux derived by Chuang and Rice (65, 73) and the nature of diffusional smoothing discussed in Chapter 5. A solution is then presented in closed form for a general model of diffusional growth of grain boundary cavities of non-equilibrium shape under creep conditions.

The symbols used in this chapter are listed in the beginning of the thesis.

6.2. Theory

6.2.1. Surface Diffusion and Cavity Shape

We start the analysis with an idealized configuration (Fig. 6.1) in which an axi-symmetric cavity located on the grain boundary is bounded by a perimeter on which periodic boundary conditions appropriate for an array of similar cavities are imposed. The entire space is

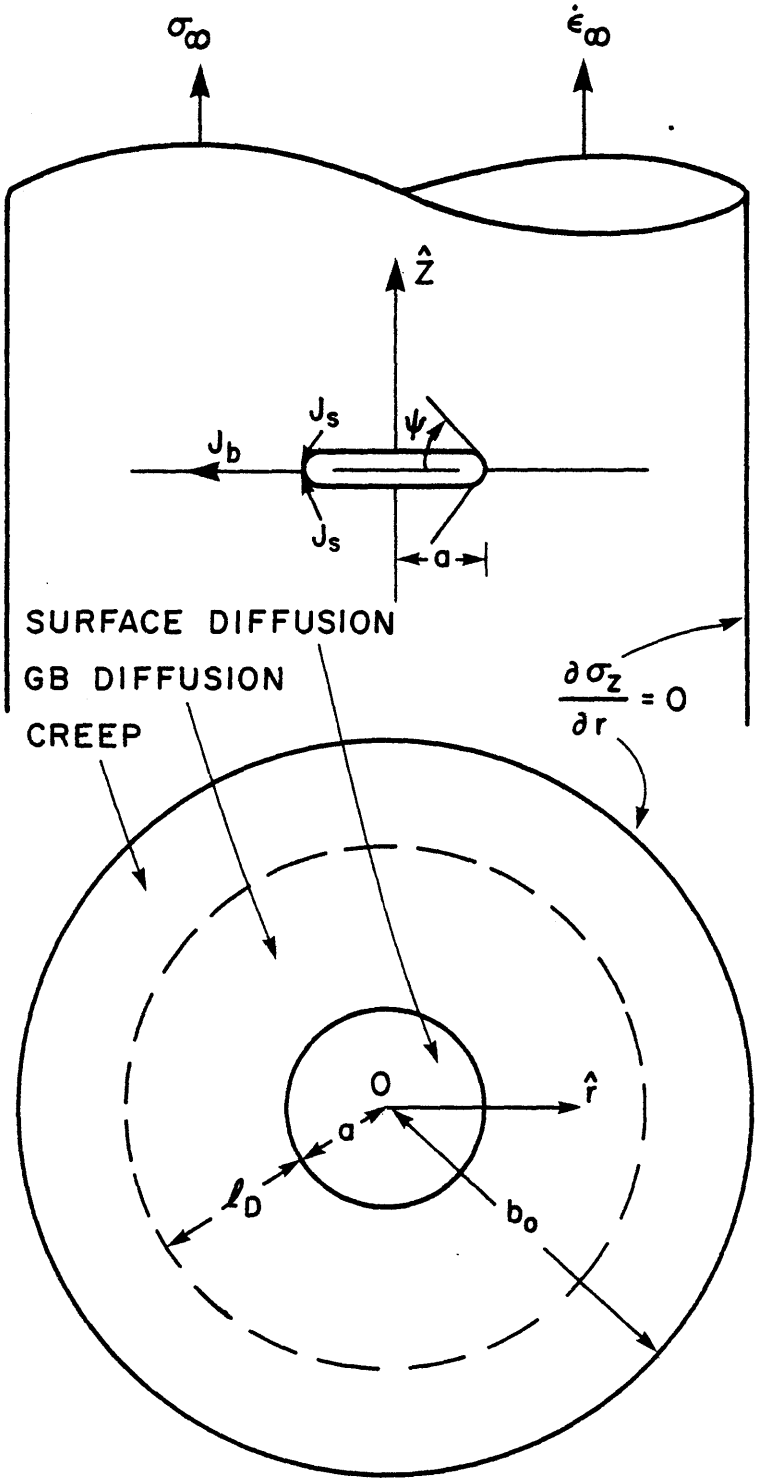

Fig. 6.1 - Configuration for an axially loaded cavity with cylindrial symmetry

subject to creep under a tensile stress in the distant field. The cavity shape is not known à priori and is to be determined as part of the analysis.

Varying curvature along the profile of the cavity gives rise to gradients of chemical potential which in turn produces a flow of matter along the cavity surface. The flow from both surfaces of the cavity eventually meets at the cavity tip and continues along the grain boundary. The following equation results from conservation of mass

$$\frac{dv}{dt} = 4\pi a\Omega J_{s(tip)} \tag{6.1}$$

It has been shown that (65, 73), for a given geometry of void tip, the surface flux is only related to a and da/dt, provided the growth is at a quasi-steady state. Corresponding to the two extreme cases, i.e., a quasi-equilibrium, spherical cap shape, and a non-equilibrium, crack-like disk shape, the surface flux is

$$J_{s(tip)} = \frac{h(\psi)}{\Omega} a \frac{da}{dt} \quad \text{(quasi-equilibrium)} \tag{6.2}$$

and

$$J_{s(tip)} = 2\sin\left(\frac{\psi}{2}\right)\left(\frac{D_s\delta_s\gamma_s}{kT}\right)\left(\frac{kT\frac{da}{dt}}{D_s\delta_s\Omega\gamma_s}\right)^{2/3} \quad \text{(crack-like)} \tag{6.3}$$

where

$$h(\psi) = \frac{v}{\frac{4\pi a^3}{3}} = [1/(1+\cos\psi) - (\cos\psi)/2]/\sin\psi$$

Using similarity solutions, the intermediate case between these extremes can also be represented (65). It is known that the intermediate case is closely approximated by an envelope which is the interpolation of the extreme solutions.

6.2.2. Grain Boundary Diffusion Coupled to Matrix Creep

Along the grain boundary, diffusion is coupled to matrix creep as described in the preceding chapter. Specifically, displacement rates at a distance on both sides of the grain boundary contain contributions from the creep accommodation throughout the region. A comprehensive numerical solution of this problem has been obtained by Needleman (94), for the special case of $a/b_o = 0.1$, $\dot{\varepsilon} = A\sigma^5$ and $\psi = 70°$ for a quasi-equilibrium cavity.

In the absence of matrix creep, the solution of this problem considering diffusion alone is well-known. Originally due to Hull and Rimmer (63), its revised form according to Speight and Harris (64) is

$$(a^3\dot{\varepsilon}_\alpha)^{-1}\, dv/dt = 2\pi\, (\ell_D/a)^3\, [\ell n(b_o/a) + (a/b_o)^2 \left(1 - \frac{1}{4}\,(a/b_o)^2\right) - 3/4]^{-1} \qquad (6.4)$$

where

$$\ell_D = (D_b\delta_b\Omega\sigma_\alpha/kT\dot{\varepsilon}_\alpha)^{1/3}$$

which was already used extensively in the discussion of visco-diffusive deformation in Chapter 5. We try, guided by the reasoning in the preceding chapter, an approximate solution by designating a diffusion zone of size ℓ_D. Thus we obtain, substituting $a+\ell_D$ for b_o in Eqn. (6.4) whenever $a+\ell_D < b_o$,

$$(a^3\dot{\varepsilon}_\alpha)^{-1}\, dv/dt = 2\pi(\ell_D/a)^3\, [\ell n(\frac{a+\ell_D}{a}) + (\frac{a}{a+\ell_D})^2\, (1 - \frac{1}{4}\,(\frac{a}{a+\ell_D})^2) - \frac{3}{4}]^{-1} \qquad (6.5)$$

The result is plotted in Fig. 6.2. As can be seen the agreement with Needleman's result (94) is excellent. Also in Fig. 6.2 are shown

* In Eqn. (6.5) $\ell_D+a \leq b_o$ is understood in the second bracket if $\ell_D+a>b_o$ where diffusion zones impinge on each other.

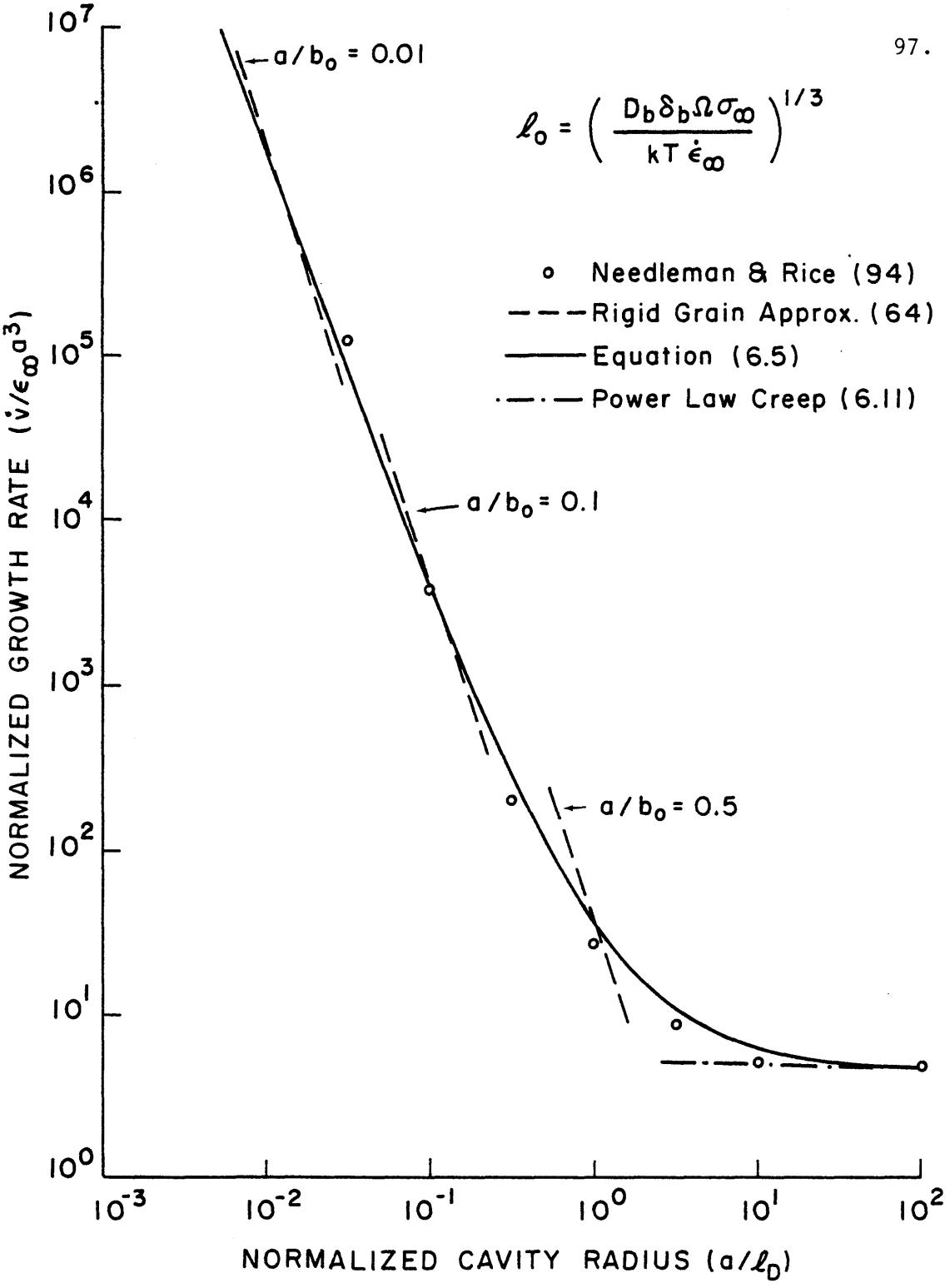

Fig. 6.2 - Normalized growth rate for quasi-equilibrium cavity

the rigid grain solutions (64) that supercede the above one at $\ell_D + a \geq b_o$ as well as the limiting condition when the growth is by matrix creep alone.

We note that nothing in the analysis that leads to Eqn. (6.5) explicitly hinges on the geometry of the axi-symmetric cavity. In view of its agreement with exact solutions and the useful feature just mentioned, Eqn. (6.5) will be used in later developments to treat cavities of other geometries.

6.2.3. Growth Rate

From conservation of mass Eqn. (6.1) and cavity expansion rate dv/dt, resulting from grain boundary diffusion coupled to matrix creep and given by Eqn. (6.5), we obtain

$$4\pi a\Omega J_{s(tip)} = \dot{\varepsilon}_\infty a^3 \left(\frac{\ell_D}{a}\right)^3 2\pi \left[\ell n\left(\frac{a+\ell_D}{a}\right)+\left(\frac{a}{a+\ell_D}\right)^2 \left(1 - \frac{1}{4}\left(\frac{a}{a+\ell_D}\right)^2\right) - \frac{3}{4}\right]^{-1} \tag{6.6}$$

The left hand side of the equation contains all the information about cavity shape and da/dt at a given a. Indeed since the flux for the general shape can be closely enveloped by the corresponding expressions for the extreme cases, described by Eqns. (6.2) and (6.3), it should be adequate to solve Eqn. (6.6) only for the extreme cases. Substituting $J_{s(tip)}$ from Eqns. (6.2) and (6.3), the growth rate of a cavity of either a quasi-equilibrium shape or a crack-like shape is, respectively,

$$\left(\frac{4\pi h(\psi)}{\dot{\varepsilon}_\infty a}\frac{da}{dt}\right)_{\text{quasi-equilibrium}} = 2\pi\left(\frac{\ell_D}{a}\right)^3\left[\ell n\left(\frac{a+\ell_D}{a}\right) + \left(\frac{a}{a+\ell_D}\right)^2\left(1 - \frac{1}{4}\left(\frac{a}{a+\ell_D}\right)^2\right) - \frac{3}{4}\right]^{-1} \tag{6.7}$$

$$\left(\frac{4\pi h(\psi)}{\dot{\varepsilon}_\infty a}\frac{da}{dt}\right)_{\text{crack-like}} = \alpha\left(\frac{\ell_D}{a}\right)^{5/2}\left[\ell n\left(\frac{a+\ell_D}{a}\right) + \left(\frac{a}{a+\ell_D}\right)^2\left(1 - \frac{1}{4}\left(\frac{a}{a+\ell_D}\right)^2\right) - \frac{3}{4}\right]^{-3/2} \tag{6.8}$$

where

$$\alpha\left(\psi, \frac{D_b\delta_b}{D_s\delta_s}, \frac{\sigma_\infty \ell_D}{\gamma_s}\right) = \frac{4\pi h(\psi)}{[4\sin(\psi/2)]^{3/2}}\left[\left(\frac{D_b\delta_b}{D_s\delta_s}\right)\left(\frac{\sigma_\infty \ell_D}{\gamma_s}\right)\right]^{1/2} \tag{6.9}$$

prescribes the ratio of effective boundary flow to the surface flow. Obviously the shape that gives the faster growth rate is favored and the actual shape of the cavity and its growth rate should resemble those in the corresponding extreme case.

The results are plotted in Fig. 6.3 for several values of α. If $\alpha = 0$, only the solution for quasi-equilibrium shape applies (Eqn. (6.7) or Eqn. (6.5)).

6.3. Application

6.3.1. Transition from quasi-equilibrium mode to crack like mode

The coefficient α in Eqn. (6.9) serves as a useful indicator of the relative importance of non-equilibrium shape in the cavitation process. As α approaches 0, cavities are of quasi-equilibrium shape and their growth is accurately described by Eqn. (6.7) (same as Needleman's solution). As α increases, the effect of non-equilibrium shape becomes more important until finally the growth and the geometry

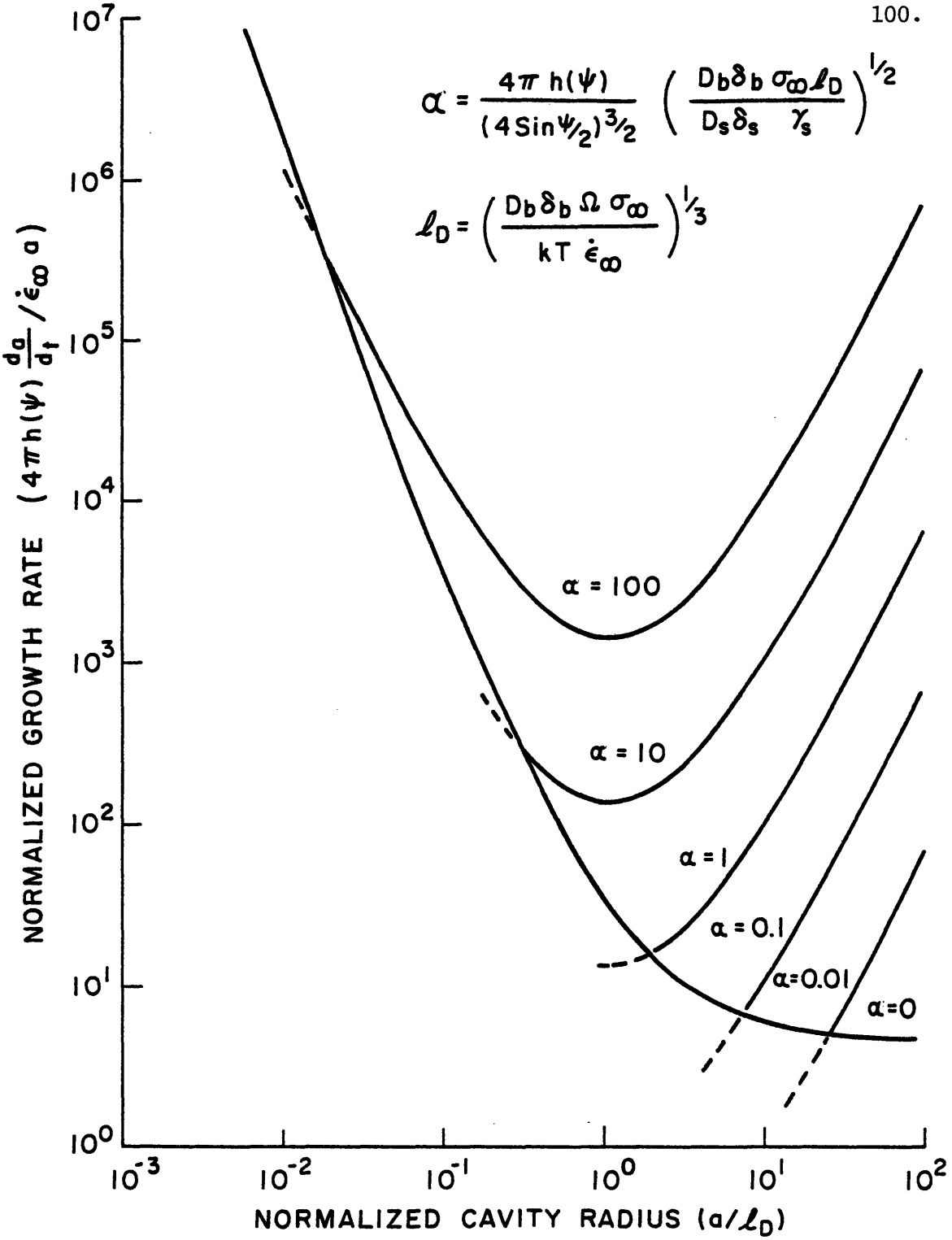

Fig. 6.3 - Growth rate for quasi-equilibrium and crack-like cavities

are characteristic of that of a crack-like cavity. The transition from a quasi-equilibrium mode to a crack-like growth mode is plotted in Fig. 6.4 as the locus of a/ℓ_D v.s. α, where a/ℓ_D are those points in Fig. 6.3 where the two branches given by Eqns. (6.7) and (6.8) intersect. Alternatively, by equating Eqns. (6.7) and (6.8), we define the transition by an equation

$$\alpha' \equiv \frac{4\pi h(\psi)}{(4\sin(\psi/2))^{3/2}}\left[\left(\frac{D_b\delta_b}{D_s\delta_s}\right)\left(\frac{\sigma_\infty a}{\gamma_s}\right)\right]^{1/2} = 2\pi\left[\ell n\ \left(\frac{a+\ell_D}{a}\right)+\left(\frac{a}{a+\ell_D}\right)^2\right.$$

$$\left.\left(1-\frac{1}{4}\left(\frac{a}{a+\ell_D}\right)^2\right)-\frac{3}{4}\right]^{1/2} \qquad (6.10)$$

which is also plotted in Fig. 6.4. The prominent constants affecting the transition are, obviously, $D_b\delta_b/D_s\delta_s$, the ratio of grain boundary diffusion to surface diffusion, $\sigma_\infty a/\gamma_s$, the ratio of applied stress to "nominal" capillary force, and a/ℓ_D, the ratio of cavity radius to diffusion distance. As these ratios, which we will call normalized grain boundary diffusion, normalized stress, and normalized cavity radius increase, the transition from the quasi-equilibrium mode to the crack-like mode eventually takes place.

A typical value of α lies between 30 and 1 while α' lies between 5 and 0.1. Since ℓ_D (see Chapter 5) is a few microns for rapid creep at 0.55 T_m and observable cavities also fall into the same range of sizes, it is very common in experiments to observe non-equilibrium cavities reported as flat disk-like voids in the literature. This situation is particularly so at lower temperatures ($\Delta G_b > \Delta G_s$), higher stresses (higher $\sigma_\infty a/\gamma_s$ and lower ℓ_D), and in the later stage of cavitation (larger a).

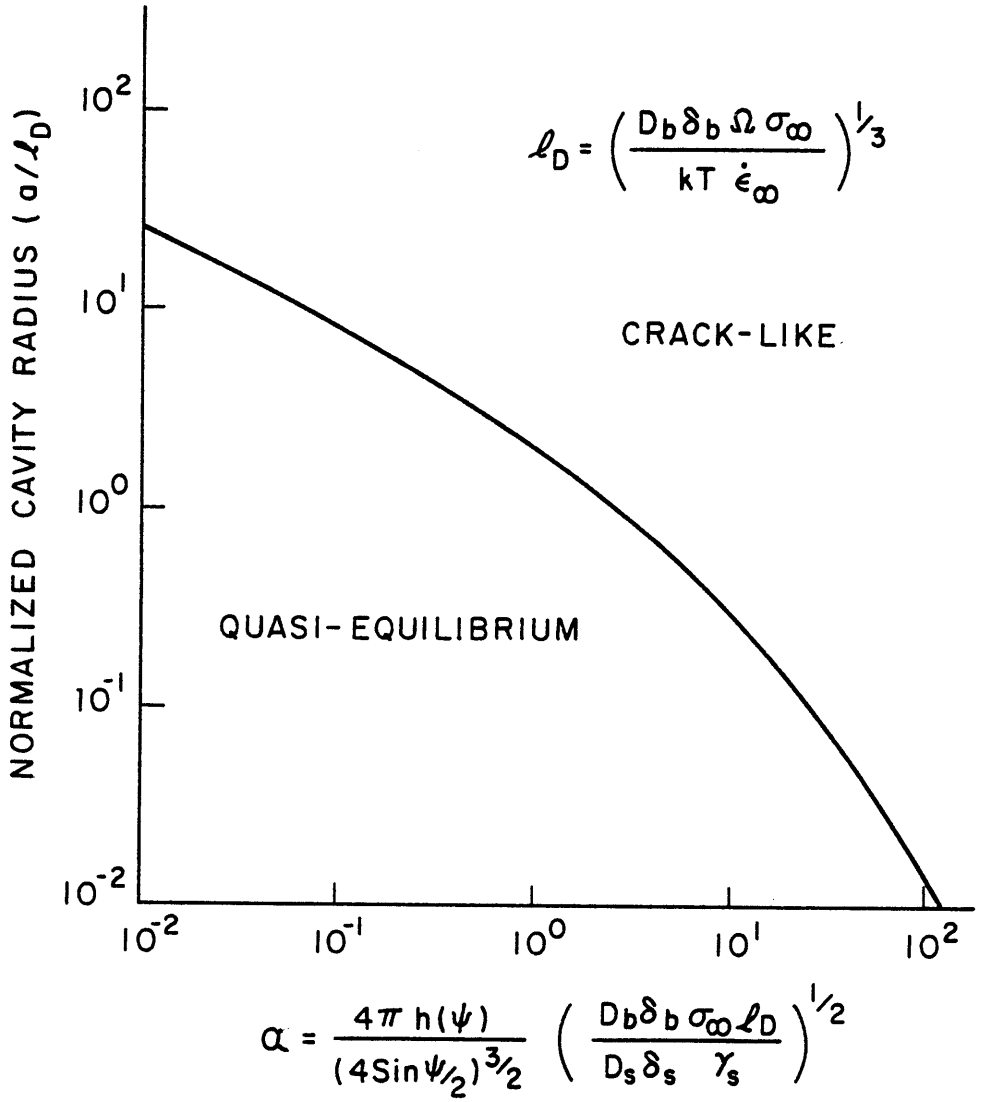

Fig. 6.4a - Transition from a quasi-equilibrium mode to a crack-like mode

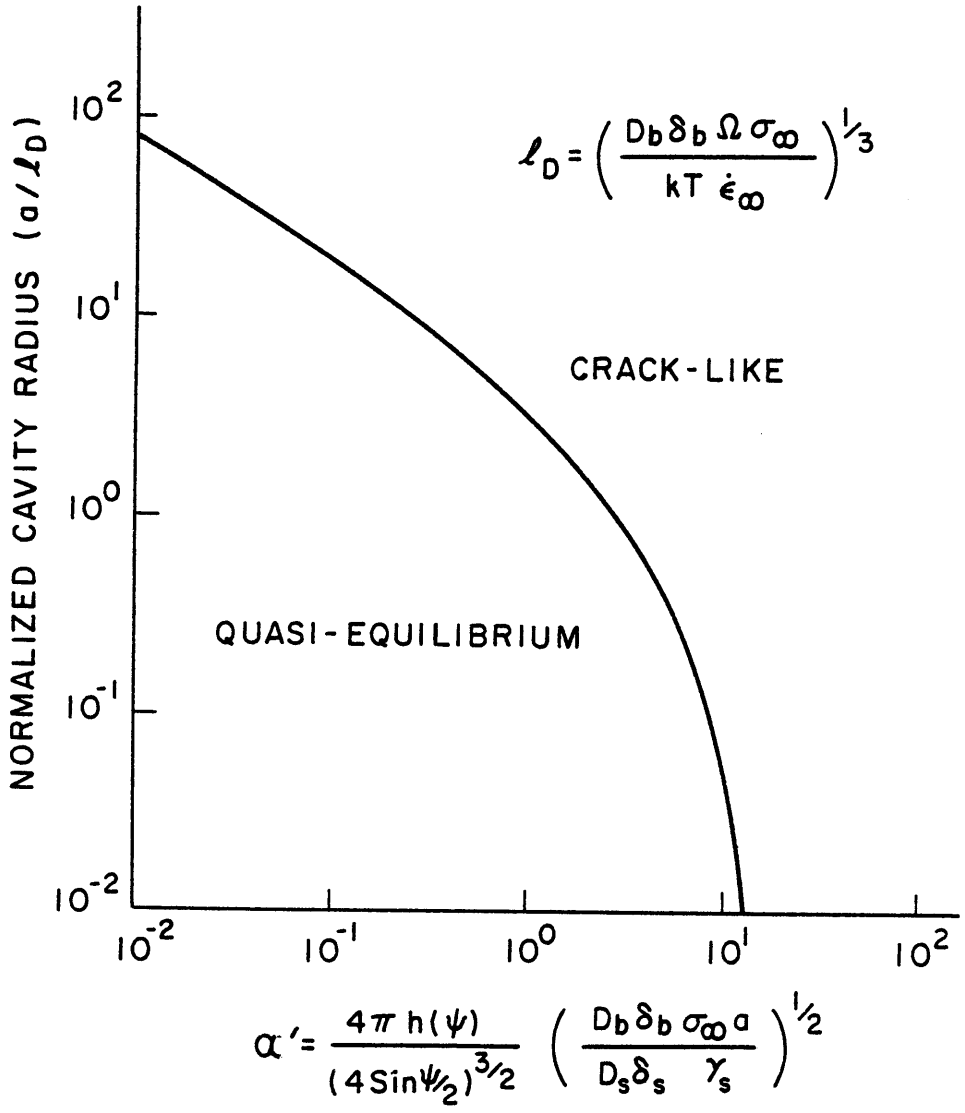

Fig. 6.4b - Transition from a quasi-equilibrium mode to a crack-like mode

In the following, limiting cases of the solutions will be examined and compared with the predications of some of the more restrictive models.

6.3.2. Quasi-Equilibrium Cavities

In this case Eqn. (6.7) reduces to Eqn. (6.5). For $a/\ell_D < a/b_o$ we recover the well-known solution of Eqn. (6.4) of the rigid grain model. Since diffusion zones of neighboring cavities impinge each other, creep is insignificant in a slab containing cavities and the entire grain boundary. The rigid grain model is satisfactory under these conditions.

For $a/\ell_D >> 1$,

$$\frac{dv}{dt} = \frac{3\pi}{2} a^3 \dot{\varepsilon}_\alpha \tag{6.11}$$

which corresponds to hole growth by matrix creep.

Of some practical interest is the intermediate range of a/ℓ_D which constitutes the bulk of creep life. Between $0.1 < a/\ell_D < 1$ the solution can be approximated by

$$\frac{4\pi h(\psi)}{\dot{\varepsilon}_\alpha a} \frac{da}{dt} = 10\pi \left(\frac{\ell_D}{a}\right)^2 \tag{6.12}$$

or

$$\frac{d}{dt} (\pi a^2) = \frac{5\pi}{h(\psi)} \ell_D^2 \dot{\varepsilon}_\alpha \tag{6.13}$$

A relation of this type, exhibiting a linear increase of cavity area with time, has been frequently reported (67, 70).

6.3.3. Crack-like Cavities

In this case, the solution is given by Eqn. (6.8). As $\alpha >> 1$ and $a/\ell_D < a/b_o$, we can compare our solution with the rigid grain model for a crack-like cavity. Substituting b_o for $a+\ell_D$ in the second bracket on RHS of Eqn. (6.8), we have

$$\frac{da}{dt} = \left(\frac{D_s \delta_s \gamma_s \Omega}{8kTb_o^3}\right)\left(\frac{D_b \delta_b}{D_s \delta_s}\right)^{3/2}\left(\frac{\sigma_\infty b_o}{\gamma_s \sin(\psi/2)}\right)^{3/2}\left(\frac{b_o}{a}\right)^{3/2}\left[\ell n\left(\frac{b_o}{a}\right) + \left(\frac{a}{b_o}\right)^2\left(1 - \frac{1}{4}\left(\frac{a}{b_o}\right)^2\right) - \frac{3}{4}\right]^{3/2} \qquad (6.14)$$

This form is identical to the result of Chuang et al. (their equation (73) and (88)) (65) except for a trivial factor $\left(1 - \left(\frac{a}{b_o}\right)^2\right)^{3/2}$ which results from a common error of most authors in this field in implementing the rigid grain approximation. (For a discussion, see Harris (105)). In this limit the cavity growth rate varies with the applied stress as $\sigma_\infty^{3/2}$.

6.4. Discussion

6.4.1. Rupture Time and Rupture Strain

A relation between rupture time and steady state creep rate has been observed by a number of authors. According to Monkman and Grant (68) a so-called Monkman-Grant relationship $\dot{\varepsilon}_{\text{steady state}}\, t_r =$ constant, holds for many materials. This relationship and several of its variations all point to a failure strain that lies between 0.05 and 0.5, depending on the material, but is otherwise insensitive to strain rate. It has been difficult to find how this relationship can be compatible with any of the models for diffusive growth of cavities

in the past.

Let $F(a/\ell_D)$ stand for the RHS of Eqns. (6.7)(6.8), then we can integrate these equations to the following form

$$\int_{t_i}^{t_f} \dot{\varepsilon} dt = \int_{\ell n(a_i/\ell_D)}^{\ell n(a_f/\ell_D)} \frac{4\pi h(\psi)}{F(a/\ell_D)} \, d\ell n(a/\ell_D) \qquad (6.15)$$

which gives an estimate of the rupture strain. Note that $F(a/\ell_D)$ can be read directly from the abscissa of Fig. 6.3. Since the most important contribution to the integral will come from the portion of a/ℓ_D where $F(a/\ell_D)$ takes on the lowest values, the rupture strain must be controlled by the lowest $F(a/\ell_D)$ during growth.

If cavities always grow in the quasi-equilibrium mode, $F(a/\ell_D)$ is a monotonically decreasing function as shown in Fig. 6.2. Since the final size of cavities does not vary greatly and is typically 0.25 b_o, a_f/ℓ_D will move to the right as strain rate increases. Thus $\varepsilon_{rupture}$ as estimated by Eqn. (6.15) also increases quickly as strain rate increases. This result of σt_r = constant in the rigid grain approximation, is inconsistent with the Monkman-Grant relationship. Likewise, cavities that always grow in the crack-like mode or by plasticity alone are not acceptable. The difficulty in that case is either an incorrect stress dependence or an unrealistic rupture strain.

In contrast, our model of cavity growth which starts in quasi-equilibrium and ends in a crack-like mode appears capable of resolving the difficulty. Typically a/ℓ_D lies between $10^{-0.5}$ and $10^{0.5}$ which coincides with the range where $F(a/\ell_D)$ has a minimum. Thus neither $F(a/\ell_D)$ nor the rupture strain should be very sensitive to the strain

rate or stress. It is also important that this minimum of $F(a/\ell_D)$ lies between $10^{2.5}$ and $10^{1.5}$ for a typical value of α between 30 and 1, thus predicting a rupture strain between 0.05 and 0.5 (for an estimate, $h(\psi) = 0.75$, $\ell n(\frac{a_f}{a_i}) = 2.$) All of this is consistent with the experiments.

Although this explanation is encouraging, we should point out in caution that it is not the only explanation for the Monkman-Grant relationship. It is likely that continuous nucleation would alter the picture considerably. This point is not pursued further in this chapter. In the end of this chapter, an example is cited in which cavities were implanted prior to test. A maximum of rupture strain is found (103) in agreement with our theory.

6.4.2. Variation of Growth Rate with Orientation

Reconsideration of the model, in the context of grain boundaries that transmit only normal stress and inclined at an angle ϕ between the normal of the boundary and the tensile axis provides some insight into the cavitation process in a polycrystal. Since only normal displacement results from grain boundary diffusion, it might be assumed that the coupling between creep and diffusion involves only the normal component of the creep field. We might expect further that ℓ_D in such coupling ($\ell_D = [(D_b\delta_b\Omega/kT)(\sigma_\alpha\cos^2\phi/\dot{\varepsilon}_\alpha\cos^2\phi)]^{1/3}$) not to be affected by ϕ, while the growth rate $1/a\ da/dt$ varies as $\dot{\varepsilon}_\infty\cos^2\phi$ (Eqn. (6.7) and (6.8)). This is what our experimental observation indicates as will be discussed in Chapter 7.

6.4.3. Limitation of the Theory

The major limitation of the theoretical model occurs for $a/\ell_D >> 1$. Since the growth by creep alone, whether the cavity is quasi-equilibrium or crack-like, is very sensitive to the boundary condition especially if m (in $\dot{\varepsilon} = A\sigma^m$) becomes large, we should not expect much accuracy for $a/\ell_D >> 1$. Fortunately this is not a major problem in applications, as a/ℓ_D in a realistic case does not exceed 5.

Although the variation of growth rate with orientation was discussed previously, it is possible that grain boundary sliding of the inclined boundary can cause some modification of the theory. At the extreme case when grain boundary sliding is very rapid, cavity growth by shearing has been observed in 304 stainless steel (Chapter 7).

Lastly, we shall comment on the capillary force at the tip of a non-equilibrium cavity. To include it in the theory, an extra term $(1 - \sigma_{capillary}/\sigma_\infty)$ should multiply the RHS of Eqns. (6.4), (6.5), (6.6). For non-equilibrium cavities, $\sigma_{capillary}$ varies with the rate of advancement of the cavity tip, da/dt, namely (65), (73)

$$\sigma_{capillary} = 2\gamma_s \sin\left(\frac{\psi}{2}\right) \left(\frac{kT\,\frac{da}{dt}}{D_s \delta_s \Omega \gamma_s}\right)^{1/3} \quad \text{(crack-like)} \qquad (6.16)$$

$$\sigma_{capillary} = \frac{\gamma_s \sin\psi}{a} \quad \text{(quasi-equilibrium)} \qquad (6.17)$$

These expressions can be incorporated, along with the modification of Eqn. (6.6), to derive a full solution corresponding to Eqns. (6.7) (6.8).

As noted by Chuang (65), it is rarely, if ever, that a modification due to capillary force is important since it requires roughly that $D_b\delta_b/D_s\delta_s$ exceeds 200 when σ_∞ = 20 MPA or 1000 when σ_∞ = 100 MPA. For this reason, our omission of this contribution is justified. It is an easy matter to check however that the modification to our theory does lead to the same growth rate proportional to σ_∞^3 when $D_b\delta_b/D_s\delta_s$ is much greater than unity, as predicted by Chuang's and Pharr's theory (65, 102).

6.5. Comparison of Theory of Diffusive Growth of Cavities with Experiment

It is generally difficult to compare rate equations of cavity growth in creep with experiments. One of the main reasons for the difficulty is the uncertainty introduced by continuous nucleation throughout the test. Two experimental studies in the literature appeared to have avoided this problem. We shall deal with each individually in the following.

(A) Cane and Greenwood on α-Iron

Cane and Greenwood studied cavitation of αF_e at 700°C (58, 101). Cavities at various stages of creep were observed by means of intergranular fracture at low temperature after the creep test. The measurement of the maximum cavity size provided a rather reliable guide to the study of cavity growth, for those cavities of maximum size could be assumed to have nucleated in the beginning of the test.

Their results show $a_i = C_i\sigma^{1.5}\, t^{0.5}$, where indices i stand for the three major dimensions of a given cavity respectively. The constants C_i are 6.5×10^{-8} m/(MPA)$^{1.5}$ (hr)$^{0.5}$, 3.5×10^{-8} m/(MPA)$^{1.5}$ (hr)$^{0.5}$

and $2.1 \times 10^{-8} m/(MPA)^{1.5}(hr)^{0.5}$. These results can be reduced to the following which bears the same form of Eqn. (5.12),

$$\frac{1}{\dot{\varepsilon}} \frac{h_i(\psi_i)}{a_i} \frac{da_i}{dt} = \left[\frac{c_i^2 h_i(\psi_i)}{2A^{1/3}} \left(\frac{kT}{D_b \delta_b \Omega}\right)^{2/3}\right] \left(\frac{\ell_D}{a_i}\right)^2$$

where A is the coefficient in the creep law $\dot{\varepsilon} = 1.77 \times 10^{-14} \left(\frac{\sigma}{MPA}\right)^7 sec^{-1}$ which was obtained by their results. Finally, coefficient in the above representation is estimated by substituting materials constants with appropriate values*, to give

$$\frac{1}{\dot{\varepsilon}} \frac{h_i(\psi)}{a_i} \frac{da_i}{dt} = 55 \times 10^{\pm 0.66} \left(\frac{\ell_D}{a_i}\right)^2$$

where the geometric mean of C_i was used for estimation. Hence the observed growth rate, interpreted in terms of growth of quasi-equilibrium cavities, is $10^{4/3}$ to $10^{2/3}$ time faster than predicted by the theory. Although the stress and time dependence are exactly the same as predicted.

(B) Goods and Nix on Silver with Implanted Water Bubbles

Goods and Nix used silver with prior implanted water bubbles in their study of cavity growth (103). Rupture time and rupture strain were recorded for each test at several temperatures between 200°C and

---

* (65,104,106,107,108)

$D_b \delta_b = 10^{-21 \pm 1} m^3/sec$, $h(\psi) = 0.75$ (65), $\Omega = 7.1 \times 10^{-6} m^3/mole$

$RT = 6.02 \times 10^{23} \times KT = 8.1 \times 10^{-3} MPA/mole$

and 550°C and a correlation $t_r \propto \sigma^{-3.7}$ exp (85.5/RT KJ/mole) was reported. These results were discussed by their authors in terms of surface diffusion controlled growth using Chuang's model (65) in the limit of $D_s\delta_s/D_b\delta_b << 1$, a condition which obviously was not satisfied in all testing conditions (104).

To apply our theory to this study, we find it convenient to express the average growth $\langle 4\pi h(\psi)/\dot{\varepsilon} a\, da/dt \rangle$ in terms of failure strain. This procedure is appropriate since, for such short testing time as was employed in this study, $a_f/a_i = 1.40$*. For $\langle\dot{\varepsilon}\rangle$, we use ε_r/t_r, for the steady rate in creep were not reached in these experiments. (ε_r/t_r is several orders of magnitude higher than the steady state creep rate.)

Since $\langle 4\pi h(\psi)/\dot{\varepsilon} a\, da/dt \rangle = 4\pi h(\psi) \ell n(a_f/a_i)/\varepsilon_r$, we can plot $4\pi h(\psi) \ell n(a_f/a_i)/\varepsilon_r$ vs. a_i/ℓ_D in Fig. 6.5. The two branches which bracket these results were from the theory, Eqn. (5.8), with α chosen as shown. The value for α is reasonable for the experimental conditions.**

---

*To obtain this estimation, we used $a_f = b_o/4 = 1.1$ μm and $a_i = 0.785$ μm. The values of these quantities were first reported by Goods and Nix (103) but were later corrected by Pharr and Nix (102) from which these values were drawn. In addition, $D_b\delta_b = 6.0 \times 10^{-15 \pm 1/2}$ exp (- 90.3/RT KJ/mole) m^3/sec, (65, 104,109,110); $\Omega = 10.3 \times 10^{-6}$ m^3/mole, RT = i.5 x 10^{-4} x T(°K) MPA m^3/mole, $h(\psi) = 0.61$ (65), $\gamma_s = 1.14$ J/m^2 (65).

**D_s for silver is not known for certainty, we found

$D_s = 2.5 \times 10^{-6}$ exp (- 84.5/RT KJ/mole) m^2/sec (102,103,111)

$D_s = 4.5 \times 10^{-6}$ exp (- 49.1/RT KJ/mole) m^2/sec (65)

and $D_s = 1.4 \times 10^{-6}$ exp (- 67.4/RT KJ/mole) m^2/sec (104).

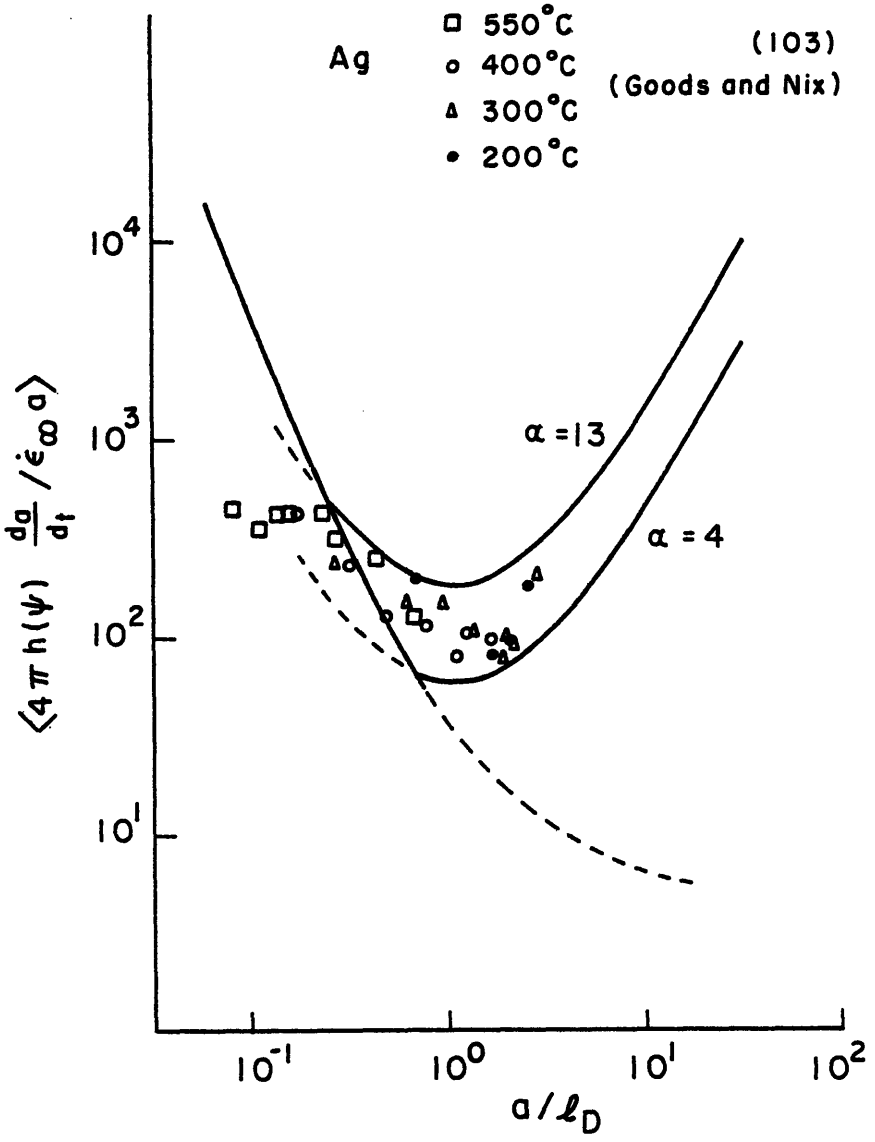

Fig. 6.5 - Comparison of the theoretical prediction with experiments of Goods and Nix

It is interesting to note that under the condition of fixed number of cavities, the rupture strain has a maximum, rather than a minimum, as stress is increased. This is in qualitative agreement with our theory.

CHAPTER 7

EXPERIMENTAL STUDIES OF INTERGRANULAR CAVITATION IN 304 STAINLESS STEEL

7.1. Introduction

Intergranular cavitation in creep has been thoroughly analyzed from the theoretical point of views in the preceding chapters. The assessment of the analysis should be made through extensive experimental studies. Despite much effort and continuing interest in this field over the past years, many fundamental questions regarding the dominant mode of cavity nucleation and growth remain mostly unanswered (34). This situation stems not only from the complicated nature of the kinetics of cavitation, in which both nucleation and growth are generally time dependent, but also from the difficulty in obtaining unambiguous measurements of the cavitation process. Moreover, creep deformation is highly inhomogeneous in nature and particularly so near the grain boundary, while cavitation is inevitably related to deformation of such nature. The lack of diffusion data, or the uncertainty in those available,further discourages attempts of making quantitative comparisons between theories and experiments.

Recently, a fractographic technique (101, 49, 62) was developed to facilitate direct observations of intergranular cavities at all stages of deformation. Another technique of superficial observation of intergranular cavities on sectioned or polished surface, in which etching is avoided, has been developed in this study. Experiments using these techniques are described in this chapter and their results are evaluated in the light of the analysis presented in the preceding chapters.

7.2. Materials and Testing

7.2.1. Materials

Two batches, I and II, of commercial 304 stainless steel were used in this study. Batch I originally came in the form of hot rolled annealed bars of 63.5 mm x 19.6 mm and was previously crept in bending at 750°C for 24 hours by Gertner (112). The grain size was determined by conventional techniques to be 0.1 mm. Six charpy bars, numbered cp1-cp6, were machined from this material with notches cut perpendicular to the principal strain direction in prior bending. The location of these specimens in relation to the pre-bending is shown in Fig. 7.1. The initial creep strain was determined from measurements of deformed circles engraved on the side surfaces of the bar prior to bending. The results are shown in Fig. 7.1.

Batch II came in the form of 7.9 mm dia. rods. This material was re-annealed at 1050°C for 0.5 hour followed by water quenching. Hour glass specimens, of 2.54 mm gauge dia. and 3.59 mm shoulder dia. with a 32.8 mm profile contour radius were machined from this material. Tensile bars of 16.5 mm gauge length and 3.59 mm dia. were also machined from the same batch.

In order to stabilize the distribution of carbides in the grain boundaries, some specimens were aged at 775°C for 40 hours. The grain size of material treated in this way was determined to be 40 μm. The distribution of carbides size (p), the ratio of coverage (f_L along grain boundaries, and the volume fraction (v_f) are given in Fig. 7.2.

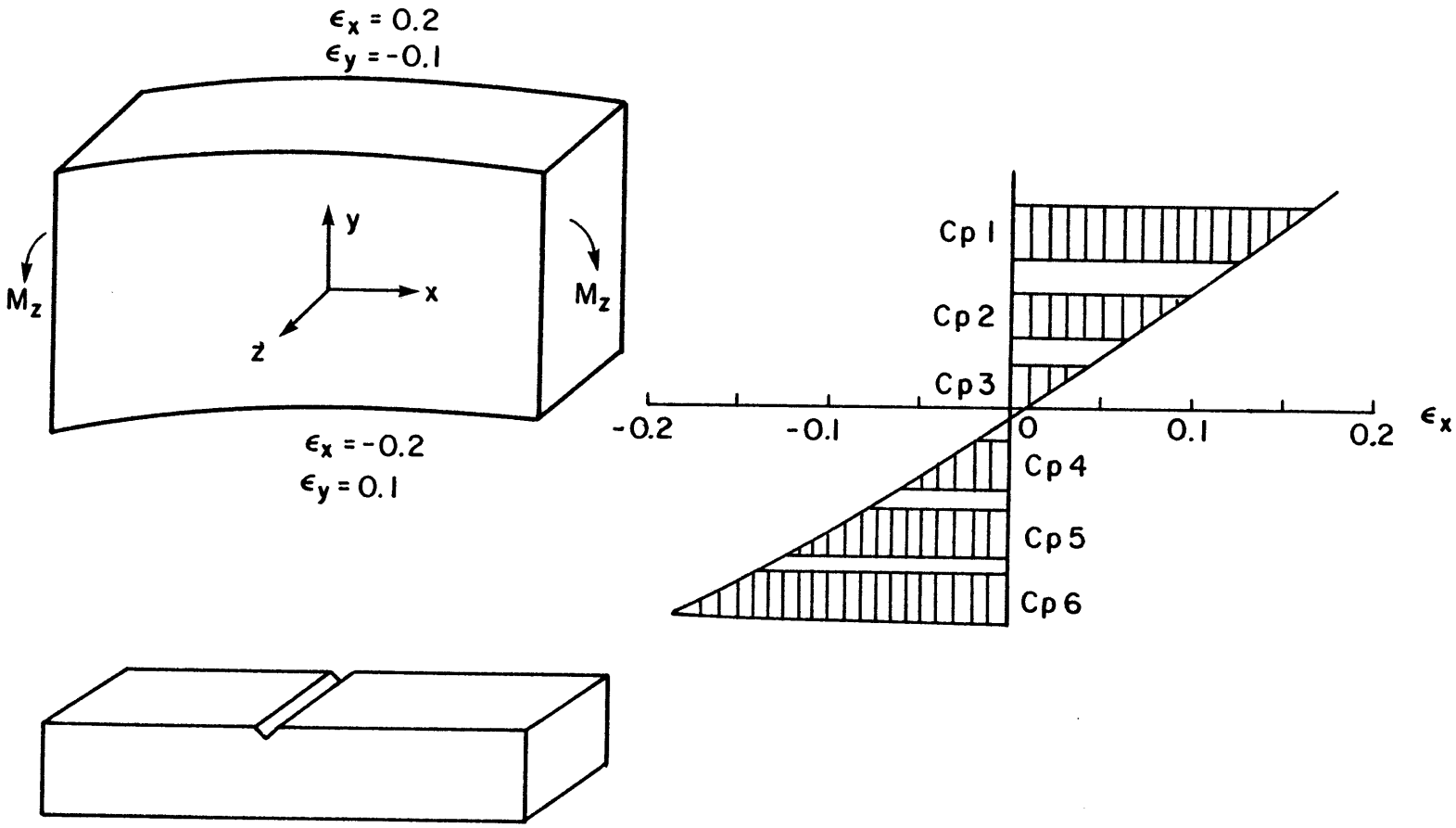

Fig. 7.1 - Configuration and strain distribution in charpy bars of prior-crept 304ss. (750°C/24 hr)

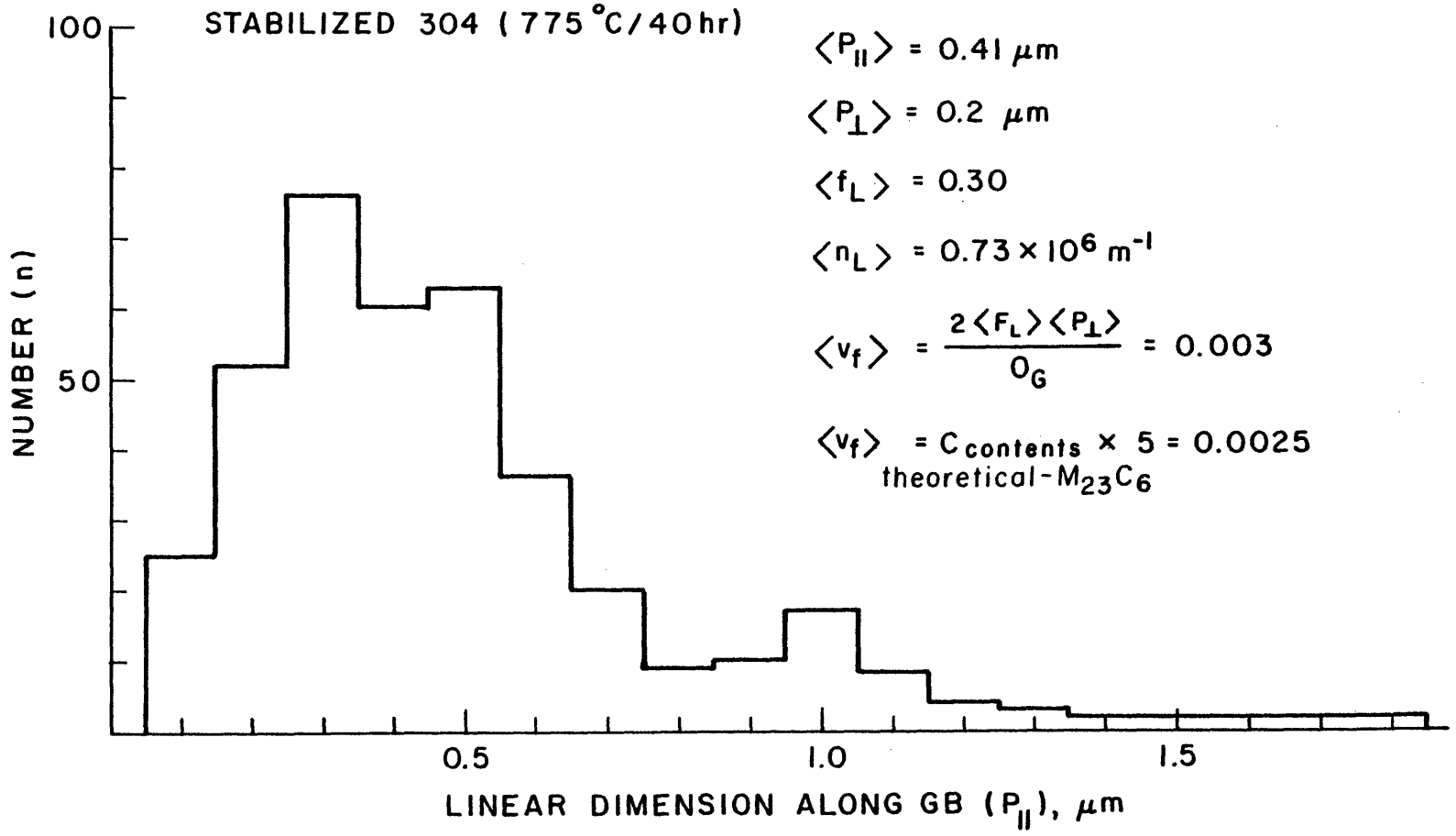

Fig. 7.2 - Distribution of GB Carbides

The carbide size p was measured by scanning electron microscopy on a polished section of the aged material which was "shock-etched" electrolytically in 10% H_2O solution of oxalic acid at room temperature. The volume fraction of carbides inferred from this measurement compares well with a theoretical estimate for that of $M_{23}C_6$ carbides in steels of 0.05% carbon content.

The size distribution of carbides shows a second peak at a size substantially larger than the more pronounced first peak. This second peak is associated with carbides which grow preferentially at intersection of grain boundaries or twin boundaries. It was also found that statistically significant variation of sizes exists among grain boundaries. In general, no simple description based on a single morphology seems appropriate for grain boundary carbides. Detailed study of this subject by Wilson et al. found a variety of carbides shaped as dendritic rods, lace-like sheets, or coarsened spheroids among others which all coexist in the same material (113, 114, 115, 116). These morphologies were also observed in the present study.

7.2.2. Testing

Specimens were loaded uniaxially in tension in vacuum in a special creep apparatus shown in Fig. 7.3. It consists of a lever loading setup which maintains fixed lines of actions tangential to two concentric circular pieces at two ends of the lever respectively. This feature is important to the accurate alignment of the specimen as well as to the implementation of a constant stress device attached to the loading pan. This device was made of a spring, whose spring constant was

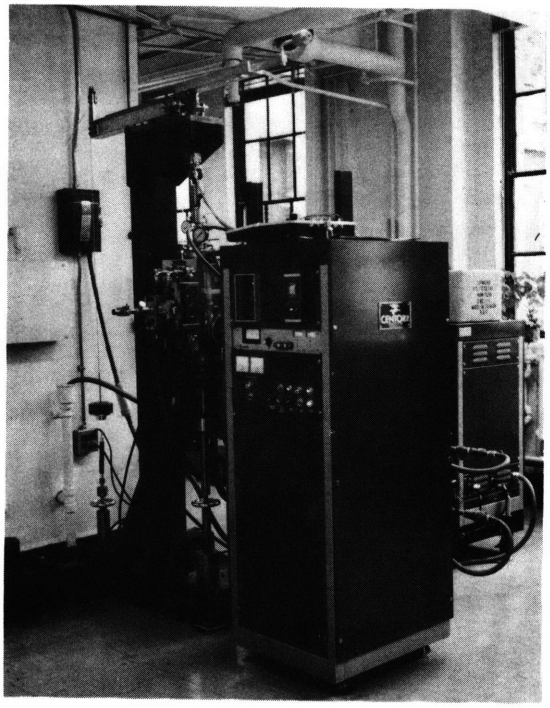

Fig. 7.3 Creep apparatus with a constant stress attachment.

adjusted by varying its length. The spring relaxes as the specimen elongates in the right amount to keep the stress constant. The device is capable of maintaining a constant stress within 1% up to 10% true strain and was used for cavity growth experiments. The specimen was engaged to a set of slotted grips into which the specimens were inserted, to be loaded at their rectangular shoulders. The vacuum during the test was better than 5×10^{-6} torr. Indeed, after an initial heating and pump out period, the vacuum was typically 5×10^{-7} torr.

Strains were measured by several methods. The total elongation between pull rods was measured using a cathetometer located outside the chamber. The measurement was compared with actual elongation of the gauge section measured optically during and after the test for calibration. Diametric contraction was also monitored optically during the test and calibrated by measurement after the test. Accurate and direct measurement however was hindered by the low magnification of the telescope due to the long working distance between the objective and the specimen surface.

7.2.3. Observation of Cavities

A. Two-Stage Creep Technique

Since etching is known to round off cavities and to attack carbides preferentially, a new technique was developed for this study which avoids etching completely. After each test, a layer of about 50 μm thickness was removed from surface by polishing using SiC paper and diamond paste. Subsequently the polished specimen was subject to a short additional increment of creep under identical conditions of the

previous test. Without exception the re-creep strain increment was less than 10% of the prior creep strain. This procedure produced a small increment of grain boundary sliding that delineated grain boundaries and revealed intergranular cavities on a generally smooth surface.

Using the technique, it was possible to detect cavities as small as 0.2 μm, as is shown in Fig. 7.4. It is to be emphasized here that cavities detected by this technique were used only for number counts, and no importance was associated to their size and shape.

B. Cryogenic Fracture Technique

Charpy bars from batch I and tensile specimens from batch II, having been held for more than 24 hours at temperature between 600°C and 775°C in aging or creep, fractured intergranularly at 77°C under impact (117). Cavities as small as 0.5 μm dia. were readily identified by this technique. In addition, examination of the mating pieces provided a powerful tool to study fine features of cavities and to ascertain that no holes accidentally introduced at particle-matrix interfaces in the intergranular cracking after the creep experiment was over were mistaken for creep cavities.*

Considerable details of grain boundary structures were seen on these fracture surfaces. Significant variation of these appearances exists among grain boundaries. Energy-Dispersive-X-ray Fluorescence technique failed to identify unambiguously these structures as carbides,

---

* It is possible that some of the separations between particles and matrix were indeed nucleated by very small creep cavities beyond our resolution.

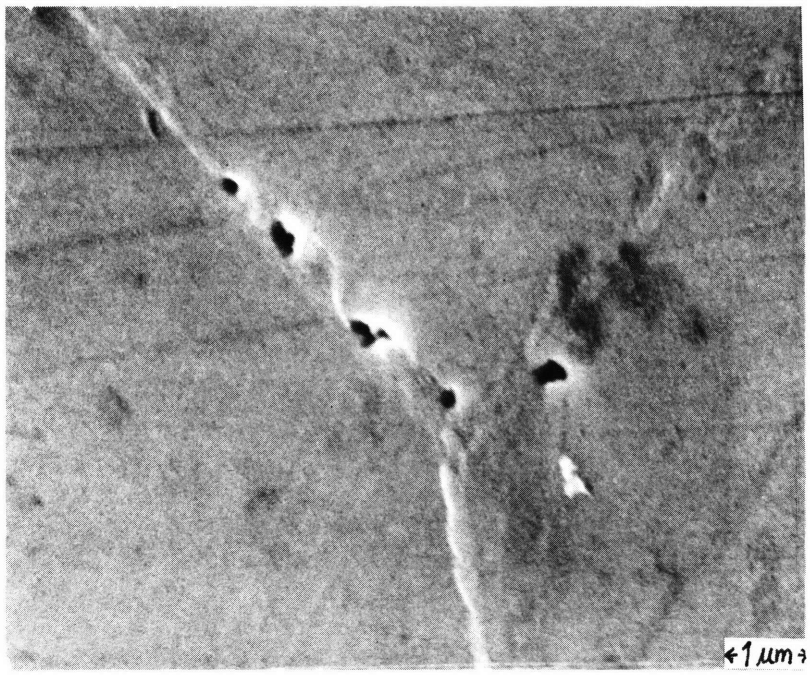

Fig. 7.4Cavities on inclined sliding boundaries,
Vertical direction is the tension direction.

presumably owing to the inadequate resolution and a nearly complete carbide coverage on grain boundaries anyway (118). The presence of such structures, typically of a wavelength of 0.3 μm or smaller, also hinders direct identification of small cavities below this size.

7.3. Results of Quantitative Studies

7.3.1. Number Densities of Cavities Measured by the two Stage Creep Technique

Results of experiments (No. 13-18) on number densities of cavities are summarized in Figs. 7.5-12. These results are from experiments conducted under constant load at 600°C and 700°C using hour-glass specimen made of aged and annealed 304 stainless steel in batch II. Major features about cavity numbers in creep can be stated as follows:

(A) Number densities of cavities increase roughly linearly with creep time in the annealed material, while a slightly downward curvature in association with the rising curve in the aged material (Figs. 7.5, 7.7, 7.9). The magnitude of number densities of cavities in both materials are comparable at any given stress and time, although creep is much faster in the aged material.

(B) The dependence of the number density of cavities on the applied stress (Figs. 7.6, 7.8, 7.10) is far too weak to be characteristic of that of the threshold stress, $\dot{\zeta} \propto \exp(-4\chi^3 F_v / kT\, \sigma_n 2)$, predicted by the classical nucleation theory (53, 97, 98).

(c) Number densities of cavities were generally enhanced on grain boundaries oriented normal to the applied stress (Figs. 7.11-12). Indeed in aged material, the correlation between the normal component of the applied stress on the inclined boundary and the number of cavities

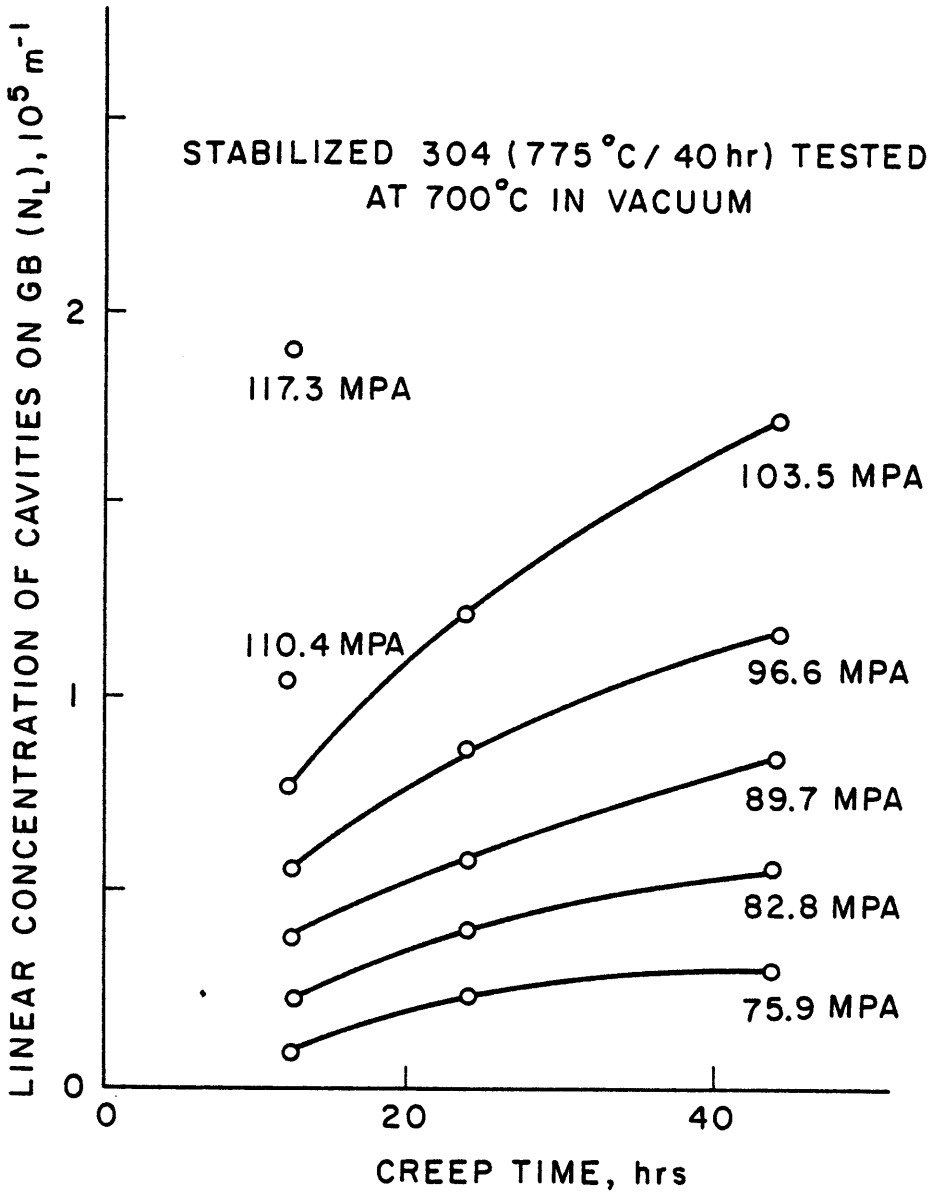

Fig. 7.5 - Variation of cavity concentrations with applied stress and creep time

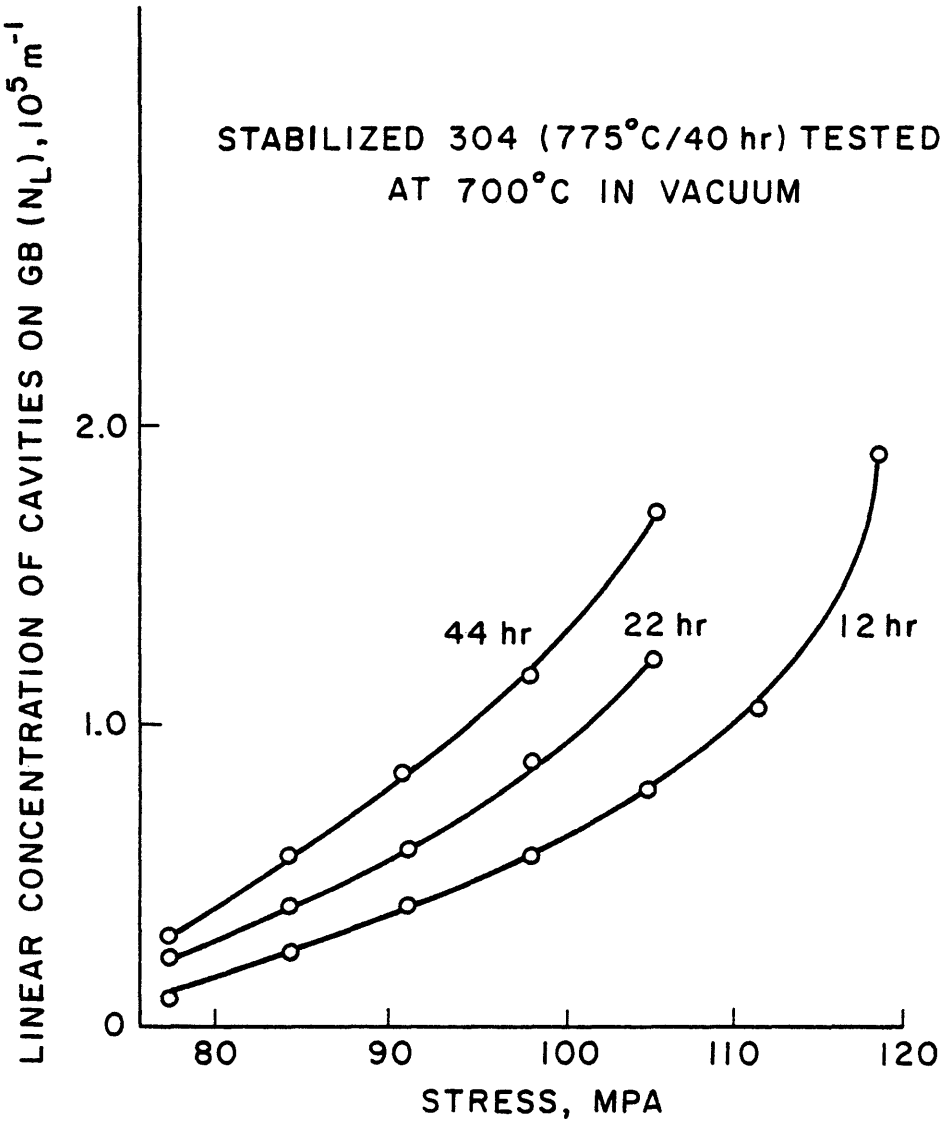

Fig. 7.6 - Variation of cavity concentrations with applied stress and creep time

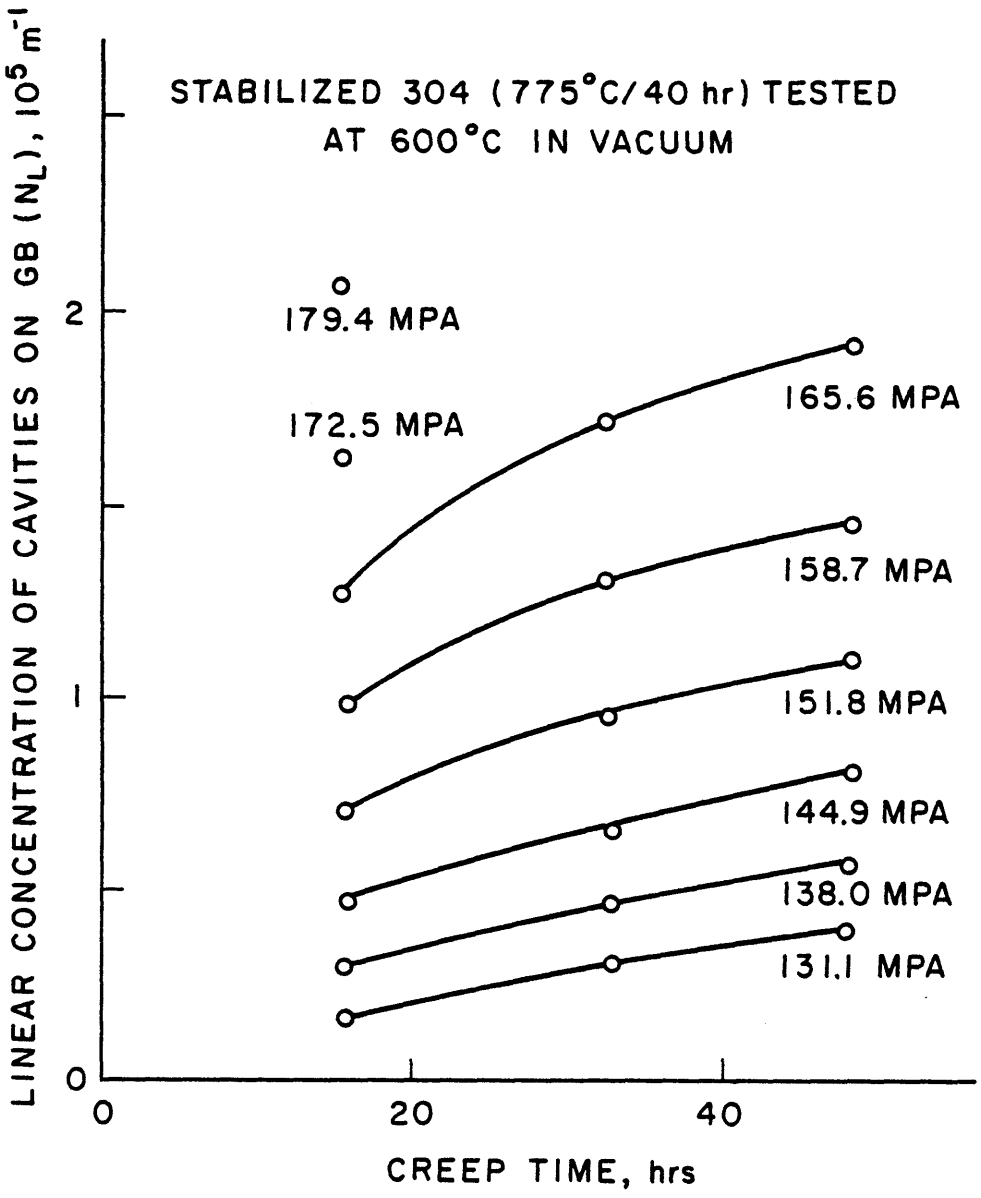

Fig. 7.7 - Variation of cavity concentrations with applied stress and creep time

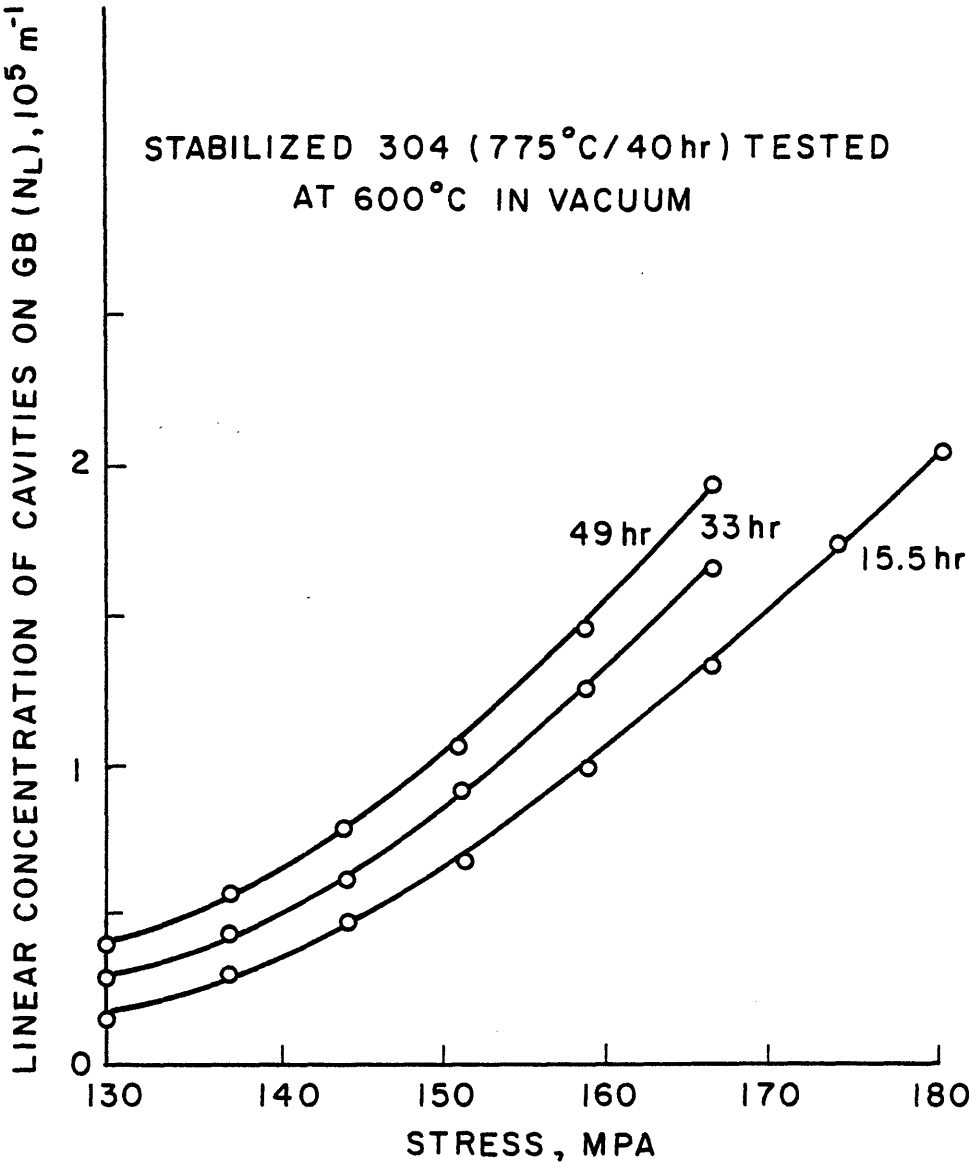

Fig. 7.8 - Variation of cavity concentrations with applied stress and creep time

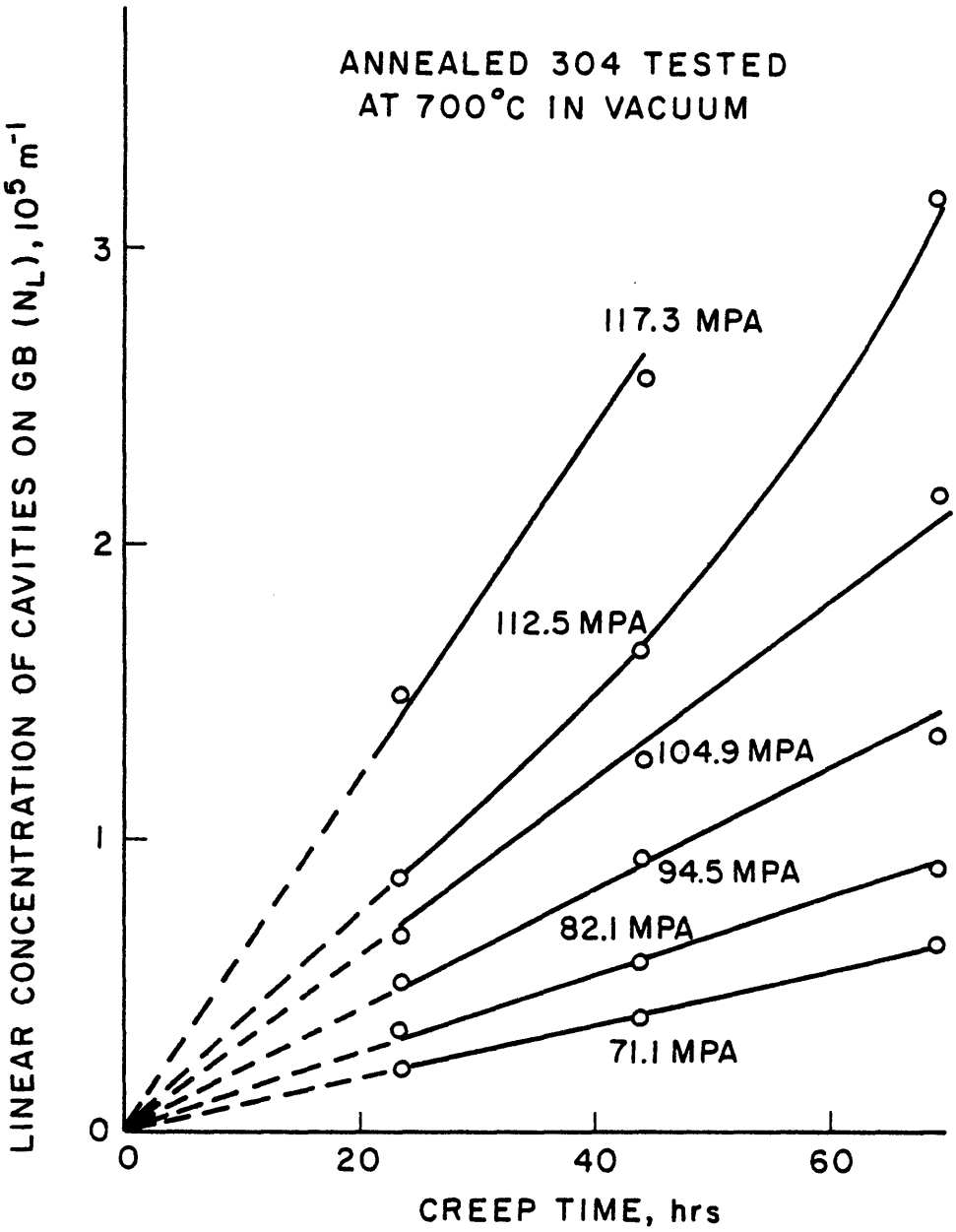

Fig. 7.9 - Variation of cavity concentrations with applied stress and creep time

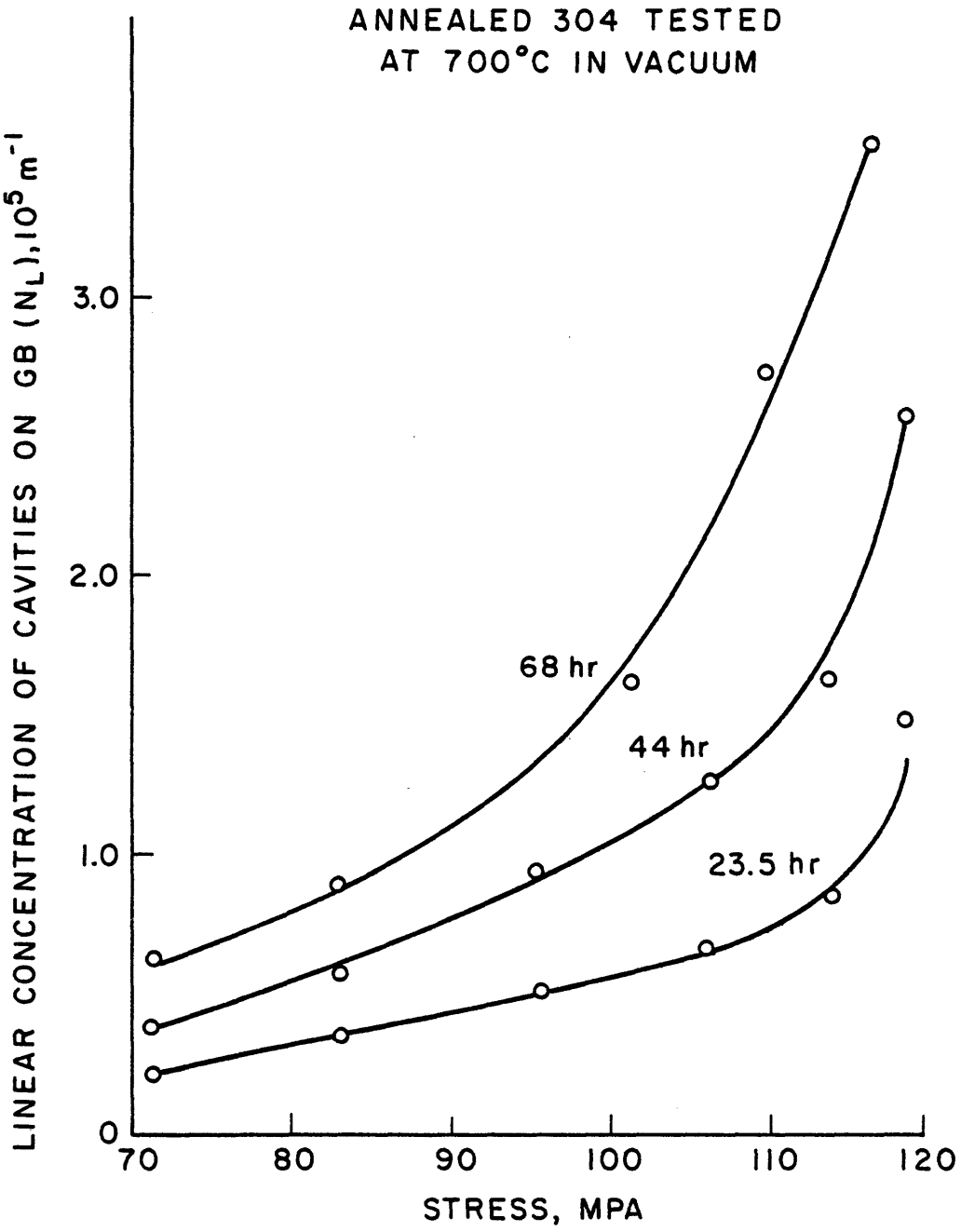

Fig. 7.10 - Variation of cavity concentrations with applied stress and creep time

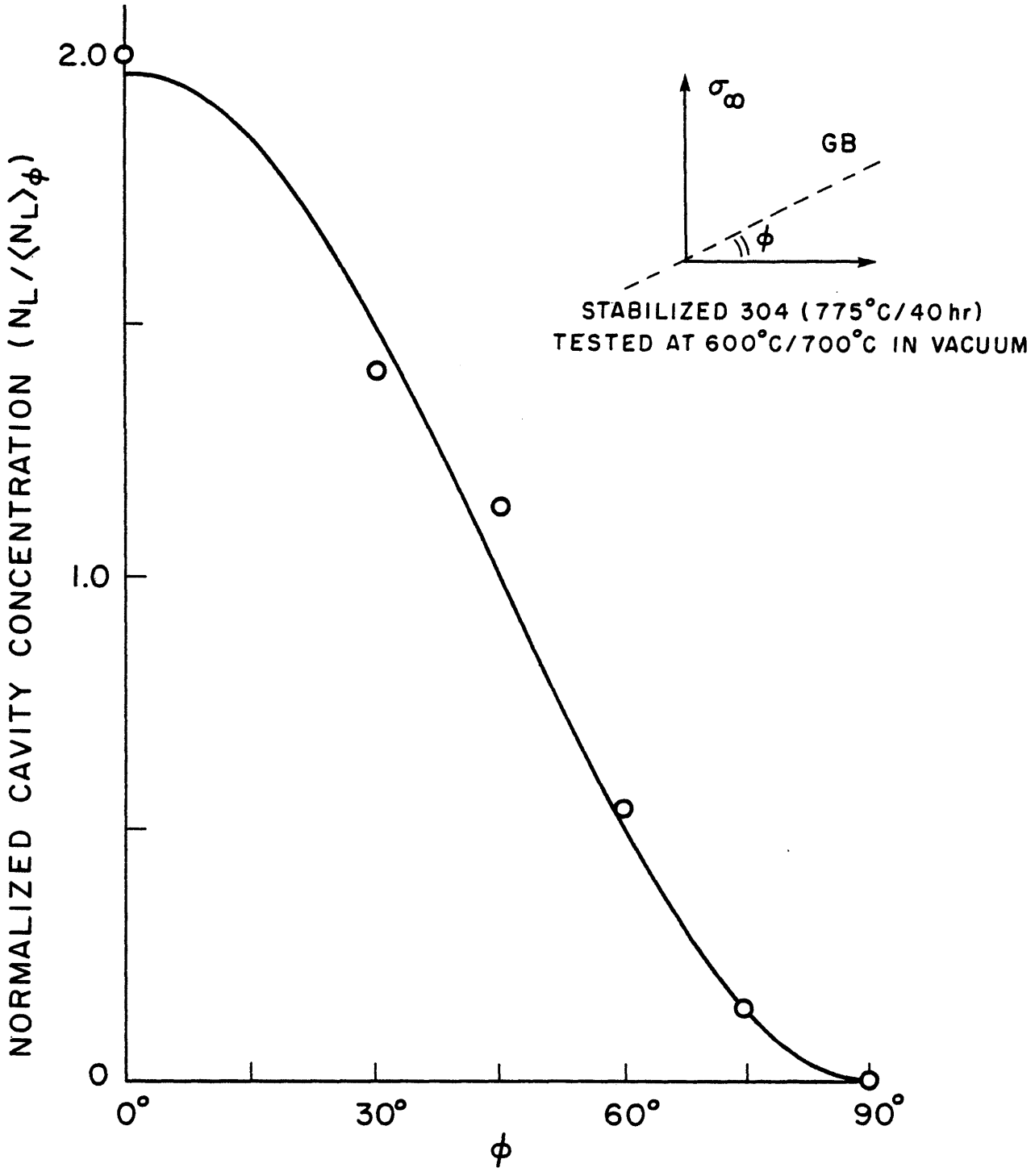

Fig. 7.11 - Variation of normalized cavity concentration with inclination between applied stresses and normal axis to GB

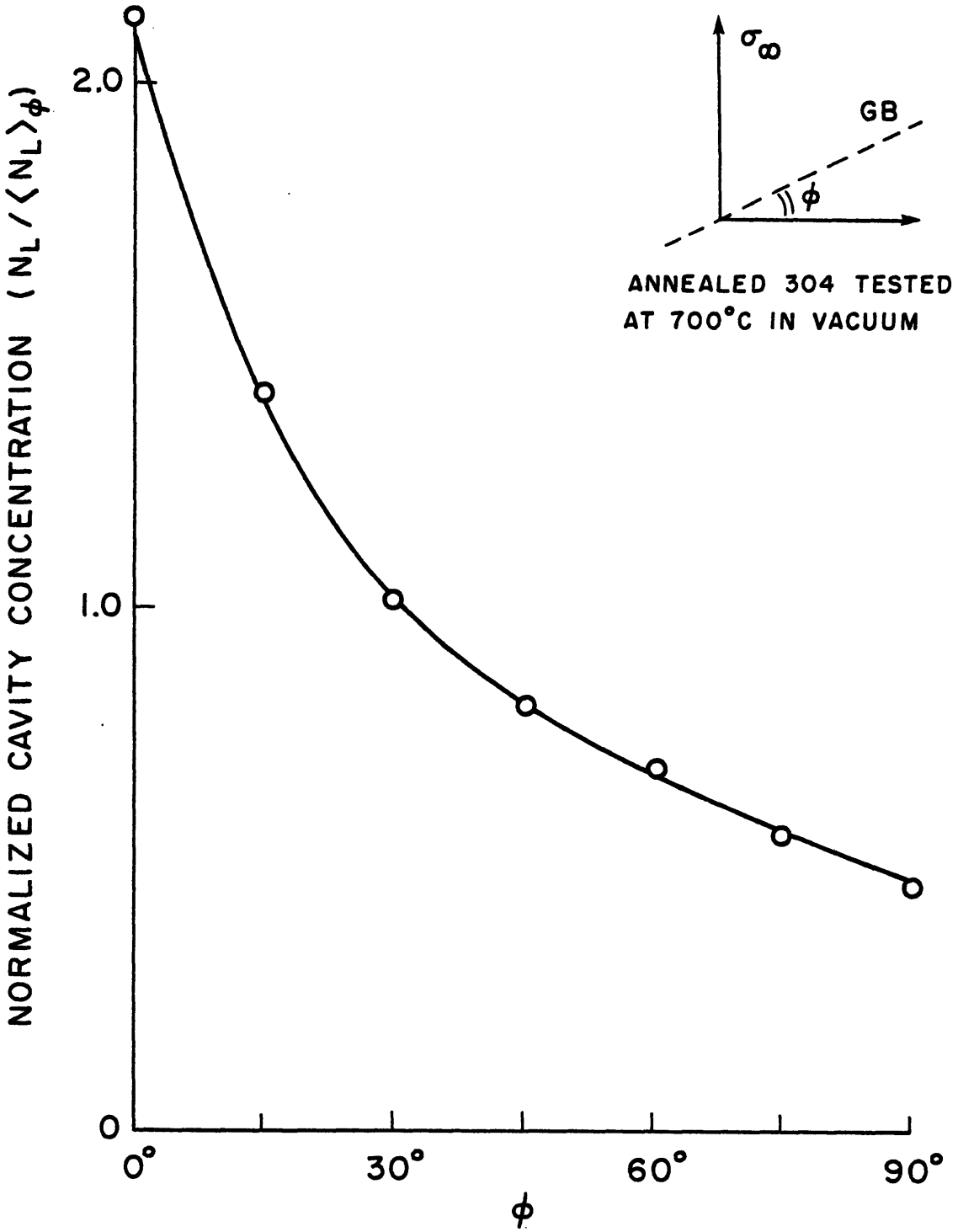

Fig. 7.12 - Variation of normalized cavity concentration with inclination between applied stress and normal axis to GB

appears to be very satisfactory.

7.3.2. Growth Kinetics Measured by the Cryogenic Fracture Technique

Growth kinetics measured by the cryogenic fracture technique from experiment (34-37) is summarized in Figs. 7.13-18. These results are from experiments conducted under constant stress (63.1 MPA) at 700°C using aged 304 stainless steel in batch II. The creep curve, together with the strain and creep duration for each specimen is plotted in Fig. 7.13. Major features about cavity growth can be stated as follows:

(A) The distributions of cavity sizes, similar throughout the creep life, is skewed toward small size cavities and has a long tail on the side of larger sizes as shown in Fig. 7.14. The peak gradually shifts toward larger sizes as creep strain increases. However, a significant increase of numbers of cavities of smaller sizes at a later stage shifts the peak backward.

(B) There are substantial variations of cavity size distribution among different grain boundaries. For example, Fig. 7.15 shows the distributions of cavities on three grain boundaries. Each of the three distributions is distinctly different from the overall distribution. Such variation and the diffuse distribution of cavities of larger sizes makes it difficult to associate the maximum cavity size with those cavities that nucleated at the very early stage as was done by Cane (101).

(C) Number densities, for each size group and as a whole, increase as creep time increases (Fig. 7.16).

(D) Accumulated damage, represented by the total cavitated area fraction on the grain boundary, given by $F_A = \pi/4 \sum_i N_{Ai} d_i^2$, increases

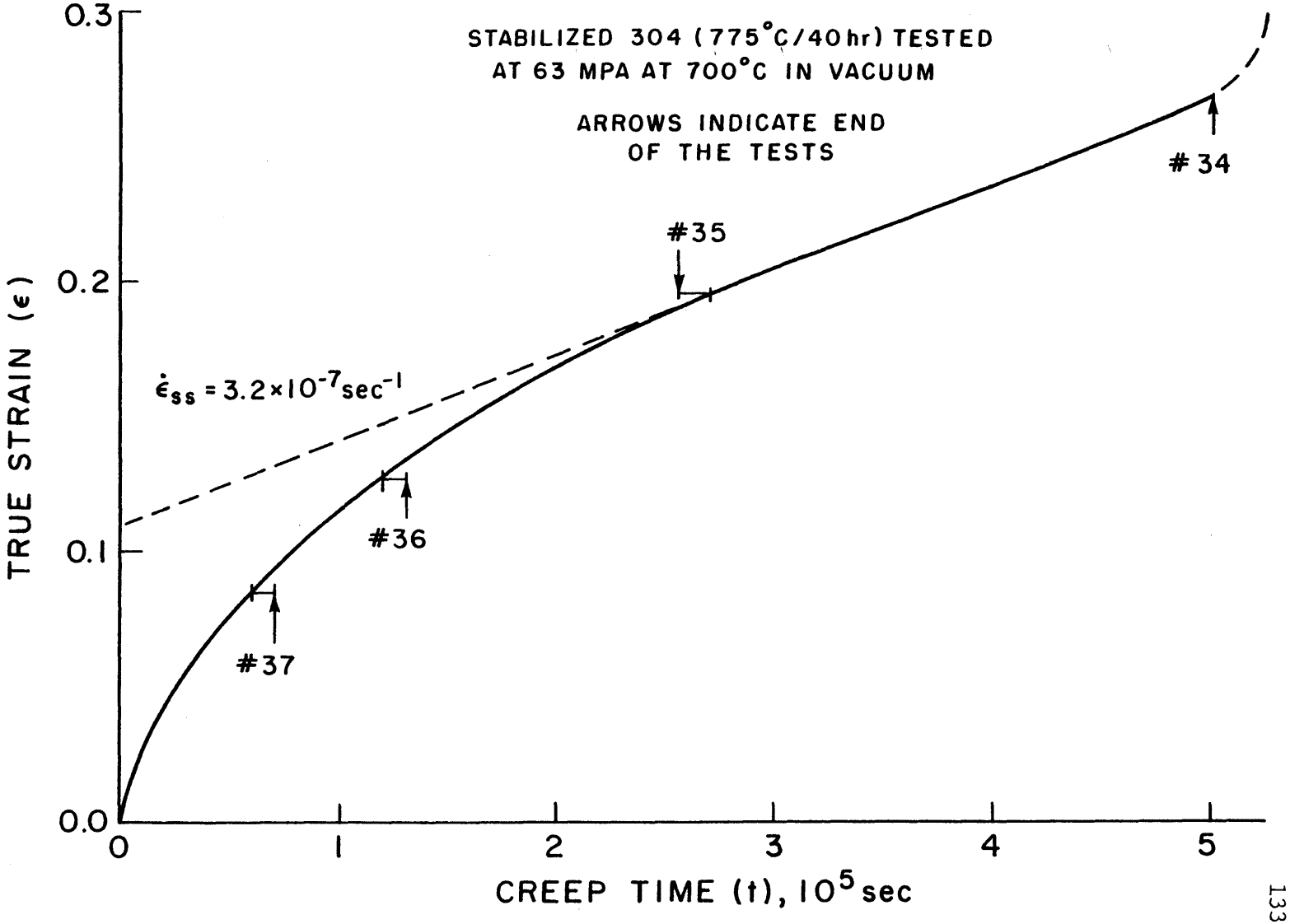

Fig. 7.13 - Creep curve of experiments on cavity growth

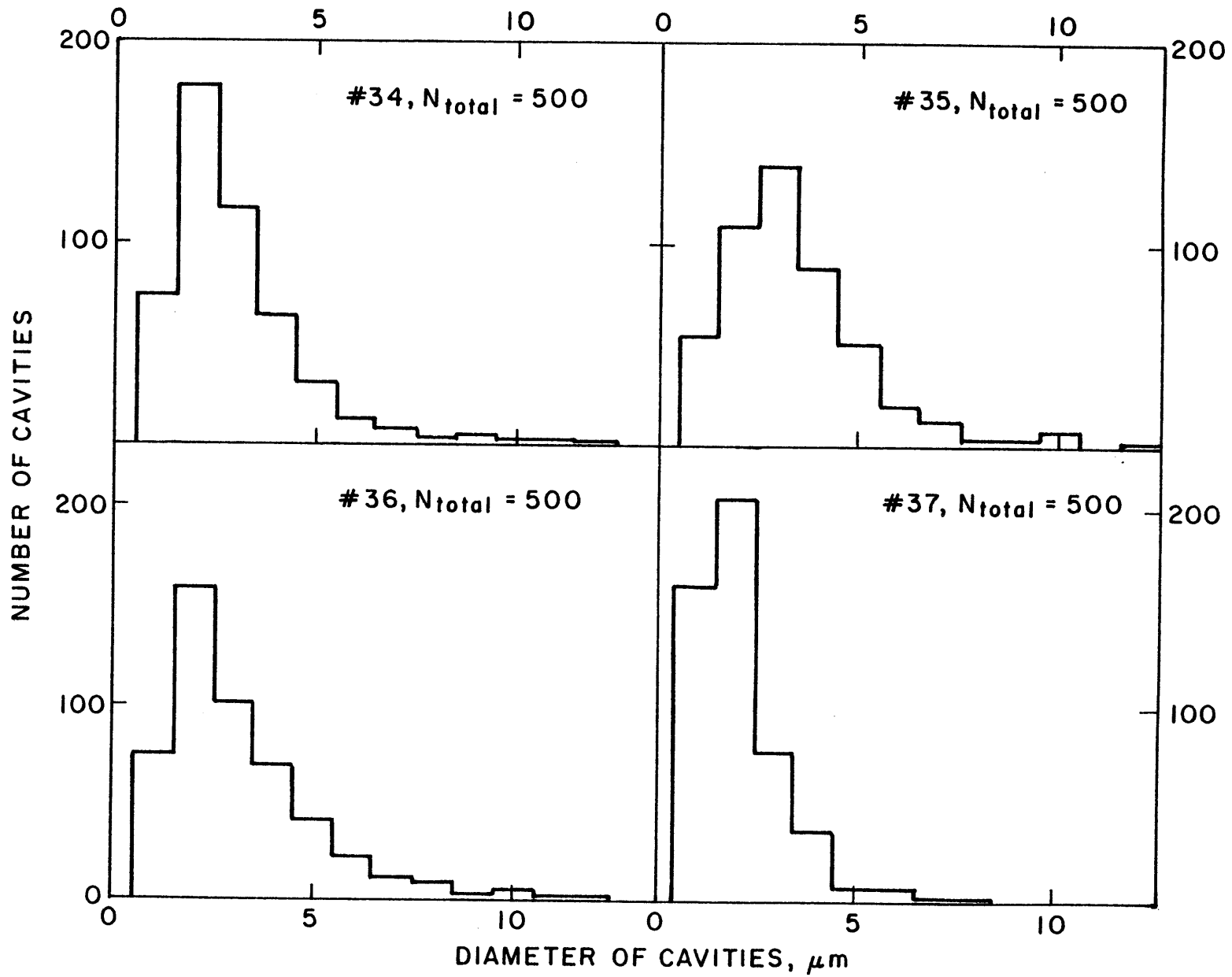

Fig. 7.14 - Size distribution of cavities

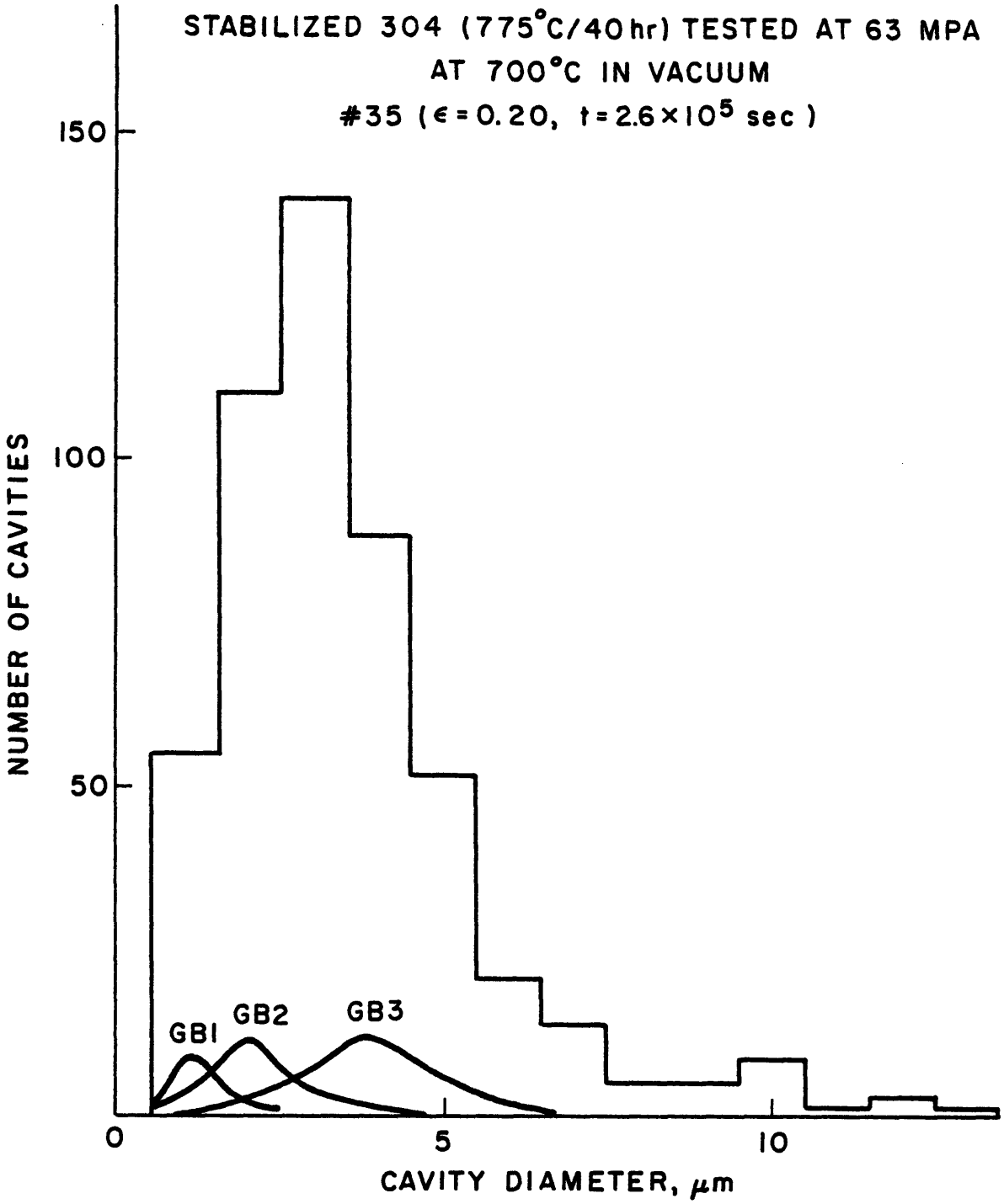

Fig. 7.15 - Overall size distribution of cavities over many GB versus size distribution of cavities on individual GB

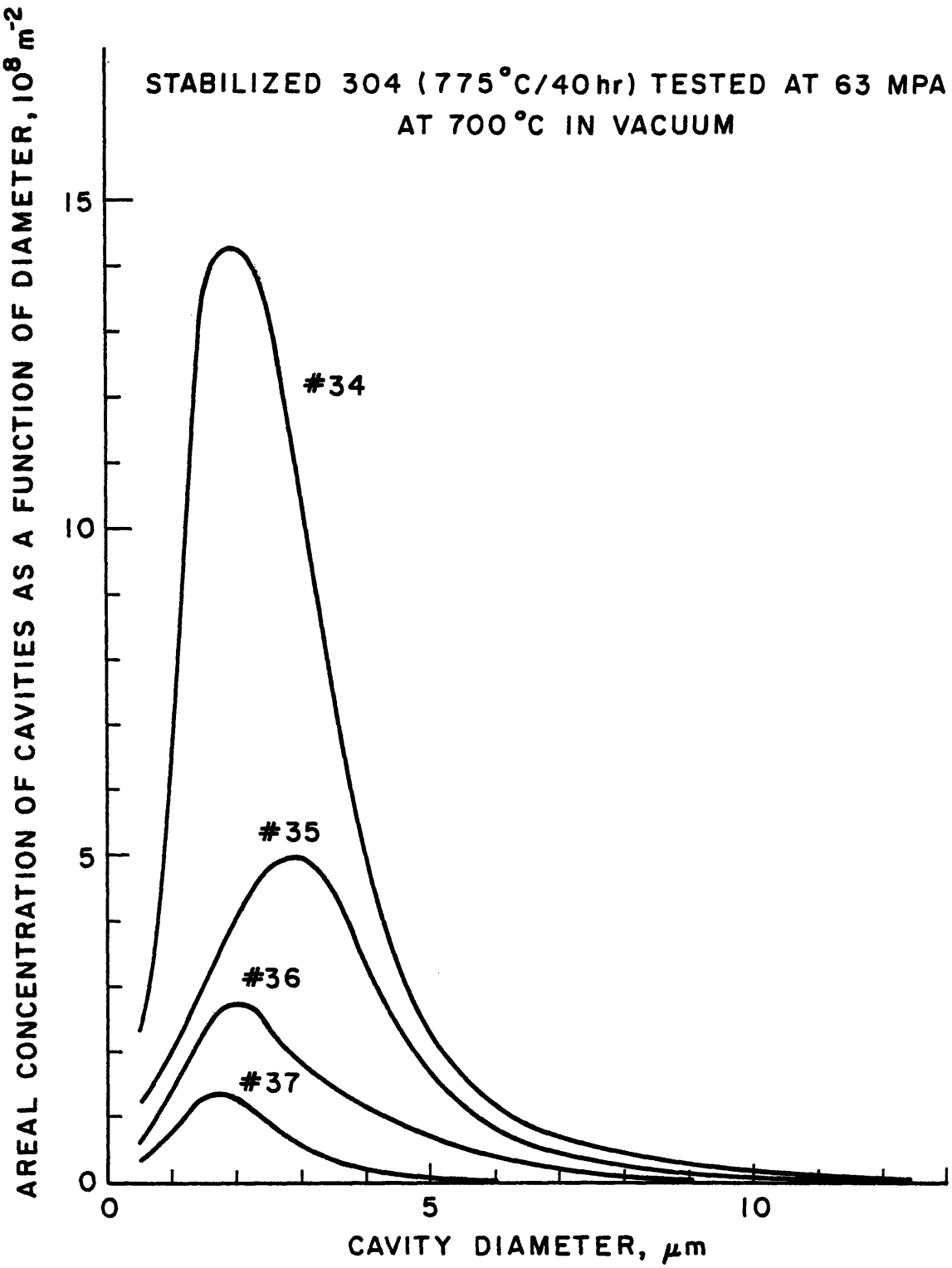

Fig. 7.16 - Variation of cavity concentration with cavity diameter and creep time

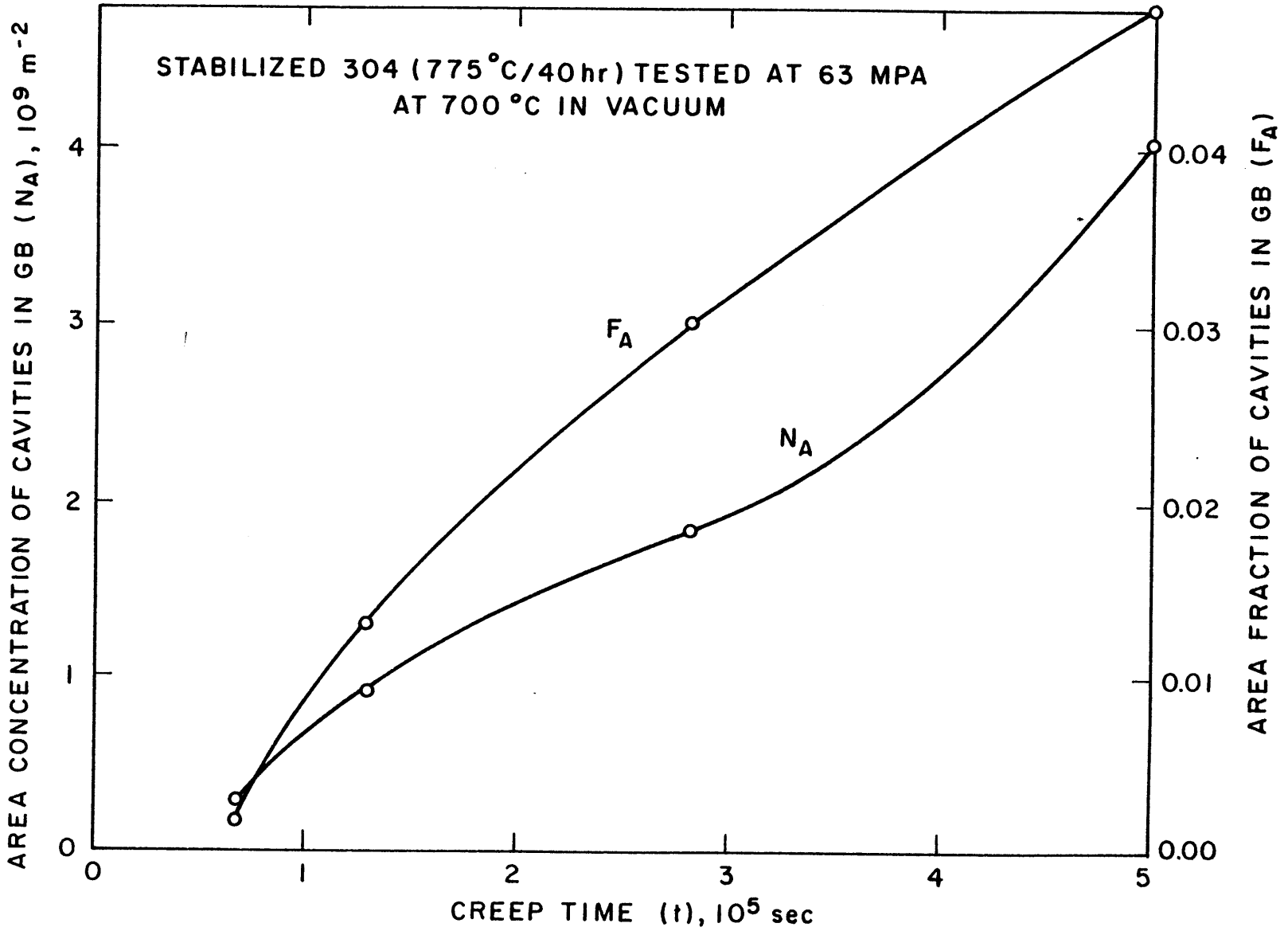

Fig. 7.17 - Variation of cavitation with creep time

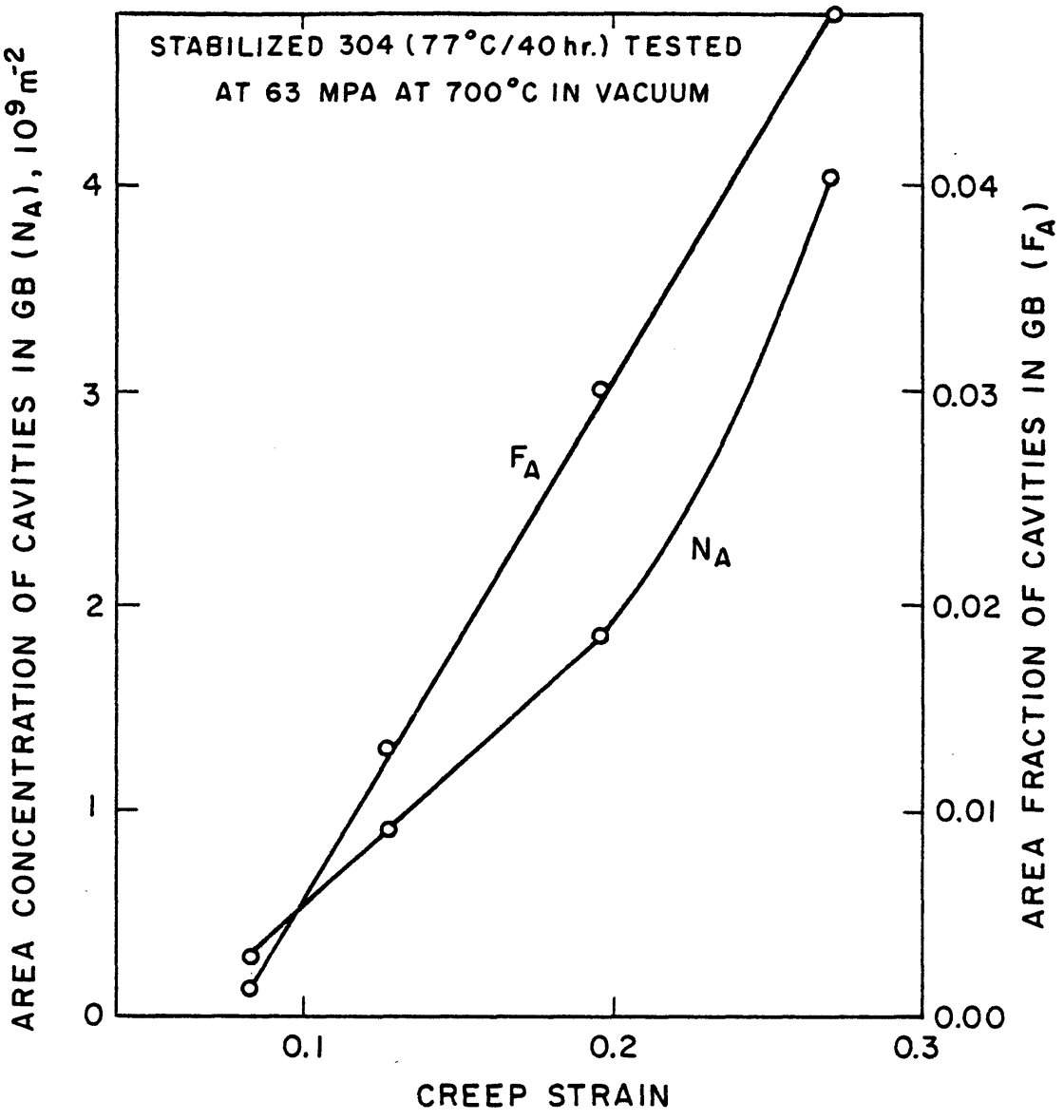

Fig. 7.18 - Variation of cavitation with creep strain

as is shown in Fig. 7.17. It is interesting to note that while F_A increases linearly with strain (Fig. 7.18), it has a downward curvature in the variation with creep time. The latter feature is also noted in the results previously described (Figs. 7.5, 7.7)*

7.4. Cavity Morphology and Distribution

In general, cavities revealed by the cryogenic fracture technique displayed the circular-disk like morphology in all specimens except at very high stresses as shown in Figs. 7.19-22. Frequently cavities were decorated with a thin film of carbide along the revealed interface which extended from the edge into the enclosed open space as shown in Fig. 7.20. In some cavities, crystallographic profiles with well-defined facets could be seen as in region A in Fig. 7.21 while for others the disk shaped profiles with shallow depth as in region B in Fig. 7.21 were entirely representative. Cavities were distributed heterogeneously throughout the grain boundaries as a typical region in Figs. 7.19, 7.21 indicates. Both the observed number and size of cavities were generally enhanced in the region of grain corners, where extensive cavity clustering and coalescence were frequently found as shown in region C of Fig. 7.21.

---

* In general, cavities observed by the two stage creep technique are more numerous in number but much smaller in size. Presumably this is due to the inability to identify small cavities by the cryogenic fracture technique. It is also possible that cavities of shallow, irregular shape, which are frequently decorated with carbides or matrix debris, may appear to be several smaller cavities on the sectioned surface.

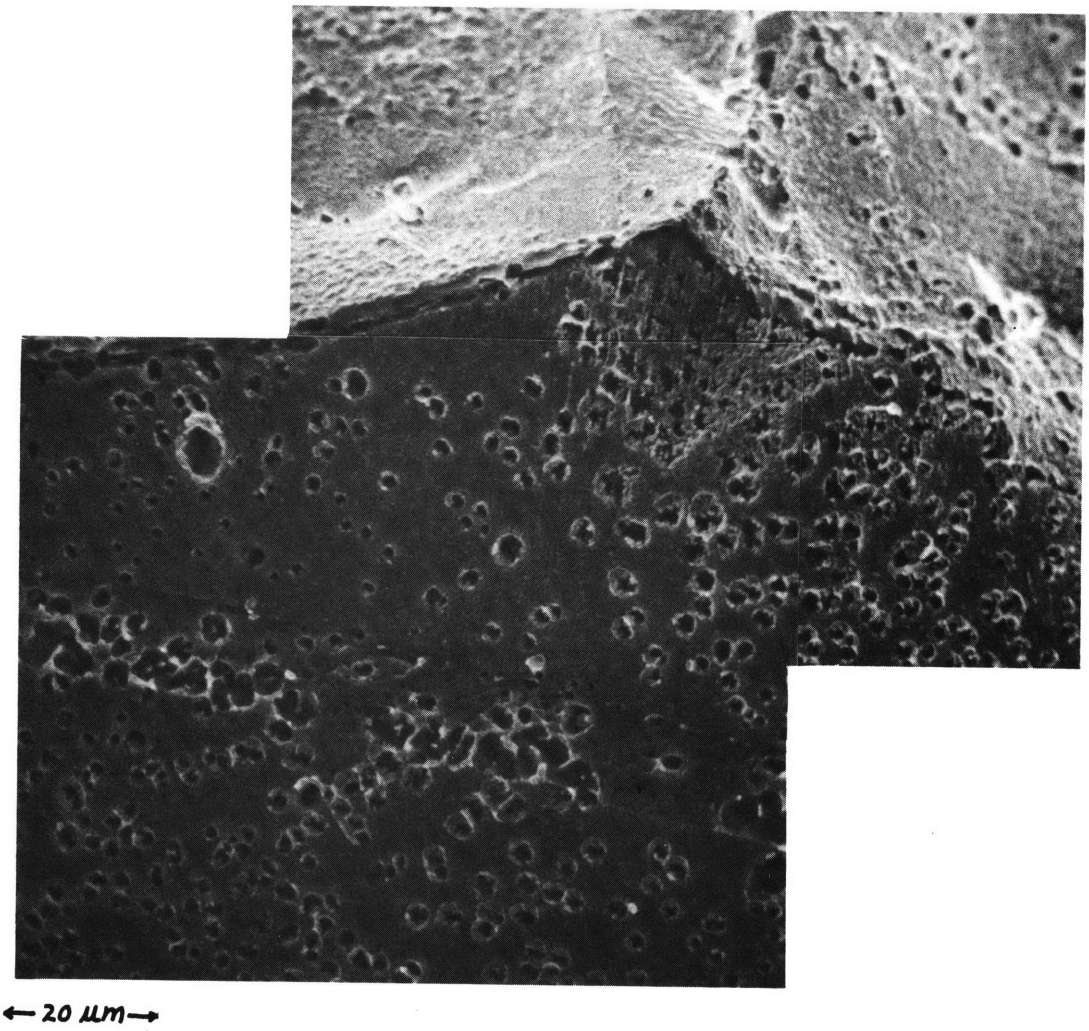

Fig. 19 ε = 17% at 750°C in 24 hours.

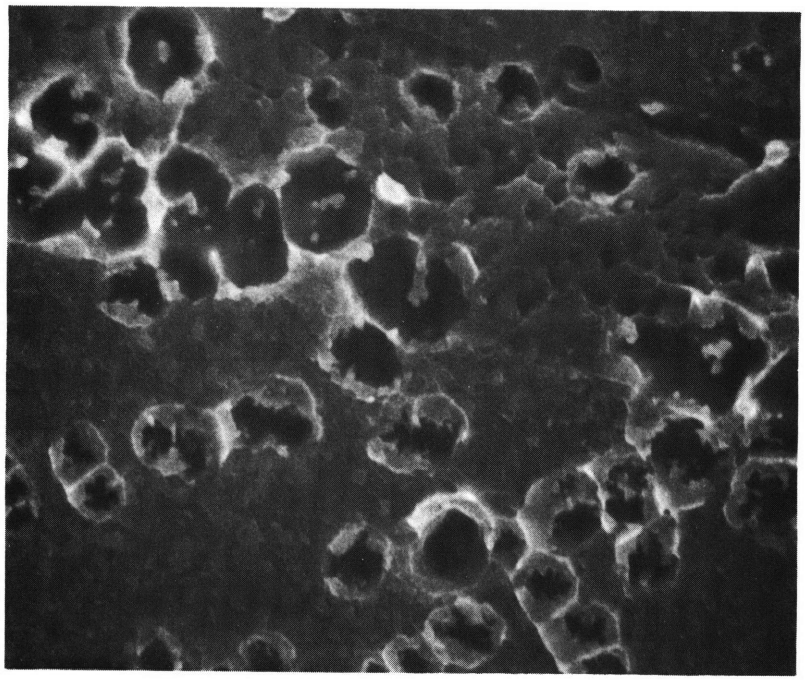

Fig. 7.20 ε = 17% at 750°C in 24 hours.

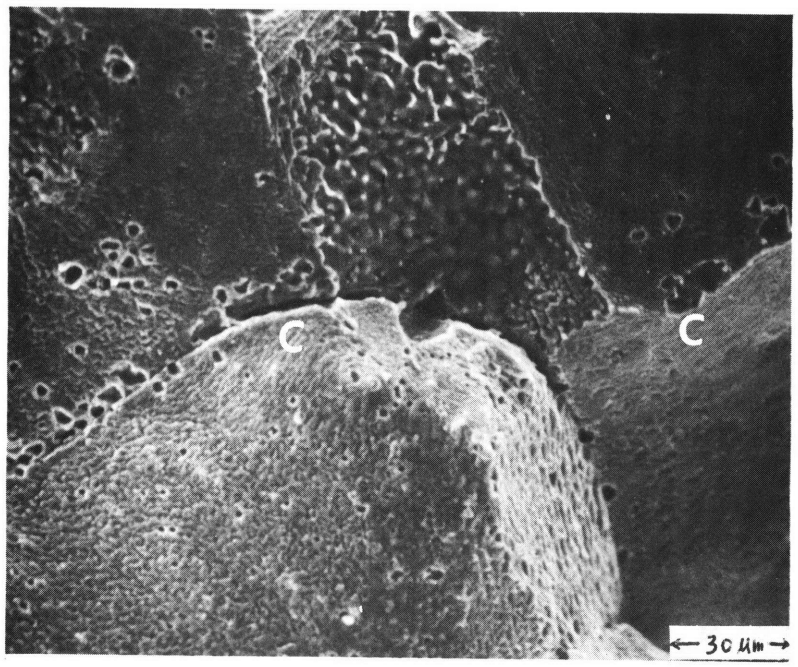

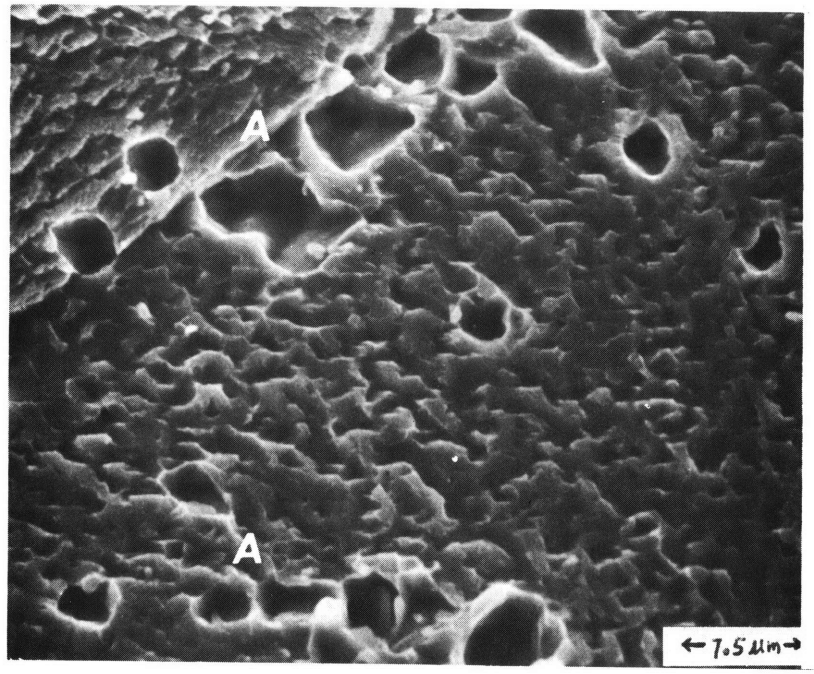

Fig. 7.21a Stress = 63 MPA
Strain = 19.5% in 72 hours at 700°C (#35).

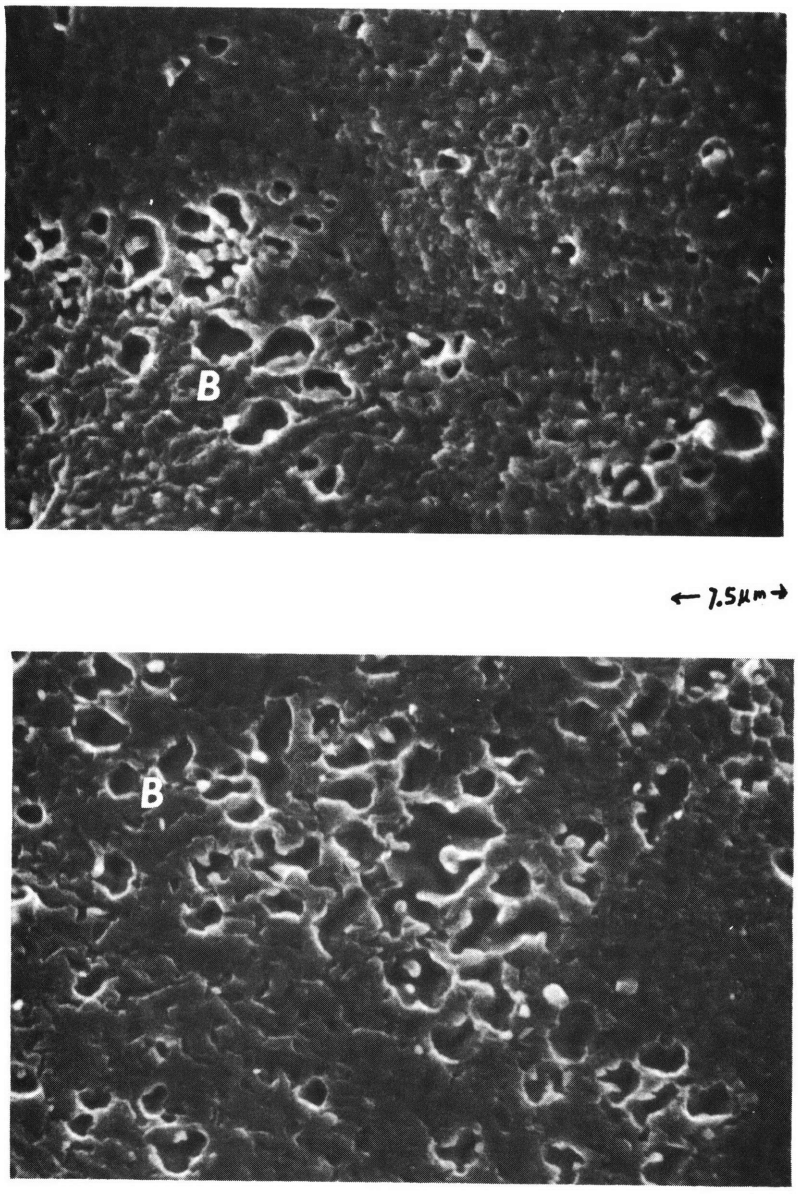

Fig. 7.21b Stress = 63 MPA
Strain = 27% in 139 hours at 700°C (#34).

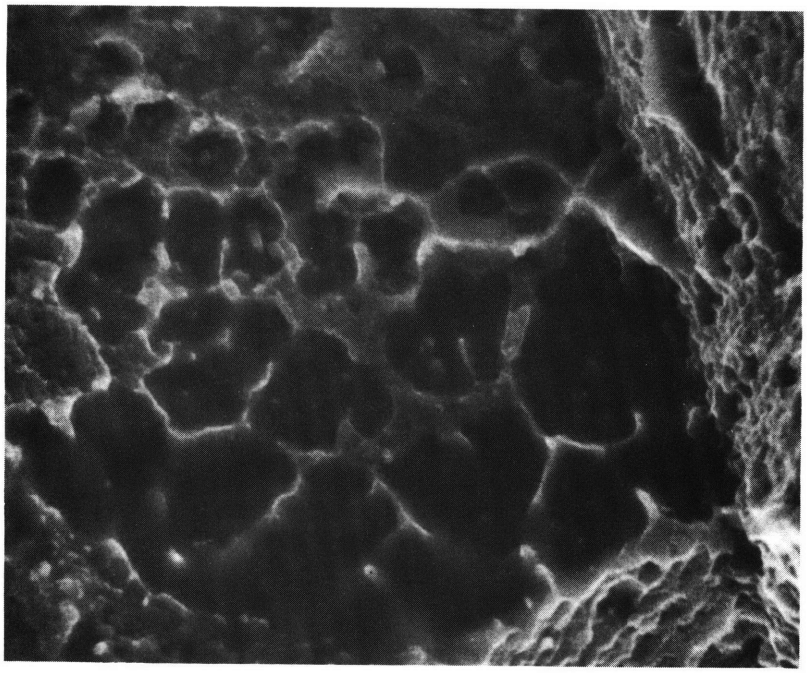

Fig. 7.22a ε = 17% at 750°C in 24 hours.

Fig. 7.22b Strain = 17% at 750°C in 24 hours.

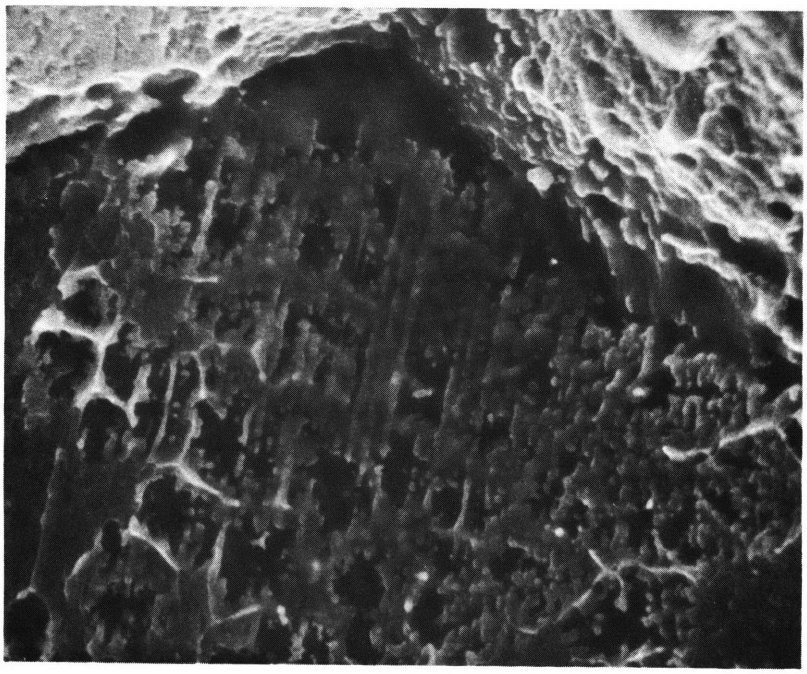

Fig. 7.22c ε = 17% at 750°C in 24 hours.

A comparison of number of cavities on grain boundaries of 90° and 45° inclination in relation to the applied stress direction was made for a specimen (Cp3) from batch I at 4% strain. The ratio of the number of cavities is roughly 2 in favor of the boundaries oriented normal to the applied stress.

Various stages of cavity coalescence were observed as is shown in Fig. 7.22. Neighboring cavities, frequently clustering, become impinge on each other and emerge as a sizable single cavity, or rather a micro-crack. A smoothed surface at the bottom of the cavity was frequently seen in such case indicating considerable surface smoothing that has occurred in time. Occasionally a dendritic structure was "deposited" on the sequence. It appears clear that all microcracks at grain corners were formed via coalescence of many smaller cavities. Indeed, this sequence of events was also observed on the surface of the specimen using the two stage creep technique and is shown in Fig. 7.23. There the coalescence of small cavities gave rise to a "wedge crack" at the triple point.

By far the most striking feature of cavitation in this material is its drastic variation with minor perturbations of the grain boundary structure. Intersection of twins with grain boundaries produces dramatic enhancement or suppression of cavitation depending on orientation and boundary structure as shown in Fig. 7.24. This was observed in every specimen tested. It was also noted that significant variation of cavitation also exists among different grain boundaries. It seems reasonable to suspect that all these variations have the same origin

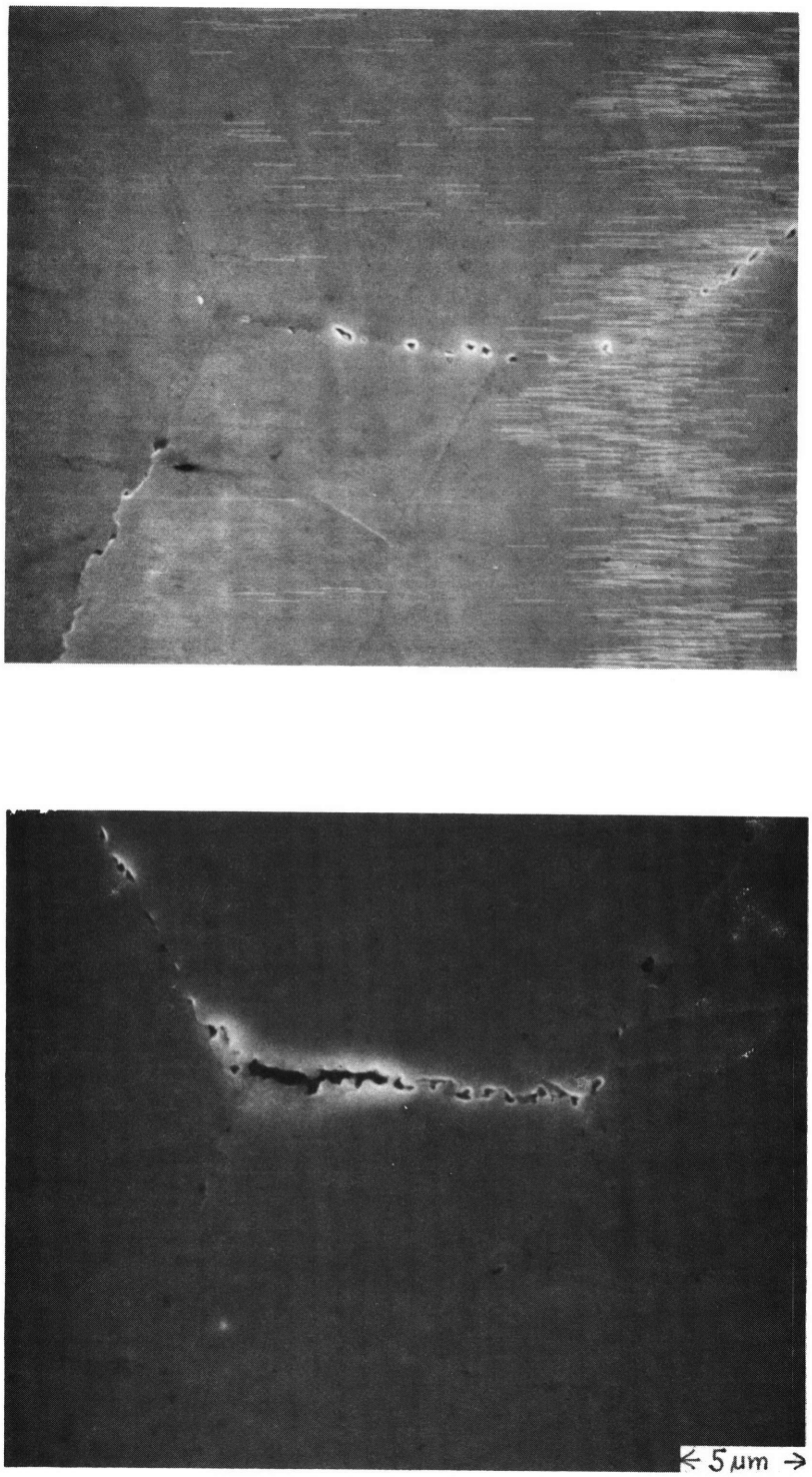

Fig. 23 Development of a wedge crack by the linkage of cavities.

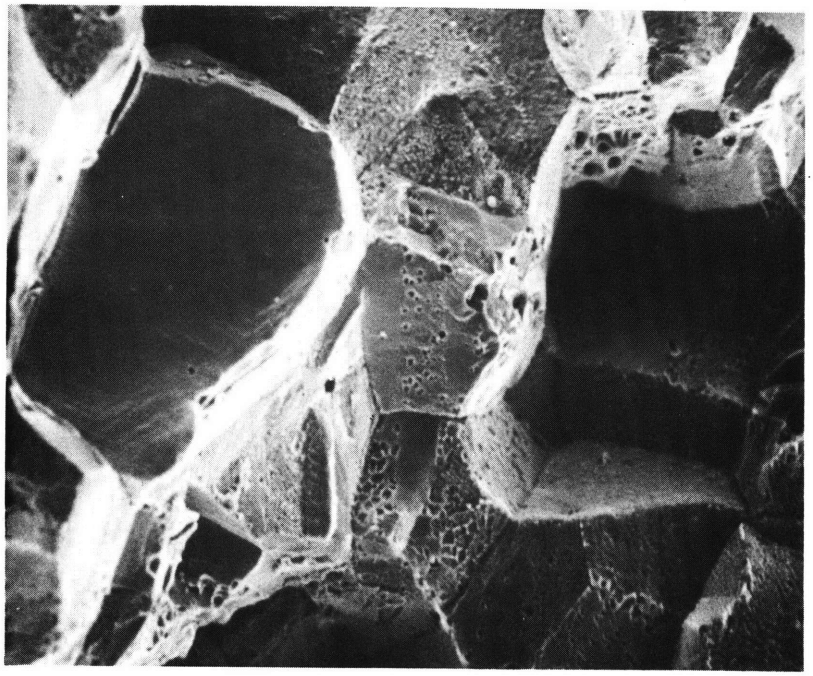

Fig. 7.24 a ε = 17% at 750°C in 24 hours.

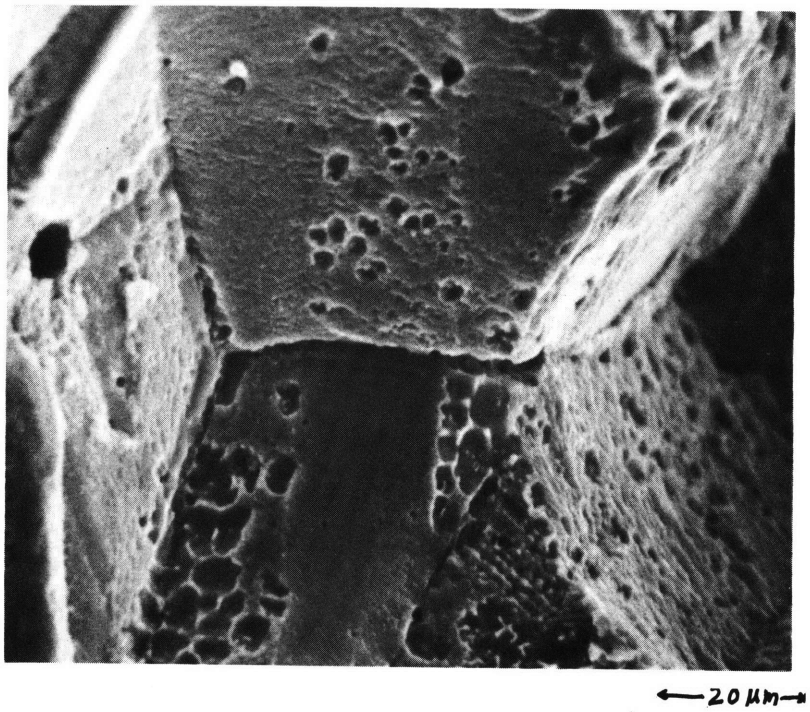

Fig. 7.24b Strain = 17% at 750°C in 24 hr

which is likely related to the misorientation between the grains which prescribed the specific boundary structure.

At high stresses and fast creep rates, another interesting feature of cavities was observed. It was found that a considerable number of cavities in the material tested at 128 MPA (#32) at 700°C displayed elongated profiles as shown in the paired cryogenic fracture surfaces of Fig. 7.25. Moreover the elongation of cavities on a grain boundary appeared well aligned and well correlated. Closer examination of the two mating pieces of the fractured specimen revealed that some cavities were made of two halves which apparently were sheared apart by grain boundary sliding as those labelled as A in Fig. 7.25. The transition from the circular disk shape to the elongated disk shape took place at a stress somewhat below 128 MPA, since the elongated profile was not observed in a test at 90 MPA (#33).

7.5. Discussion

7.5.1. Nucleation of Cavities

The very weak dependence of number densities of cavities on the applied stress is not compatible with any nucleation model based on the classical nucleation theory (53, 97, 98) outlined in a previous chapter. This, however, should not be a great cause for concern since cavities of the size of 0.2 μm and larger are well past the stage of nucleation. Typically a critical size nucleus is of the order of 50 Å or smaller and is nearly two orders of magnitude below the resolution of our two stage creep technique as well as that of any other currently available technique used in this field. An inevitable conclusion is then that

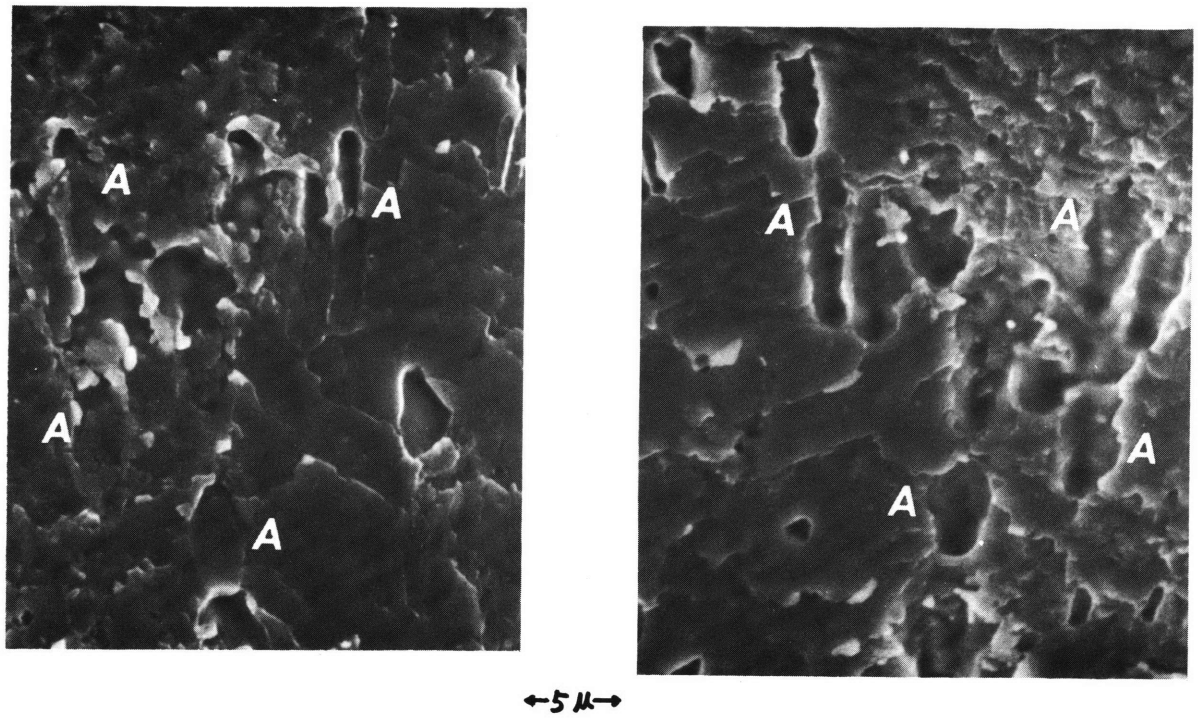

Fig. 7.25 Stress = 128 MPA
$Strain_{ss} = 3.5 \times 10^{-5} Sec^{-1}$ at 700°C for 97.5 min.(#32).

growth has already played a major role affecting the cavity size and distribution in our measurements. Indeed the excellent correlation between the number densities of cavities and the normal component of the applied stress across boundaries lends further support to this interpretation. We recall that both the classical theory of Hull and Rimmer (63) and our general theory of cavity growth predict such a correlation.

Nevertheless the sensitive dependence of cavitation on grain boundary structures could be taken as evidence that nucleation has a profound influence on later cavitation. As noted earlier, the heterogeneous and selective cavitation on certain portions of boundaries is likely related to the misorientation of the two grains bordered by the grain boundary in question. The misorientation can be altered by a twin which intersects the grain boundary. Although many physical properties are dependent on the misorientation, the most critical one for which a drastic difference in cavitation can be caused by a small change of the magnitude of the property is the interfacial energy $\chi(\dot{\zeta} \sim \exp - 4\chi^3/\sigma_n^2 kT))$. It is possible that variation of interfacial energy, in addition to the extreme cases such as the ones caused by twin intersections, is very common and widespread throughout grain boundaries. A broad spectrum would then be possible for χ^3 which would correspond to a gradual dependence of number of cavities on stress.

It was also pointed out earlier that substantial interfacial stresses only exist during intermediate transients in which relaxation along grain boundary is complete while that around inclusions is not yet accomplished. It is possible that similar events can recur in the

course of the later history of the sample even at the steady state which after all for polycrystals can be defined only in a macroscopic sense and involves repeated acceleration and deceleration of boundary sliding. Such behavior could explain the phenomenon of continuous nucleation and furnishes an additional possibility for the observed weak dependence of nucleation rates on applied stress.

In summary, cavities observed in this study or in most others are well past the nucleation stage. Their distribution in relation to the applied stress reflects more strongly the effect of the features of cavity growth rather than that of nucleation. On the other hand, cavitation is influenced by the interfacial energy which affects nucleation drastically by prescribing the presence or absence of sites for particles that are responsible for the cavities. In general, a broad spectrum of nucleation barrier seems plausible, although the activation of even the preferable nucleation site is only possible during transients of grain boundary sliding. Recurrence of these transients even at a macroscopically steady state can be responsible for continuous increase of number of cavities during creep.

7.5.2. Growth of Cavities

Diffusion distance ℓ_D and coupling coefficient α have been shown to be important parameters in the characterization of cavity growth. Choosing the constants as in the footnote,* we find ℓ_D to be 5.5 μm at 63 MPA and 1.5 μm at 128 MPA, while α to be 26 and 19 res-

* $D_b\delta_b = 10^{-21} m^3/sec$ (104), $D_s\delta_s = 10^{-20} m^3/sec$ (99, 104), ψ =1.37 (65), γ_s= 2.5 J/m^2(65), $\Omega = 7.0 \times 10^{-6} m^3/mole$, d_G = 40 μm, $\dot{\varepsilon}_{s.s}$=3.2 x 10^{-7} sec^{-1} at 63MPA, 4.1 x 10^{-6} sec^{-1} at 90 MPA, and 3.5 x 10^{-5} sec^{-1} at 128 MPA.

pectively. The transition from the quasi-equilibrium mode to the crack-like growth mode should occur at a = 0.54 μm at 63 MPA and a = 0.22 μm at 128 MPA. This is consistent with the morphology of cavities at 63 MPA where they are either disc-like or slightly faceted. The growth rate predicted by the theory, 4×10^{-5} sec^{-1} at 63 MPA is also consistent with the observed growth rate, although a detailed comparison is not possible due to the distribution of cavity sizes.

The interesting feature of cavities grown by grain boundary sliding is also examined. It can be shown that the diffusion time for a cavity of diameter d sheared apart by sliding to recover the equilibrium shape is

$$\tau_s = \frac{kT}{D_s \delta_s \Omega \gamma_s} \frac{d^4}{(2\pi)^4}$$

using simple analysis such as that given by Rice (65) and Harris (45). Thus the additional growth due to grain boundary sliding and sintering is, at a sliding rate $\dot{u}_{GB}$,

$$\left(\frac{\delta d}{\delta t}\right)_{GBS} = \dot{u}_{GB} - \frac{d}{\tau_s}$$

Since $\dot{u}_{GB}$ can be estimated from creep rate and grain size (35), namely, $\dot{u}_{GB} = \alpha_{GB} \dot{\varepsilon}_{GB} d_G$, where α_{GB} is roughly 0.3, we find, for d = 5 μm

$$\frac{d}{\tau_s} = 2.8 \times 10^{-10} \text{ m/sec and}$$

$$\dot{u}_{GB} = 4.2 \times 10^{-10} \text{ m/sec at 128 MPA}$$

$$= 4.9 \times 10^{-11} \text{ m/sec at 90 MPA}$$

$$= 3.8 \times 10^{-12} \text{ m/sec at 63 MPA respectively.}$$

These values are in good agreement with the observation that only at 128 MPA cavity growth was affected by grain boundary sliding. Note that for smaller sized cavities, recovery due to surface diffusion will suppress any shearing caused by grain boundary sliding and the growth rate should be governed by the two limiting modes discussed earlier.

In summary, cavity growth in most circumstances in this study is controlled by grain boundary diffusion which is coupled to surface diffusion and power law creep in the way described in the preceding chapter. At 63 MPA, most cavities looked like amorphous disks and with facets occasionally. They had just past the transition from the quasi-equilibrium mode and were more characteristic of the crack-like mode . At very high stress and creep rate (128 MPA and 3.5×10^{-5} sec^{-1}), shearing caused by grain boundary sliding becomes the fastest mode of growth. The transition can be satisfactorily explained by the competition between surface diffusion and grain boundary sliding spreading out the cavities.

CHAPTER 8

CONCLUSIONS

A micromechanical analysis of deformation and fracture in creeping alloys is presented based on a mechanistic approach utilizing continuum mechanics. It is shown that the effect of small volume fractions of included equiaxed phases with large deformation resistance in a creeping matrix will produce only a very modest rise in overall creep resistance provided the alloys have coarse microstructure. Thus the relatively large creep exponents in microcomposite alloys having superior creep resistance in comparison with the constituent pure matrix phases, is only attributable to the deformation restraint due to non-local processes initiated by the less deformable phases where dislocation-obstacle interactions play an essential role. In spite of this, analysis of interfacial stress on grain boundary particles under certain conditions can still rely on continuum mechanics provided diffusional flow is incorporated in the formulation. Such continuum approaches are useful as a smoothed-out representation of statistical "dislocation flow" processes around particles which otherwise become intractable. Furthermore, the important presence of diffusional flow that can occur in atomic size volume elements serves to justify further the use of continuum field approaches around particles on sliding grain boundaries. These local mechanistic approaches based on continuum mechanics lead us to conclude that along interfaces of relatively large particles on sliding grain boundaries high interfacial stresses that are instrumental in cavity nucleation can occur only in transients of grain boundary sliding. Such transients can take place even under conditions of

macroscopic steady state which, as is well known, involves random accelerations and decelerations of boundary sliding that must be related to microstructural evolution and spurts of grain boundary migration.

In Chapters 5 and 6, we introduce general concepts, such as characteristic diffusion time and characteristic diffusion distance which serve as important scaling parameters in visco-diffusive deformation of materials. A simple theoretical approach based on dimensional analysis to the general problem of cavity growth where surface diffusion, grain boundary diffusion and power-law creep are coupled together was developed. This analysis embraces most of the features of previous successful models in the field and makes it possible to furnish a satisfactory account of the process of microscopical damage production.

An experimental study of creep cavitation in 304 stainless steel at around 0.5 T_m was conducted to test the theoretical models. Cavities were found to nucleate heterogeneously throughout the creep history. Comparison of these observations with a proper rendering of the classical nucleation theory, developed specifically for cavity nucleation at stressed interfaces, suggests that a broad spectrum of interfacial energy may exist, and that microstructural changes during the creep process can alter cavitation drastically. In particular, it was found that some portions of boundaries, where twins impinged on grain boundaries, are sufficiently different from their surroundings to suggest that changes in the microstructure result from changes in misorientation between bordering grains and that this can be a key factor in the consideration of cavity nucleation. Cavities grow in most cases by coupled diffusion and matrix creep, somewhat restricted

by surface diffusion across the cavity which becomes increasingly important at an intermediate stage of growth. Experiments demonstrate, however, that grain boundary sliding can be a dominant mode of cavity growth at high stresses and for large cavities. This last mechanism may play a more important role near the tip of a macroscopic crack and possibly in non-steady loading.

BIBLIOGRAPHY

1. F. A. McClintock and A. S. Argon, "Mechanical Behavior of Materials," Addison-Wesley, Reading, Massachusetts (1966).
2. S. H. Crandall and N. C. Dahl, "An Introduction to the Mechanics of Solids", McGraw-Hill, New York (1959).
3. G. I. Taylor, J. Inst. Metals, 62, 307 (1938).
4. R. Hill, J. Mech. Phys. Solids 5, 66 (1956).
5. M. F. Ashby, G. H. Edward, J. Davenport and R. A. Verrall, Acta Met. 26, 1379 (1978).
6. Z. Hashin and S. Strickman, J. Mech. Phys. Solids, 10, 343 (1962).
7. Z. Hashin, J. Appl. Mechanics, 29, 143 (1962).
8. A. Gurson, Ph.D. Thesis, Brown University (1975).
9. M. P. Cleary, I.W. Chen and S. M. Lee, "Self Consistent Techniques for computing the Effective Response of Heterogeneous Materials" Paper in print (1980).
10. A. V. Hershey, J. Appl. Mech., 21, 236 (1954).
11. E. Kröner, Z. Physik, 151, 504 (1958).
12. B. Budiansky, J. Mech. Phys. Solids, 13, 223 (1965).
13. R. Hill, J. Mech. Phys. Solids, 13, 89 (1965).
14. R. Hill, J. Mech. Phys. Solids, 13, 213 (1965).
15. J. W. Hutchinson, Proc. Roy. Soc. 319A, 247 (1970).
16. J. W. Hutchinson, Proc. Roy. Soc. A. 348, 101 (1976).
17. W. Huang, J. Comp. Mater. 5, 320 (1971).
18. J. D. Eshelby, Proc. Roy. Soc., A. 241, 376 (1957).
19. L. M. Brown and W. M. Stobbs, Phil. Mag. 23, 1185 (1971).
20. L. M. Brown and W. M. Stobbs, Phil. Mag. 23, 1201 (1971).

21. L. M. Brown and W. M. Stobbs, Phil. Mag. 34, 351 (1976).

22. C. Zener, Phys. Rev., 60, 906 (1941).

23. T. S. Ke, J. Appl. Phys. 22, 274 (1949).

24. N. F. Mott, Proc. Phys. Soc. (London), 60, 391 (1948).

25. H. Gleiter and B. Chalmers, Progress in Materials Science, Vol. 16, Pergamon, N.Y. (1972).

26. E. W. Hart, Acta Met., 15, 1545 (1967).

27. F. W. Crossman and M. F. Ashby, Acta Met., 23, 425 (1975).

28. F. Ghahremani, Ph.D. thesis, Harvard University (1979).

29. C. W. Lau and A. S. Argon, Proc. 4th Int. Conf. Fracture (Waterloo) V. 2, p. 595 (1977).

30. J. W. Hutchinson, J. Mech. Phys. Solids, 16, 13 (1968).

31. H. C. Chang and N. J. Grant, Trans. AIME, 197, 1175 (1953).

32. R. Raj and M. F. Ashby,Met. Trans., 2, 1113 (1971).

33. R. Raj, Met. Trans., 6A, 1499 (1975).

34. A. J. Perry, J. Mat. Sci., 9, 1016 (1974).

35. R. C. Gifkins, "Fracture" ed., B. L. Averbach, MIT Press (1959).

36. D. McLean, J. Inst. Met., 85, 468 (1956-1957).

37. C. Zener, "Fracturing of Metals," ASM, Clevaland (1948).

38. A. N. Stroh, Proc. Roy. Soc. 233A, 404 (1954).

39. J. N. Greenwood, D. R. Miller and J. W. Suiter, Acta Met., 2, 250 (1954).

40. R. Resnick and L. Seigle, Trans. AIME, 209, 87 (1957).

41. R. W. Balluffi and L. L. Seigle, Acta Met., 3, 170 (1955).

42. D. McLean, "Grain Boundaries in Metals" Oxford U. Press, Oxford (1957).

43. R. C. Gifkins, Acta Met., 4, 98 (1956).

44. C. W. Chen and E. S. Machlin, Acta Met., 4, 655 (1956).

45. J. E. Harris, Trans., AIME, 233, 1509 (1965).

46. P. W. Davis and J. P. Dennison, Nature, 182, 131 (1958).

47. I. S. Servi and N. J. Grant, Trans. AIME, 191, 909 (1951).

48. N. J. Grant and A. R. Chaudhuri, "Creep and Rupture," ASM, Cleveland (1957).

49. E. D. Hyam, "Structural Processes in Creep," Iron Steel Inst., London (1961).

50. C. W. Weaver, J. Inst. Met., 88, 296 (1959-60).

51. E. S. Machlin, Trans. AIME, 206, 106 (1956).

52. A. H. Cottrell, "Structural Processes in Creep" Iron Steel Inst. London (1961).

53. R. Raj, Acta Met., 26, 995 (1978).

54. R. C. Boettner and W. D. Robertson, Trans. AIME, 221, 613 (1961).

55. D. M. R. Taplin and L. J. Barker, Acta Met., 14, 1527 (1966).

56. R. T. Ratcliffe and G. W. Greenwood, Phil. Mag., 12, 59 (1965).

57. G. W. Greenwood, Phil. Mag., 19, 423 (1969).

58. B. J. Cane, Met. Sci, 12, 102 (1978).

59. A. Gittins and H. D. Williams, Phil. Mag., 16, 849 (1967).

60. A.E.B. Presland and R.I. Hutchinson, J. Inst. Met., 90, 239 (1961-61).

61. R.G. Fleck, D.M.R. Taplin, G.I. Beevers, Acta Met., 23, 415 (1975).

62. D.M.R. Taplin and A.L. Wingrove, Acta Met., 15, 1231 (1967).

63. D. Hull and D.E. Rimmer, Phil. Mag., 4, 673 (1959).

64. M.V. Speight and W. Beere, Met. Sci., 9, 190 (1975).

65. T. Z. Chuang, K.I. Kagawa, J.R. Rice, L.B. Sills, Acta Met., 27, 265 (1979).

66. A. L. Wingrove and D.M.R. Taplin, J. Mat. Sci., 4, 789 (1969).

67. I.J. Spark and D.M.R. Taplin, J. Australian, Inst. Met., 14, 298 (1968).

68. F. C. Monkman and N.J. Grant, Proc. ASIM, 56, 593 (1956).

69. A. Gittins, cited by R. C. Gifkins, "Fracture" (Butterworths), London (1963).

70. D. Kramer and E.S. Machlin, Acta Met., 6, 454 (1958).

71. J. Intrater and E.S. Machlin, Acta Met., 7, 140 (1959).

72. R. J. Fields and M.F. Ashby, Phil. Mag. 33, 33 (1976).

73. T. Z. Chuang and J.R. Rice, Acta Met., 21, 1625 (1973).

74. W. Beere and M.V. Speight, Met. Sci., 12, 172 (1978).

75. G. H. Edward and M.F. Ashby, Acta Met., 27, 1505 (1979).

76. A. S. Argon, "Surface Effects in Crystal Plasticity" (edited by R. M. Latanision and J.F. Fourie), p. 383, Noordhoff International Publishing, Netherland (1977).

77. L. J. Walpole, J. Mech. Phys. Solids, 17, 235 (1969).

78. J. W. Hutchinson, Met. Trans., 8A, 1465 (1977).

79. A. S. Argon, unpublished paper presented at the Symposium "Advances in Metal Deformation: Phenomena and Mechanism" at Cornell University, USA (1976).

80. N. J. Hoff, Quart. Appl. Math., 12, 49 (1954).

81. J. E. Gubernatis and J. A. Krumhansl, J. Appl. Phys., 45, 5 (1975).

82. J. R. Willis, J. Mech. Phys. Solids, 25, 185 (1977).

83. W. Huang, Int. J. Solids Struct., 8, 149 (1972).

84. A. Needleman, Ph.D. Thesis, Harvard University (1970).

85. T. T. Wu, Int. J. Solids Struct., 2, 1 (1966).

86. B. Budiansky and R. J. O'Connell, Int. J. Solids Struct., 12, 81 (1976).

87. H. Brunner and N. J. Grant, J. Inst. Metals, 85, 77 (1957).

88. C. W. Lau, Ph.D. Thesis, MIT (1980).

89. M. V. Speight, Acta Met., 24, 725 (1976).

90. I.M. Lifshitz, Soviet Phys. JETP, 17, 909 (1963).

91. A. I. Luré, "Three-Dimensional Problems of the Theory of Elasticity," Inter. Sci. (1964).

92. H. Riedel, Z. Metallkde, 69, 12 (1978).

93. J. Bassani, Private communication (1979).

94. A. Needleman and J. R. Rice, Private communication (1979).

95. S. P. Timoshenko and J. N. Goodier, "Theory of Elasticity," 3rd ed., McGraw-Hill, New York (1970).

96. M. L. Williams, J. Appl. Mech., Trans. ASME, 74, 526 (1952).

97. A. S. Argon, Paper presented in AIME Fall Meeting, Milwaukee (1979).

98. R. Raj and M.F. Ashby, Acta Met., 23, 653 (1975).

99. D. A. Mortimer and M. G. Nicholas, Met. Sci., 10, 326 (1976).

100. R. W. Little, "Elasticity", Prentice-Hall, Englewood Cliff (1973).

101. B. J. Cane and G. W. Greenwood, Met. Sci., 9, 55 (1975).

102. G. M. Pharr and W. D. Nix, Acta Met., 27, 1615 (1979).

103. S. H. Goods and W. D. Nix, Acta Met., 26, 739 (1978).

104. N. A. Gjostein, "Diffusion Seminar," ASM, Cleveland (1974).

105. J. E. Harris, Met. Sci., 12, 321 (1978).

106. V. J. Borisov, V. M. Golikov and G. V. Scherbedinskiy, Phys. Met. and Metallog, 17, 6, 80 (1964).

107. C. Leyymonie and P. Lacombe, Rev. Metal., 57, 285 (1960).

108. D. W. James and G. M. Leak, Phil. Mag., 12, 491 (1965).

109. D. Turnbull, J. Appl. Phys., 22, 634 (1951).

110. J. T. Robinson, and N. L. Peterson, Surface Sci., 31, 586 (1972).

111. V. V. Gall, P.L. Gruzin and G. Y. Yudina, Phys. Met. and Metallog., 30, 204 (1973).

112. J. Gertner, Ph.D. Thesis, MIT (1978).

113. F. G. Wilson, J. Iron Steel Inst., 209, 126 (1971).

114. M. H. Lewis and B. Hattersley, Acta Met., 13, 1159 (1965).

115. C. Novak, "Handbook of Stainless Steels," ed. D. Peckner and I.M. Bernstein, McGraw-Hill, New York (1977).

116. L. K. Singhal and J. W. Martin, Trans. AIME, 242, 814 (1968).

117. J. Y. Park and S. Danyluk, Corrosion, 33, 304 (1977).

118. S. Danylux, J.Y. Park, D.E. Busch, Script Met., 13, 857 (1979).